RESONANCE RAMAN STUDIES
ON
CHROMOPROTEINS
AND
THEIR MODEL COMPOUNDS

YASUHISA MIZUTANI

School of Mathematical and Physical Sciences
The Graduate University for Advanced Studies

Preface

Resonance Raman (RR) spectroscopy is a versatile spectroscopic technique for studying the structure of biological molecules. The resonance condition arises when the wavelength of the laser light used to excite Raman scattering falls within an electronic absorption band, causing Raman intensity of the vibrations of the absorbing species to be selectively enhanced. This makes it possible to obtain the vibrational spectrum of a chromophore in a protein without interference from the vibrations of other parts of protein and solvent. The vibrational spectra provide detailed information about the geometry and electronic structure of the chromophore. The chromophore of biological molecules usually serves as an active site of their physiological functions. Therefore, the analysis of RR spectra is expected to provide some unique and essential information about the structure-function relationship of biomolecules.

The author has been interested in applying the RR technique to structural studies of biomolecules and their related model compounds, and selected phytochrome and iron porphyrins as objects. Phytochrome is one of the most important photoreceptors in higher plants. It is used to sense the light environment and to transduce the environmental information into a form to which plants can respond by modification of growth and development. Phytochrome has two stable forms, red- (P_r) and far-red-absorbing forms (P_{fr}), and the phototransformation between them is a trigger reaction of signal transduction. The final purpose of this study is to elucidate the mechanism of phototransformation and that of signal transduction from phytochrome to next signal transducing proteins. However, as the first step, the practical goal in this dissertation is to characterize the differences in molecular structure between P_r and P_{fr}, and the reaction intermediates by using RR spectroscopy.

In addition to the phytochrome study, the author had been engaged in the study on the iron porphyrins with higher oxidation states in the earlier part of this course. Iron porphyrin is a prosthetic group of heme proteins and those with higher oxidation states are essentially important as the model compounds of intermediates in their physiological reactions.

This dissertation consists of two parts. In Part I, the results about the phytochrome study are described. Studies on functions, molecular properties, phototransformation pathway and reaction kinetics are reviewed in Chapter I. In Chapter II RR spectra, which were observed in a natural state for the first time, are presented. Pea

"large" phytochrome, which lacks ca. 7-kDa polypeptide of intact pea phytochrome, was used in the first stage of this course because of ease for its preparation. Differences in protonation structure of the chromophore of P_r, P_{fr} and the reaction intermediate (I_{bl}) are discussed there. RR spectra of pea "intact" phytochrome are presented in Chapter III. A difference in protonation structure of the chromophore and a role of 7-kDa segment are discussed. In addition, the results about the model compounds of the chromophore and specification of the protonation site on the chromophore by using ^{1}H- and ^{15}N-NMR technique are also described in this chapter. In Chapter IV the vibrational assignments of model compounds of phytochrome chromophore are discussed on the basis of the spectra of their isotopic derivatives. Chapter V aims to detect the conformational change of phytochrome upon phototransformation by using ultraviolet RR spectroscopy. Environments of some aromatic amino acid residues and conformational change upon phototransformation are discussed there.

In Part II the results about iron porphyrins in higher oxidation states are described. A historical review of studies on oxyferrous-, oxoferryl-porphyrins, and π cation radicals is described in Chapter I. In Chapter II, RR spectra of the intermediates in autoxidation of four-coordinated ferrous porphyrin at low temperature are presented. The Fe^{II}-O_2 and O-O stretching Raman bands, which were simultaneously observed, of the oxyferrous intermediate, and the Fe^{IV}=O stretching Raman band of the oxoferryl intermediate are presented in this chapter. In Chapter III porphyrin π cation radicals and their Fe^{IV}=O stretching vibration are characterized by RR spectroscopy. The assignments of several porphyrin in-plane vibrations and Fe^{IV}=O stretching vibration of π cation radical on the basis of isotopic frequency shifts are described in this chapter.

Acknowledgements

November, 1991
Okazaki,

Yasuhisa Mizutani

Publication List

1. "Effect of Urea on Hydrophobic Interaction: Raman Difference Spectroscopy on the C-H Stretching Vibration of Acetone and the C-N Stretching Vibration of Urea",
   Yasuhisa Mizutani, Keiji Kamogawa and Koichiro Nakanishi,
   Journal of Physical Chemistry **1989**, *93*, 5650-5654.

2. "Synthetic Model for Dioxygen Binding Sites of Non-Heme Iron Proteins. X-ray Structure of Fe(OBz)(MeCN)(HB(3,5-iPr$_2$pz)$_3$) and Resonance Raman Evidence for Reversible Formation of a Peroxo Adduct",
   Nobumasa Kitajima, Hideno Fukui, Yoshihiko Moro-oka, Yasuhisa Mizutani and Teizo Kitagawa,
   Journal of the American Chemical Society **1990**, *112*, 6402-6403.

3.* "Resonance Raman Spectra of Large Pea Phytochrome at Ambient Temperature",
   Satoru Tokutomi, Yasuhisa Mizutani, Helen Anni and Teizo Kitagawa,
   FEBS Letters **1990**, *269*, 341-344.

4.* "Resonance Raman Pursuit of the Change from Fe^{II}-O$_2$ to Fe^{III}-OH via Fe^{IV}=O in the Autoxidation of Ferrous Iron-Porphyrin",
   Yasuhisa Mizutani, Shinji Hashimoto, Yoshitaka Tatsuno and Teizo Kitagawa,
   Journal of the American Chemical Society **1990**, *112*, 6809-6814.

5. "Solution Structures and Phase Separation in Fluoro Alcohol/Water Mixtures: A Study with Raman Difference and ^{13}C NMR Spectroscopy",
   Yasuhisa Mizutani, Keiji Kamogawa, Teizo Kitagawa, Akio Shimizu, Yoshihiro Taniguchi and Koichiro Nakanishi,
   Journal of Physical Chemistry **1991**, *95*, 1790-1794.

6.[*] "Resonance Raman Characterization of Ferric- and Ferrylporphyrin π Cation Radicals and the $Fe^{IV}=O$ Stretching Frequency",
Shinji Hashimoto, Yasuhisa Mizutani, Yoshitaka Tatsuno and Teizo Kitagawa,
Journal of the American Chemical Society **1991**, *113*, 6542-6549.

7.[*] "Resonance Raman Study on Intact Pea Phytochrome and Its Model Compounds: Evidence for Proton Migration during the Phototransformation",
Yasuhisa Mizutani, Satoru Tokutomi, Katsuhiro Aoyagi, Keisuke Horitsu and Teizo Kitagawa,
Biochemistry **1991**, *30*, 10693-10722.

8. "μ-Alkoxo-Diiron(II,II)Complexes of *N,N,N',N'*-tetrakis-(2-(6-methylpyridyl)-1,3-diaminopropan-2-olato and the Reversible Formation of the O_2-Adducts",
Yoshihito Hayashi, Masatatsu Suzuki, Akira Uehara, Yasuhisa Mizutani and Teizo Kitagawa,
Chemistry Letters **1992**, 91-94.

(*) Articles marked by an asterisk are included in this dissertation.

Contents

(vii)

Part I.

Resonance Raman Studies on
the Phototransformation Mechanism
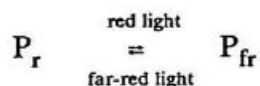# of Phytochrome

1

Chapter I.

Overview: Physical Chemistry of Phytochrome

I-1. Phytochrome in Photomorphogenesis

Light plays various key roles in the life of plants, animals and microorganisms.[1] Light is particularly crucial in green plants not only as the source of energy for photosynthesis but as an environmental signal which regulates diverse elementary processes at the molecular, cellular and organ levels. The former process converts light energy into chemical energy that can be used for carbon dioxide fixation, while the latter utilizes light as a signal to detect information about the environment. As plants are unable to change their location to avoid dangerous or unfavorable conditions, they must safeguard themselves for their existence by responding promptly and efficiently to sudden, diurnal or seasonal changes in their environment.

Light capture by photoreceptor pigments in organisms is the first step of all signal transduction chains that induce some developmental responses. Phytochrome is the only photoreceptor that has been identified biochemically so far among those of photomorphogenesis and the most important phototransducer for the photoregulation in plants.[2,3] Undoubtedly, the most striking feature of phytochrome is the photoreversible change of its absorption, which occurs upon irradiation with visible light. Namely, phytochrome has two stable absorbing forms, the red light absorbing form and the far-red light absorbing form:

$$P_r \overset{\text{red light}}{\underset{\text{far-red light}}{\rightleftharpoons}} P_{fr}$$

where P_r and P_{fr} represent the two forms of phytochrome absorbing maximally at 660nm and 730 nm, respectively. This phototransformation of phytochrome results eventually in a wide variety of physiological and developmental responses in plants, such as stem elongation, leaf expansion, spore and seed germination, photoperiodic floral induction, hyponatic leaflet movement and several other phenomena.[4] Phytochrome also regulates the progression of cell cycles,[5] phototactic chloroplast movements,[6] chloroplast biogeneses,[7] activities of several enzymes[8] and gene expressions.[9]

Recently it has been shown that conidation in the filamentous asomycete *Aspergillus nidulans*, which has no photosynthetic system, is induced by red light and that this induction is reversed by an immediate shift to far-red light, reminiscent of the phytochrome-mediated responses observed in higher plants.[10] This is particularly interesting from a view of evolution.

4

I-2. Discovery of Phytochrome

Red/Far-red Light Photorevesible Reactions. The discovery of phytochrome is a fascinating event of biological research in which botanists cooperated with physicochemists and biochemists in an ideal way.[2] An important step was the discovery of photoreversivility: Lettuce seeds, only 25% of which had been germinated in the dark, were induced to more germinate (up to 70-80%) by red light illumination (maximum at about 660 nm). The irradiation of far-red light was able to inhibit germination not only of the original seeds but also of the red-irradiated seeds (down to 6-7% germination). Germination of the latter seeds could be reinduced by red light and then again inhibited by far-red light. This could be repeated up to 100 times with always the same effect. Thus, the last light treatment determined the physiological response irrespective of the pretreatment. Since then, the red/far-red light photoreversible reactions have been observed extensively in morphogenesis phenomena of higher plants.[4]

After the discovery of the red/far-red photoreversible effect, Borthwick and Hendricks were able to make a unique prediction concerning the nature of the photoreceptor for the red/far-red photoreversible responses. They proposed that the physiological response pattern observed could be most simply explained by assuming that the photoreceptor existed in two interconvertible forms, one of which had an absorption maximum at 660 nm, and the other at 730 nm, and absorption of light by either form would result in conversion to the other form. Using a two-wavelength difference spectrometer, they succeeded in measuring photoreversible changes in optical density at 660 nm and 730 nm in etiolated maize seedlings and crude extract.[3] This photochromic pigment was named '*phytochrome*' (*phyto*=plant, *chrome*=pigment) in their paper in 1960.

Phytochrome Isoforms. In the 1980's biochemical evidence that suggests the existence of isoforms of phytochrome has been accumulated.[11] The level of the phytochrome species which is present in abundance in etiolated seedlings ('type I phytochrome' according to Furuya[11]) is controlled by light very sensitively; it decreases rapidly under a white-light condition. The level of the other isoform is not so sensitive to the light condition that it becomes a major species in green plants ('type II phytochrome'). A different subunit with the molecular mass of 118kDa and the blue-shifted absorption maximum (654nm) are also reported for the green-tissue phytochrome.[12,13] At least three different phytochrome genes, *phy A*, *phy B* and *phy*

5

C, are present in *Arabidopsis thaliana*.[14] Effects of light conditions on the expression of these genes suggest that *phy A* gene may code for type I phytochrome and the other genes for type II phytochromes. However, information of type II phytochrome is not sufficient at the present stage. Therefore, in this chapter, hereafter, only type I phytochrome will be discussed.

I-3. The Mechanism of Signal Transduction Mediated by Phytochrome

The mechanism of the phytochrome-mediated signal transduction is far from being fully understood. The physiological behavior of plants indicates that P_{fr} is the active form and that P_r is the inactive form.[16] It has also been demonstrated that the isolated phytochrome in P_{fr} enhances mRNA synthesis in isolated nuclei.[17] The question about a specific receptor for the P_{fr} remains unanswered. It has been reported that phytochrome accelerates the inositolphospholipid turnover via Ca^{2+} ion mobilization[18] and activates a protein kinase.[19] In animal signal transduction, G-proteins play a pivotal role. Very recently, Romero et al. suggested that a G-protein-based signal cascade is involved in the phytochrome-mediated responses *in vivo*.[20] On the other hand, enzymatic activity of phytochrome has been discussed since the discovery of phytochrome.[4] Wong et al. reported that polycation-dependent protein kinase activity associated with purified *Avena* phytochrome,[21] although, later, an argument against their result was reported.[22] While various hypotheses have been proposed for signal transduction pathway as described above, none of them can not be taken for granted yet.

I-4. Molecular Properties of Phytochrome

Polypeptide Size and Terminology of Phytochromes. Biochemical researches on phytochrome have been hampered by a partial enzymatic degradation during its purification since the first extraction.[23] Thus, most phytochrome samples prepared in the 1960's were probably molecular species with about 60kDa, and in fact, it was later revealed to be the chromophore-bearing, N-terminal half of phytochrome.[24] Phytochrome samples in the 1970's were mostly composed of two identical subunits with 114-118kDa. In the early 1980's, it became evident that the 6-8kDa segment from the N-terminus was extremely sensitive to proteolysis by endogeneous proteases when phytochrome was in P_r. The polypeptide size of native phytochrome was evaluated to be 121-124kDa depending on plant species.[25,26] The molecular size of native phyto-

6

chrome was later confirmed by the nucleotide sequence of phytochrome cDNA.[27] It took more than 20 years to conclude the dispute over the size of native phytochrome polypeptide. In this dissertation terminology used in the historical background is adopted to specify the partially degraded products of phytochrome: The chromophore-bearing fragment whose molecular mass is around 60kDa is called '*small phytochrome*'; the less degraded phytochrome whose subunit molecular mass ranges 114-118kDa is called '*large phytochrome*'; the no degraded, native phytochrome whose molecular mass ranges 121-124 kDa is called '*intact phytochrome*' (Figure I-1).

Chromophore Structure. As an absorption spectrum of P_r is similar to that of phycobiliprotein, especially to that of allophycocyanin, phytochrome has been presumed to be a biliprotein since the beginning of the biochemical research of phytochrome.[28] In fact, the chromophore of phytochrome, phytochromobilin, is closely related to phycocyanobilin, which is a chromophore of allophycocyanin and phycocyanin from blue-green algae (Figure I-2). The only difference between them is that the ethyl group attached to ring D in phycocyanobilin is replaced with a vinyl group in phytochromobilin. Both chromophores are bound covalently to their polypeptide chains in the identical manner: ring A of the open tetrapyrrole links to the cysteine residue through a thioether bond.[29]

Primary Structure. In the last five years amino acid sequences of phytochrome have become available thanks to molecular cloning of phytochrome cDNA. So far the sequences of phytochrome from six different plant species and two phytochrome isoforms have been determined.[27,30] Monocot and dicot phytochromes isolated from the etiolated tissue show a high homology within each group (80-90%) and a lower homology of about 65% is observed between monocot and dicot phytochromes.[31]

Domain Structure. The partial degradation of phytochrome during preparation often frustrates phytochrome studies, but, on the other hand, the process of finding a native phytochrome has led us to understand the domain structure of phytochrome. When phytochrome is extracted and purified in P_r from etiolated pea seedlings, the large phytochrome which lacks N-terminal 52 amino acid residues is obtained.[32] In comparison the absorption spectrum of native phytochrome with that of large phytochromes, it becomes evident that upon losing the N-terminal 6-kDa domain, the absorption peak of P_{fr} blue-shifts from 730 to 724nm, while the absorption of P_r is not influenced.[33,34] The CD signal due to the P_{fr} chromophore increases in its magnitude.[35,36] The chromophore configuration of P_{fr} probably changes depending

7

on the presence of that domain. Generally speaking, spectral properties of large phytochrome after red light irradiation highly depend on environmental factors such as pH,[37] ionic composition,[38] reducing reagent[39] and so on. In contrast, spectral properties of intact phytochrome are much less affected by environmental factors. The rate of reversion from P_{fr} to P_r in the dark is also affected: it is negligibly slow on intact phytochrome, while it is fast on large phytochrome.[35,40] These phenomena indicate that the domain interacts with the chromophore in P_{fr}. A conformational change (3% increase in α-helix) is detected by a far-UV CD measurement for intact phytochrome during a photoreaction from P_r to P_{fr}.[37] No CD change has been detected for large phytochrome.[41] When the monoclonal antibody which binds with the N-terminal 6-kDa domain is added to intact phytochrome, the CD change is suppressed.[42]

When phytochrome is subjected to prolonged purification, a small phytochrome whose molecular weight is around 60kDa is obtained. The small phytochrome was shown to be a chromophore-bearing fragment ranging about 60th to 600th residues.[32,43] The protein does not form a homodimer any longer. It displays the photoreversible conversion between P_r and P_{fr}, which is similar to that of large and intact phytochromes, indicating that main machinery of light absorption locates within the 60-kDa domain of phytochrome.

When phytochrome is treated with proteases strongly, chromophore-bearing 33-39kDa fragments of a single polypeptide are obtained.[32,44] These preparations do not show photoconversion between P_r and P_{fr} any longer. When phytochrome is digested by proteases in P_r, the new absorbing form with absorption maximum at 658nm, P_{658}, is obtained. Irradiation of P_{658} with red light yields a bleached form instead of P_{fr}. This bleached form has a broad, but weak absorption band in the red and far-red regions, and is, therefore, called a bleached form, P_{bl}. P_{bl} also is phototransformed to P_{658} by a prolonged exposure to far-red light, and reverts to P_{658} very slowly in the dark. P_{bl} shows an absorption spectrum similar to that of the bleached intermediate, I_{bl}, which appears during phototransformation (see I-6). P_{bl} can be obtained by irradiating large phytochrome in P_r with red light following the treatment with formic acid or by irradiation it with red light under an alkaline condition ($\sim$ pH 11).

Subunit Structure and Molecular Shape. It is made evident by sodium dodecyl-sulfate-polyacrylamide gel electrophoresis that phytochrome consists of a polypeptide

of about 120kDa. On the other hand, the molecular mass of 240kDa is estimated by the sedimentation equilibrium centrifugation (SEC) for both large and intact phytochromes.[45,46] It is concluded that phytochrome is composed of two identical subunits. The contact site between the two subunits of intact oat phytochrome has been localized within 42kDa from the C-terminus,[36,46] because all the trypsin digested segments containing the C-terminal 42-kDa portion migrate as aggregates in SEC, while trypsin digested segments derived from N-terminal 82-kDa portion behave as globular monomers. A similar conclusion is reached for pea large phytochrome.[47]

For elucidating the tertiary and quarternary structures of phytochrome it is difficult to apply X-ray crystallography, since it has not been crystallized due to its high molecular mass. The application of the high-resolution NMR spectroscopy to polypeptides with a molecular mass of more than about 20kDa is still limited. The molecular shape of phytochrome in P_r has been recently studied by small-angle X-ray scattering (SAXS).[48] The obtained best-fit model is shown in Figure I-3. It is called 'four-leaved shape model' based on a view from the Z-axis. The shape of large pea phytochrome in P_r has also been investigated by rotary shadowing electron microscopy.[48b,c] Essentially the same images have been observed for pea intact phytochrome.[48c] These results indicate that the N-terminal 6-kDa domain does not influence the overall shape of phytochrome.

I-5. Difference between P_r and P_{fr}

It is one of the major goal of the research on phytochrome to determine which molecular properties are different between P_r and P_{fr} besides an apparent difference, since understanding of the difference could be a starting point in elucidation of the transducing chain of phytochrome actions.

Chromophore Structure. There is a proposal that the primary photoreaction ($P_r \rightarrow I_{700}$ (see I-6)) involves $Z \rightarrow E$ isomerization of the chromophore (Figure I-4).[49] Positive evidence for $Z \rightarrow E$ isomerization so far available is the difference between P_r chromophore and P_{fr} chromophore as analyzed for small chromopeptides.[29] But such an isomerization of intact phytochrome remains to be established. The H_2O/D_2O dependence of the rate constant suggests proton transfer in a photoreaction of phytochrome.[50] It remains to be elucidated at what stage of the phototransformation an intramolecular proton migration takes place along the thermal pathway leading to P_{fr} and is responsible to proton release/uptake in solution (*vide infra*).

9

Conformational Changes of the Protein. There are some clearly recognizable conformational changes in the phototransformation of phytochrome. High-performance SEC of oat and rye intact phytochromes indicated a measurable, photoreversible change in the molecular shape.[51] Hydrogen-tritium exchange measurements on *Avena* phytochrome revealed an increase in the ^1H-^3H exchange kinetics upon P_r to P_{fr} phototransformation.[52] Native phytochrome in P_{fr} has three to four more reactive SH groups than P_r.[53] Similar results are also obtained for large phytochrome. Phosphorylation sites by protein kinases also change depending on individual forms of phytochrome.[21,54] It was suggested that the P_{fr} chromophore was substantially exposed, as compared with the P_r chromophore.[55] But there is no information about the concrete differences of molecular structure to which these differences between two forms are ascribed.

Difference in Hydrophobicity of Two Absorbing Forms. So far many experimental results show that P_{fr} is more hydrophobic than P_r. Large pea phytochrome in P_{fr} forms an aggregate in the presence of 10mM Ca^{2+}.[56] When a membrane fraction is added, the phytochrome in P_{fr} binds it *in vitro*. Since phytochrome is also evenly distributed as a soluble cytosolic protein *in vivo* but tends to form sequestered bodies in the P_{fr} form, it is highly possible that the difference in hydrophobicity is related to the physiological function of phytochrome. Interestingly, small phytochrome in P_{fr} shows neither self aggregation nor binding to the membrane, which indicates that the small phytochrome loses the hydrophobic surface of phytochrome associated with the photoreversible change.

Proton Transfer. Like bacteriorhodopsin, pea large and small phytochromes were found to release or take up protons photoreversibly during interconversion between P_r and P_{fr}.[57] Contrary to this, intact phytochrome seems to hardly release or take up protons between the protein and bulk medium. On the other hand, only proton release is observed for a change from P_{658} to P_{bl} occurring in the 39-kDa fragment or partially denatured large phytochrome by saponin. This suggests that proton release and uptake take place in the steps of $P_r \rightarrow I_{bl}$ and $I_{bl} \rightarrow P_{fr}$, respectively.

I-6. Phototransformation Pathway and Reaction Kinetics of Phytochrome

A characteristic feature of phytochrome photochemistry is the formation of reaction intermediates between P_r and P_{fr}. The initial photoreaction via the excited state of the chromophore is followed by a series of dark relaxation processes in both

directions. Intermediates of the forward reaction ($P_r \to P_{fr}$) seem to be different from those of the backward reaction.[58] Studies on the intermediates have been mainly done for the forward reaction since pure P_{fr} solutions free from P_r are very difficult to prepare. The phototransformation pathway and reaction kinetics of phytochrome have been studied mainly by flash absorption and low temperature spectroscopies.

Flash Photolysis Studies. Flash absorption studies using single or double flashes have provided information with regard to the transient intermediates along the photo-transformation pathway. It has been revealed that there is at least two spectrally-identifiable intermediates in the forward reaction, each of which decays thermally by complex kinetics. The first stage is represented by intermediates which appear within nanoseconds of an actinic flash and are identified by their enhanced absorbance near 700nm compared to P_r, therefore, being named I_{700}. These intermediates decay thermally on a microsecond time scale, which comprise the second stage of the process. The second stage is characterized by a reduced absorbance near 700nm with no corresponding absorbance increase at nearby wavelengths, therefore being named I_{bl} (bl. = bleached). The second intermediates decay to P_{fr} on millisecond or longer time scale. I_{700} and I_{bl} are equivalent to lumi-R and meta-R of Kendrick and Spruit,[59] respectively.

$$P_r \to I_{700}(=\text{lumi-R}) \to I_{bl}(=\text{meta-R}) \to P_{fr}$$
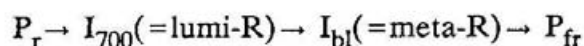
Double flash studies of Pratt et al.[60] with large *Avena* phytochrome corroborated earlier low temperature studies by showing that I_{700} was directly photoconverted back to the P_r form. Furthermore, evidence was also presented that I_{bl} can also be photoconverted back to the P_r form albeit via a different pathway. The photochromism of intermediates on the P_r to P_{fr} pathway also occurs *in vivo*, which was demonstrated by Scheuerlein and Braslavsky[61] using a double flash analysis for lettuce seed germination.

Picosecond fluorescence decay measurements and fluorescence quantum yields have been reported for small, large and intact phytochromes from etiolated oat seedlings.[62] Interestingly, the measured lifetime for the P_r excited state of 45 ± 3ps was identical for all three phytochrome species. These results imply that the rate of the primary photoprocess is not affected by regions of the protein removed by proteolysis.[63]

It is clear that the Z → E isomerization would be a good candidate for the primary photoreaction (P_r → I_{700}) in phytochrome since the photochemical isomerization of the C=C conjugated chain is well known and it has been shown that P_r and P_{fr} of small chromopeptide have Z, Z, Z and Z, Z, E configurations,[29] respectively. But it should be stressed that the photochemical isomerization can not yet be taken for granted. The proposal of proton transfer for the primary photoreaction has been made by Song et al. from fluorescence measurement of P_r.[50] Time resolved fluorescence measurements showed, however, that the deuterium effect was found only for a non-photoreversible chromophore with a long lifetime of fluorescence. No deuterium effect was found for the photoreversible chromophore with a short lifetime of fluorescence.[63,64] Therefore it is unlikely that a proton transfer is involved in the primary photoreaction (P_r → I_{700}). Proton transfer reactions should take place in the later process, if it is involved in the phototransformation of phytochrome.

Low Temperature Spectroscopy. Low temperature absorption measurements and flash absorption measurements on large and intact *Avena* phytochromes revealed the identical intermediates.[58] At low temperature, the photoconversion of phytochrome does not proceed to completion but stops at intermediates which are stable under these conditions.

$$P_r \quad \xrightarrow{\quad} \quad I_{700} \quad \xrightarrow{-100°C} \quad I_{bl} \quad \xrightarrow{-65°C} \quad P_{fr}$$
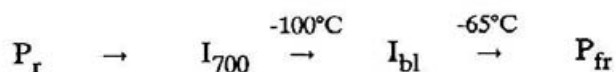
In addition, because of a wide range of these low temperature measurements, the ratio of the oscillator strength of the blue and red absorptions of the intermediates could be determined. Since the oscillator strength ratio is a measure of the overall conformation of tetrapyrrole, a model for kinetics and mechanisms of the light-induced conformational changes of the phytochrome chromophore based on these measurements has been proposed.[58] But, because various assumptions have to be made in deriving the spectra of intermediates, it is still early to wholly embrace either model.

I-6. Problems to be Solved and Summary of Studies in Part I

Chromophore Structure. In order to understand the phototransformation mechanism of phytochrome, it is indispensable to elucidate its chromophore structure, because the phototransformation is undoubtedly induced by the structural change of the chromophore following absorption of light. As the candidates for structural change in the chromophore, proton migration as well as the Z → E isomerization

should be examined, because, if true, it is particularly interesting for phytochrome to have similarity to other photoactive proteins, such as bacteriorhodopsin and rhodopsin, of which photoreaction processes also involve proton migration following photoisomerization.

Resonance Raman (RR) spectroscopy is a powerful technique for studying the structure of chromophore in chromoprotein.[65] Since Raman excitation in resonance with the first absorption band of P_r brings about intense fluorescence background, the RR technique had not been successfully applied to phytochrome until Fodor et al. measured the RR spectra of oat intact phytochrome at 77 K by using far-red-light excitation to avoid much of the inherent fluorescence.[66] Song and his coworkers have employed surface enhanced resonance Raman spectroscopy (SERRS).[67] In both kinds of studies, the sample solutions were frozen, which might cause possible changes in its tertiary and/or quarternary structures and, moreover, SERRS might suffer from a possible structural change of the protein which was induced by the adsorption onto the substrate. In order to study the structural changes of the chromophore accompanied by phototransformation, it is highly desirable to observe RR spectra of phytochrome in a natural state at an ambient temperature. Accordingly, we started this project.

We attempted to measure RR spectra in resonance with the second absorption band in order to avoid the inherent fluorescence and, moreover, adopted two color excitation technique to bias the equilibrium of photo-steady state toward the species to be observed. We used pea large phytochrome in the first stage of this study because of ease for its preparation. We succeeded in observing RR spectra of P_r, I_{bl} and P_{fr} and demonstrating the change in chromophore protonation during the phototransformation as described in Chapter II: Chromophore is protonated in P_r and deprotonated in I_{bl} and P_{fr}; probably deprotonation occurs in the process, $I_{700} \rightarrow I_{bl}$. As described in Chapter III, we also extended this technique to pea intact phytochrome and obtained the results similar to those for large phytochrome although it is suggested for intact phytochrome that proton release/uptake between the protein and bulk medium scarcely occurs.

During the course of three years (1989-1991), vibrational spectra of phytochrome have been reported by several groups including us.[66-68] In order to interpret vibrational spectra of phytochrome, band assignments of the bile chromophore is indispensable. Although the bile chromophore is important as a prosthetic group in

the world of plant not only for phytochrome but also for phycocyanin and phycoery-thrin, a detailed vibrational analysis has not yet been carried out owing to its largeness and low symmetry. As the first ambitious attempt to analyze vibrational spectra of the bile chromophore, we studied RR spectra of the related model compounds, octaethyl-biliverdin and dihydorooctaethylbiliverdin, and their isotopic derivatives. The results are described in Chapter IV. Although the band assignment is incomplete in the study, the results provided some new and important information.

Protein Structure. Since it is well known that most of signal transducing proteins utilize their conformational change, characterization of the conformational change involved is an important subject to be examined in order to understand the signal transduction mechanism. For this purpose ultraviolet RR (UVRR) spectroscopy is helpful because it provides structural information on aromatic amino acid residues.[69] Accordingly we observed UVRR spectra of pea large and intact phytochrome success-fully and detected some spectral differences between P_r and P_{fr} (Chapter V).

References

(1)   Clayton, R. K. In *Light and Living Matter*; McGrow Hill: London, 1970.

(2)   Borthwick, H. A.; Hendricks, S. B.; Parker, M. B.; Toole, E. H.; Toole, V. K. *Proc. Natl. Acad. Sci. U.S.A.* **1952**, *38*, 662-666.

(3)   Butler, W. L.; Norris, K. H.; Siegelman, H. W.; Hendricks, S. B. *Proc. Natl. Acad. Sci. U.S.A.* **1959**, *45*, 1703-1708.

(4)   Borthwick, H. A.; Hendricks, S. B. *Science* **1960**, *132*, 1223-1228.

(5)   (a) Mohr, H. In *Lectures on Photomorphogenesis*; Springer-Verlag: Berlin, 1972. (b) Smith, H. In *Phytochrome and Photomorphogenesis*; McGrow Hill: London, 1975. (c) Kendrick, R. E.; Frankland, B. In *Phytochrome and Plant Growth*; Edward Arnold Ltd.: London, 1976.

(6)   Furuya, M.; Wada, M.; Kadota, A. In *Blue Light Syndrome*; Senger, H. Ed.; Springer-Verlag: Berlin, 1980.

(7)   Haupt, W. In *Phytochrome and Photoregulation in Plants*; Furuya, M. Ed., Academic Press: Tokyo, 1987.

(8)   Jenkins, G. I.; Hartly, M. R.; Bennett, J. *Phil. Trans. Roy. Soc. London* **1983**, *B303*, 419-431.

(9)   Sharma, R. S. *Photochem. Photobiol.* **1985**, *41*, 747-751.

(10)   (a) Tobin, E. M.; Silverthorne, *Ann. Rev. Plant Physiol.* **1985**, *36*, 569-643.   (b) Kuhlemeier, C.; Green, P. J.; Chua, N.-H. *Ann. Rev. Plant Physiol.* **1987**, *38*, 221-278.

(11)   Mooney, J. L.; Yager, Lawrence. N. *Genes Develop.* **1990**, *4*, 1473-1482.

(12)   Furuya M. *Adv. Biophys.* **1989**, *25*, 133-167.

(13)   Tokuhisa, J. G.; Daniels, S. M.; Quail, P. H. *Planta* **1985**, *164*, 321-322.

(14)   Tokuhisa, J. G.; Quail, P. H. *Photochem. Photobiol.* **1989**, *50*, 143-152.

(15)   Scharrock, R. A.; Quail, P. H. *Genes Develop.* **1989**, *3*, 1745-1757.

(16)   Pratt, L. H. In *Photochemical and Photobiological Reviews*; Smith, K. C. Ed.; Plenum Press: New York/London, 1979.

(17)   Ernst, D.; Oesterhelt, D. *EMBO J.* **1984**, *13*, 3075-3078.

(18)   Morse, M. J.; Crain, R. C.; Satter, R. L. *Proc. Natl. Acad. Sci. U.S.A.* **1987**, *84*, 7075-7078.

(19)   Ranjeva, R.; Boudet, A. M. *Ann. Rev. Plant Physiol.* **1987**, *38*, 73-79.

(20)   Romero, L. C.; Sommer, D.; Song, P.-S. *FEBS Lett.* **1991**, *282*, 341-346.

(21)   Wong, Y.-S.; Cheng, H.-C.; Walsh, D. A.; Lagarias, J. C. *J. Biol. Chem.* **1986**,

261, 12089-12097.

(22) Kim, I.-S.; Bai, U.; Song, P.-S. *Photochem. Photobiol.* **1989**, *49*, 319-323.

(23) Briggs, W. R.; Rice, H. V. *Ann. Rev. Plant Physiol.* **1972**, *23*, 293-334.

(24) Gardner, G.; Pike, C.; Rice, H. V.; Briggs, W. R. *Plant Physiol.* **1971**, *48*, 686-693.

(25) Kerscher, L.; Nowitzki, S. *FEBS Lett.* **1982**, *146*, 173-175.

(26) Vierstra, R. D.; Quail, P. H. *Proc. Natl. Acad. Sci. U.S.A.* **1982**, *79*, 5272-5276.

(27) Hershey, H. P.; Barker, R. F.; Idler, K. B.; Lissemore, J. L.; Quail, P. H. *Nucleic Acids Res.* **1985**, *13*, 8543-8559.

(28) Siegelman, H. W.; Turner, B. C.; Hendricks, S. B. *Plant Physiol.* **1966**, *41*, 1289-1292.

(29) Lagarias, J. C.; Rappoport, H. *J. Am. Chem. Soc.* **1975**, *102*, 4821-4828.

(30) (a) Kay, S. A.; Keith, B.; Shinozaki, K.; Chye, M. L.; Chua, N.-H. *Plant Cell* **1989**, *1*, 351-360. (b) Sato, N. *Plant Mol. Biol.* **1988**, *11*, 697-710. (c) Scharrock, R. A.; Lissemore, J. L.; Quail, P. H. *Gene* **1986**, *47*, 287-.

(31) Yamamoto, K. T. *Bot. Mag. Tokyo* **1990**, *103*, 469-491.

(32) Yamamoto, K. T. In *Phytochrome and Photoregulation in Plants*; Furuya, M. Ed.; Academic Press: Tokyo, 1987.

(33) Vierstra, R. D.; Quail, P. H. *Planta* **1982**, *156*, 158-165.

(34) Lumsden, P. J.; Yamamoto, K. T.; Nagatani, A.; Furuya, M. *Plant Cell Physiol.* **1985**, *26*, 1313-1322.

(35) Litts, J. C.; Kelly, J. M.; Lagarias, J. C. *J. Biol. Chem.* **1983**, *258*, 11025-11031.

(36) Vierstra, R. D.; Quail. P. H.; Hahn, T.-R.; Song, P.-S. *Photochem, Photobiol.* **1987**, *45*, 429-432.

(37) Tokutomi, S.; Inoue, Y.; Sato, N.; Yamamoto, K. T.; Furuya, M. *Plant Cell Physiol.* **1986**, *27*, 765-773.

(38) Yamamoto, K. T.; Smith, W. O., Jr. *Plant Cell Physiol.* **1981**, *22*, 1149-1158.

(39) Mumford, F. E.; Jenner, E. L. *Biochemistry*, **1971**, *10*, 98-101.

(40) Vierstra, R. D.; Quail, P. H. *Plant Physiol.* **1983**, *72*, 264-267.

(41) Tobin, E. M.; Briggs, W. R. *Photochem. Photobiol.* **1973**, *18*, 487-495.

(42) Chai, Y.-G.; Song, P.-S.; Cordonnier, M.-M.; Pratt. L. H. *Biochemistry* **1987**, *26*, 4947-4952.

(43) Grimm, R.; Lottspeich, F.; Schneider, H. A. W.; Rüdiger, W. *Z.Naturforsch.* **1986**, *41C*, 993-1000.

(44) Yamamoto, K. T.; Furuya, M. *Plant Cell Physiol.* **1983**, *24*, 713-718.

(45) Hunt, R. E.; Pratt, L. H. *Biochemistry* **1980**, *19*, 390-394.

(46) Jones, A. M.; Quail, P. H. *Biochemistry* **1986**, *25*, 2987-2995.

(47) Yamamoto, K. T.; Tokutomi, S. *Photochem. Photobiol.* **1989**, *50*, 113-120.

(48) (a) Tokutomi, S.; Kataoka, M.; Sakai, J.; Nakasako, M.; Tokunaga, F.; Tasumi, M.; Furuya, M. *Biochim. Biophys. Acta*, **1988**, *953*, 297-305. (b) Tokutomi, S.; Nakasako, M.; Sakai, J.; Kataoka, M.; Yamamoto, K. T.; Wada, M.; Tokunaga, F.; Furuya, M. *FEBS Lett.* **1989**, *247*, 139-142. (c) Nakasako, M.; Wada, M.; Tokutomi, S.; Yamamoto, K. T.; Sakai, J.; Kataoka, M.; Tokunaga, F.; Furuya, M. *Photochem. Photobiol.* **1990**, *52*, 3-12.

(49) Rüdiger, W.; Thümmler, F.; Cmiel, E.; Schneider, S. *Proc. Natl. Acad. Sci. U.S.A.* **1983**, *80*, 6244-6248.

(50) Song, P.-S. In *Sensory Perception and Transduction in Organisms*; Lenci, F.; Song, P.-S. Ed.; Plenum Press: London, 1985.

(51) Lagarias, J. C.; Mercurio, F. M. *J. Biol. Chem.* **1985**, *260*, 2415-2423.

(52) Hahn, T.-R.; Chae, Q.; Song, P.-S. *Biochemistry* **1984**, *23*, 107-110.

(53) Smith, W. O., Jr.; Cyr, K. L. *Plant Physiol.* **1988**, *87*, 185-200.

(54) McMicheal, R. W., Jr.; Lagarias, J. C. *Biochemistry* **1990**, *29*, 3872-3878.

(55) Song, P.-S. *J. Photochem. Photobiol.* **1988**, *2*, 43-57.

(56) Yamamoto, K. T.; Smith, W. O., Jr.; Furuya, M. *Photochem. Photobiol.* **1980**, *32*, 233-239.

(57) (a) Tokutomi, S.; Yamamoto, K. T.; Furuya, M. *Photochem. Photobiol.* **1982**, *35*, 431-433. (b) Tokutomi, S.; Yamamoto, K. T.; Furuya, M. *Photochem. Photobiol.* **1988**, *47*, 439-445.

(58) Eilfeld, P.; Rüdiger, W. *Z. Naturforsch.* **1984**, *40c*, 109-114.

(59) Kendrick, R. E.; Spruit, C. J. P. *Photochem. Photobiol.* **1977**, *26*, 201-214.

(60) Pratt, L. H.; Inoue, Y.; Furuya, M. *Photochem. Photobiol.* **1984**, *39*, 241-246.

(61) Scheuerlein, R.; Braslavsky, S. E. *Photochem. Photobiol.* **1985**, *42*, 173-178.

(62) (a) Wendler, J.; Holzwarth, A. R.; Braslavsky, S. E.; Schaffner, K. *Biochim. Biophys. Acta* **1984**, *786*, 213-221. (b)Holtzwarth, A. R.; Wendler, J.; Ruzsicska, S. E.; Braslavsky, S. E.; Schaffner, K. *Biochim. Biophys. Acta* **1984**, *791*, 265-273.

(63) Ruzsicska, B. P.; Braslavsky, S. E.; Schaffner, K. *Photochem. Photobiol.* **1985**, *41*, 681-688.

(64) (a) Brock, H.; Ruzsicka, B. P.; Arai, T.; Schlamann, W.; Holtzwarth, A. R.; Bras-

lavsky, S. E.; Schaffner, K. *Biochemistry* **1987**, *26*, 1412-1417. (b) Aramendía, P. F.; Ruzsicska, B. P.; Braslavsky, S. E.; Schattner, K. *Biochemistry* **1987**, *26*, 1418-1422.

(65)   Spiro, T. G. Ed.; In *Biological Applications of Raman Spectroscopy*; Wiley: New York, 1987.

(66)   Fodor, S. P. A.; Lagarias, J. C.; Mathies, R. A. *Photochem. Photobiol.* **1988**, *48*, 129-136.

(67)   (a) Rospendowski, B. N.; Farrens, D. L.; Cotton, T. M.; Song, P.-S. *FEBS Lett.* **1989**, *258*, 1-4. (b)   Farrens, D. L.; Holt, R. E.; Rospendowski, B. N.; Song, P.-S.; Cotton, T. M. *J. Am. Chem. Soc.* **1989**, *111*, 9162-9169.

(68)   (a) Tokutomi, S.; Mizutani, Y.; Anni, H.; Kitagawa, T. *FEBS Lett.* **1990**, *269*, 341-344. (b) Mizutani, Y.; Tokutomi, S.; Aoyagi, K.; Horitsu, K.; Kitagawa, T. *Biochemistry* **1991**, *30*, 10693-10722. (c) Fodor, S. P. A.; Lagarias, J. C.; Mathies, R. A. *Biochemistry* **1990**, *29*, 11141-11146. (d) Sakai, J.; Morita, E. H.; Hayashi, H.; Furuya, M.; Tasumi, M. *Chem. Lett.* **1990**, 1925-1926. (e) Siebert, F.; Grimm, R.; Rüdiger, W.; Schmidt, G.; Scheer, H. *Eur. J. Biochem.* **1990**, *194*, 921-928.

(69)   (a) Spiro, T. G.; Grygon, C. A. *J. Mol. Struct.* **1988**, *173*, 79-90. (b) Asher, S. A. *Ann. Rev. Phys. Chem.* **1988**, *39*, 537-588.

Functional Domains of Pea Phytochrome

intact P   (121 kDa)

large P   (114 kDa)

small P   (62 kDa)

(39 kDa)

Gly-52   Cys-322 Arg-413   Arg-622

H_2N —‖——————————————————— COOH

N-terminal   chromophoric   C-terminal
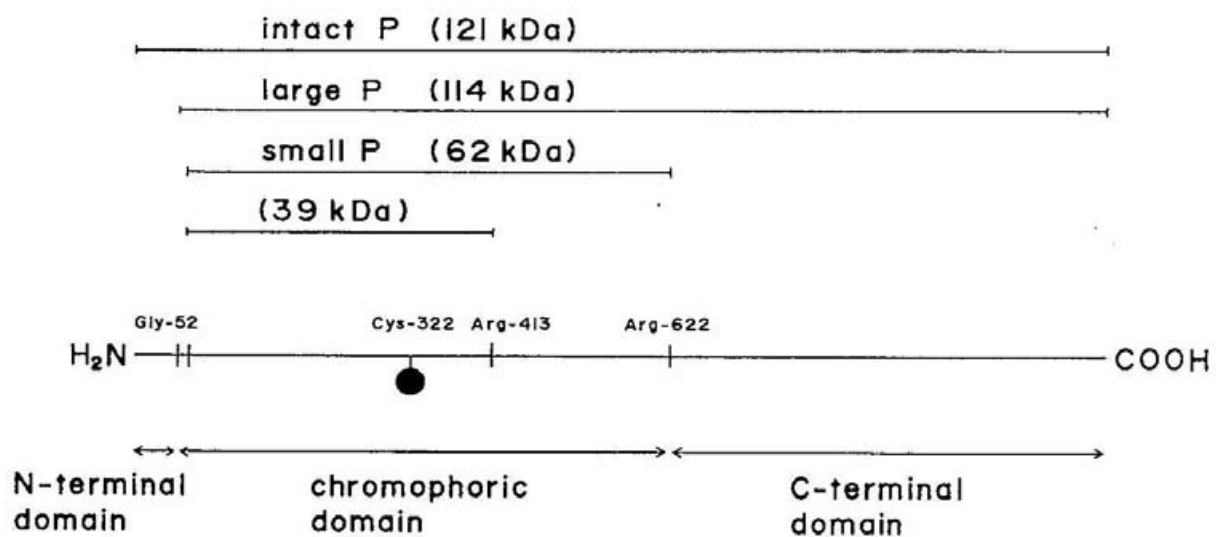domain   domain   domain

Figure I-1. Relative alignment of the 121-kDa, 114kDa phytochrome and its tryptic fragments with the amino acid sequence deduced from the cDNA base sequence of oat phytochrome. A solid circle at Cys-322 denotes phytochrome chromophore.
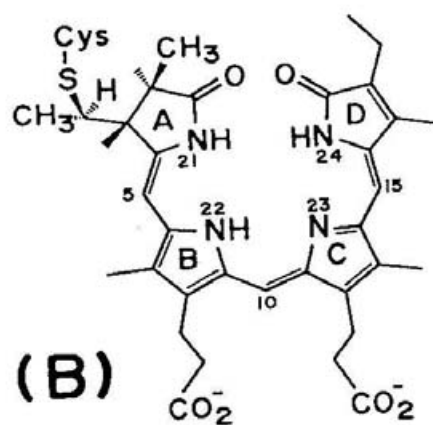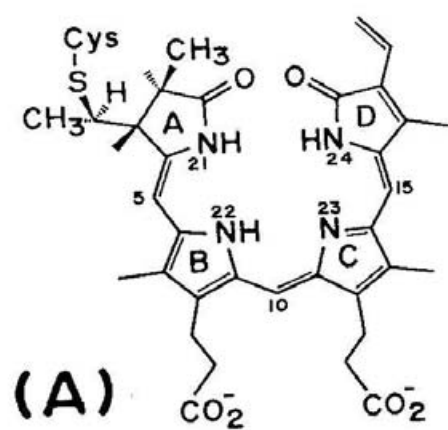
Figure I-2. Comparison of chromophore structure between phytochrome (A) and phycocyanin (B).
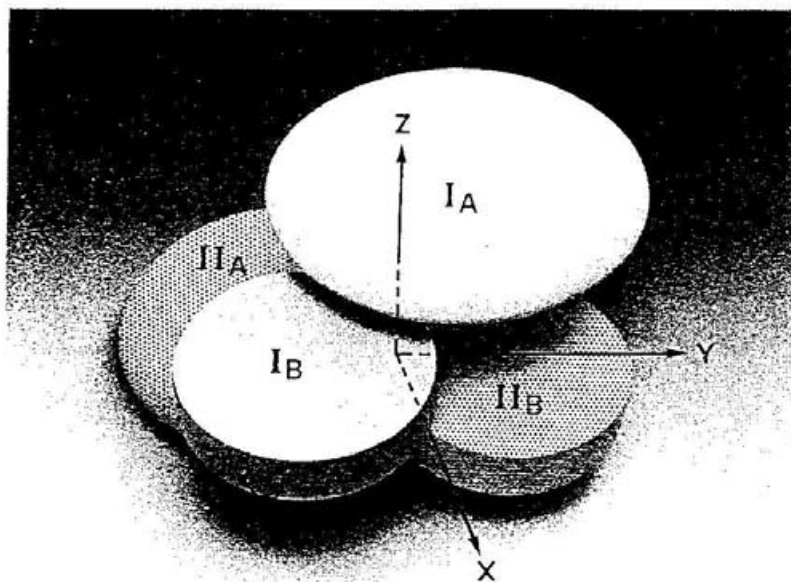
Figure I-3. Domain structure elucidated from SAXS study in P_r (from ref. 48b). The molecule consists of two identical subunits: upper subunit I and lower subunit II (dotted). Each subunit consists of chromophoric domain, A, and C-terminal domain, B. The domains A and B in a subunit are attatched to each other at the edge of the ellipsoidal and flat plane with their rotational axes oriented in pararell. The subunits I and II make contact at the margin of the lower flat plane of I_B and the upper flat plane of II_B with their rotational axes oriented in pararell.

21

Figure I-4. Possible mechanism for the phototransformation of phytochrome based on the isomerization at the 15, 16-C=C bond in the primary photoprocess of P_r (left).
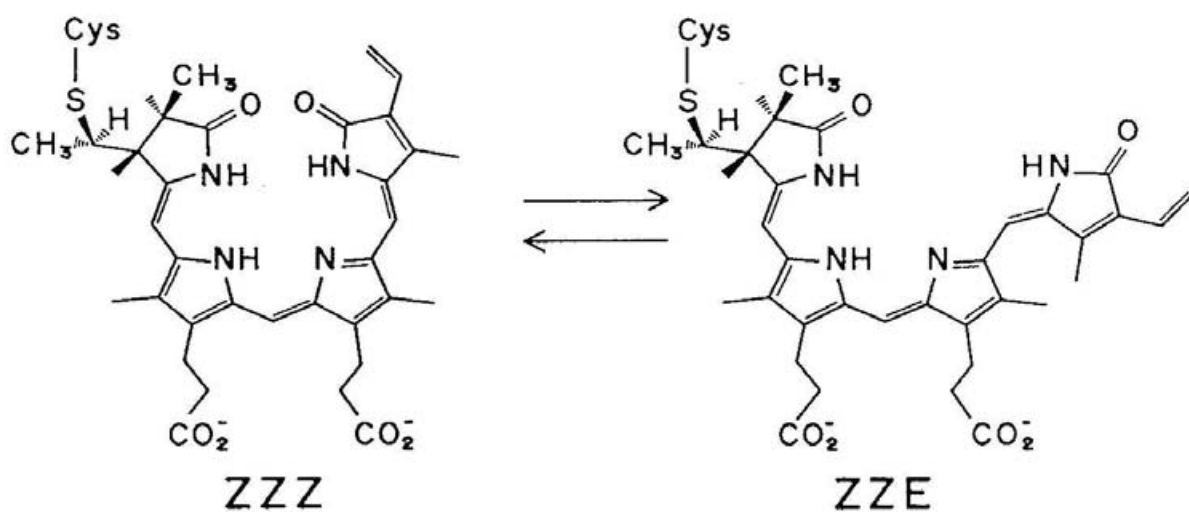
Chapter II

Resonance Raman Studies of Large Pea Phytochrome at Ambient Temperature: Difference in Chromophore Protonation between Red and Far-red Absorbing Forms

Abstract

Resonance Raman (RR) scattering from large pea phytochrome was observed at ambient temperature for the first time by using a micro-spinning cell and the two color excitation technique. The relative population of the red-absorbing form (P_r), the far-red- absorbing form (P_{fr}), and the bleached intermediate (I_{bl}) under laser illumination was estimated from the absorption spectra. The RR spectrum of P_r obtained by the 364 nm excitation under the 740 nm pumping exhibited a frequency shift between the H_2O and D_2O solutions. On the other hand, the RR spectra of P_{fr} and I_{bl} obtained by 407 nm excitation under 633 nm pumping and 364 nm excitation under 633 nm pumping, respectively, did not exhibit such a deuteration shift. This indicates distinct differences in protonation levels between the former and the latter two, presumably in protonation of C-ring.

II-1. Introduction

Phytochrome is a noble photoreceptor chromoprotein in green plants and performs a variety of reversible morphogenetic and developmental responses upon red/far-red light illumination.[1,2] The molecule consists of two identical subunits,[3] with a 2,3-dihydrobiliverdin chromophore in each one.[4,5] It undergoes a photoreversible transformation between a red-absorbing form (P_r) and a far-red-absorbing form (P_{fr}) via intermediates like a bleached form (I_{bl}). Although isomerization of the chromophore[6-8] and proton migration[9-11] have been proposed for the phototransformation and a structure of the chromophore with an undeca-peptide from P_r was determined by NMR spectroscopy,[5] the chromophore structures in the P_r and P_{fr} proteins have not been clarified yet.

Resonance Raman (RR) spectroscopy is a powerful technique for studying the structure of chromophores in chromoproteins.[12] However, application of this technique to phytochrome had long been unsuccessful due to its intense fluorescence. Recently RR spectra of oat phytochrome in the P_r form were obtained at 77K with far-red excitation[13,14] and also a surface enhanced resonance Raman (SERR) study of oat phytochrome was reported with blue excitation.[15-17] However, in order to obtain information on structural differences between the two phytochrome forms, it is indispensable to observe the RR spectra of the P_r and P_{fr} forms in a natural state at ambient temperature. Accordingly, we have studied the RR spectra of phytochrome in a natural state by using a two-color excitation technique and report here the blue excited RR spectra of the P_r and P_{fr} forms of large pea phytochrome at 288K for the first time. We propose that the P_r and P_{fr} forms have different protonated structures.

II-2. Experimental Section

Phytochrome Preparation. Large pea phytochrome was isolated according to the reported method[19], precipitated by ammonium sulfate [$(ND_4)_2SO_4$ in D_2O for the deuterated preparation] and resuspended in 50 mM HEPES and 1 mM Na_2EDTA, pH 7.8 to a final concentration of 8.0 cm^{-1} in terms of A_{667} ($\epsilon_M = 1.3 \times 10^5$ cm^{-1}). The solution was dialyzed for complete removal of ammonium sulfate. The stable bleached form, P_{bl}, was prepared by the following way: after pH of the solution of large phytochrome resuspended in 50 mM CHES and 1 mM Na_2EDTA was raised from pH 9.0 to 11.0 by the addition of 5M NaOH, the red light was irradiated and, then, pH of the solution was lowered to pH 9.0 by the addition of 5M HCl.

RR measurements. Figure II-1 schematically shows the RR measurement system used in this study. RR spectra were measured for 50 μL of the phytochrome preparation in a micro spinning-cell at 1600 rpm, kept at 288 ± 3 K by flushing with cold N_2 gas, and detected by a photodiode array (PAR 1420) attached to a Spex 1404 double monochromator. Raman scattering was excited at 407 nm (Kr$^+$ laser) or 364 nm (Ar$^+$ laser) under continuous illumination to another spot of the cell at 740 nm (Ti-doped sapphire laser) or at 633 nm (He/Ne laser) to bias the equilibrium in photosteady state toward either P_r or P_{fr}, respectively. However, in the photosteady state under double laser illumination, the third component[19,20], which was previously demonstrated to have an absorption spectrum close to that of the bleached form and is considered to be the same as I_{bl}[21], was appreciably present besides P_r and P_{fr}. The relative population of P_r, P_{fr}, and I_{bl}, under double laser illumination was estimated separately from visible absorption spectra[22] that were measured by irradiating the continuously stirred sample solution in the sample compartment of a spectrophotometer (Shimadzu UV-240) with the two laser beams. RR measurements at low temperature were performed by using a cryostat which was cooled by cold nitrogen gas. After the double laser experiments the sample was confirmed to preserve its original photoreversibility and showed no degradation or aggregation products in SDS polyacrylamide gel electrophoresis patterns. The sensitivity differences of individual elements of the diode-array detector was corrected through measurements of white light. The background due to fluorescence was removed by polinominal subtraction.

II-3. Results and Discussion

RR spectra of phytochrome observed upon excitation at 364 nm are depicted in Figure II-2. The left and right columns are for H_2O and D_2O solutions, respectively. The top (A and A') and the middle spectra (B and B') were obtained under far-red and red-light illumination, respectively, and the bottom ones (C and C') are the difference between them. The 1625/1618 cm^{-1} and 1599 cm^{-1} bands are assignable to P_r and I_{bl}, because the main component under 740 nm and 364 nm illumination (top spectra) are P_r (66%) and I_{bl}(29%) and, among P_r, I_{bl} and P_{fr}, the former two have the second absorption band around 380 nm. Moreover, since the 1599 cm^{-1} band is intensified in comparison with the 1625/1628 cm^{-1} band by red light illumination, it is most plausible to assign the 1625/1618 cm^{-1} to P_r and the 1599 cm^{-1} to I_{bl}.

In order to confirm the assignments, RR spectra of phytochrome at low temper-

26

ature and P_{bl} were measured. The RR spectra of large phytochrome at low temperature are shown in Figure II-3. Spectra A and B were obtained at -120 and -80°C, respectively. Since I_{700}, which is the first photointermediate so far identified, can not be converted to I_{bl} at -120°C, the components in a sample solution are considered to be P_r and I_{700}. At this temperature the 1599 cm^{-1} band is not observed, although 1625 cm^{-1} band and an additional band at 1648 cm^{-1} are clearly seen. Upon raising temperature to -80°C, where thermal conversion from I_{700} to I_{bl} proceeds, a shoulder band at 1597 cm^{-1} appears and the 1648 cm^{-1} band decreases. Therefore the appearance of the 1599 cm^{-1} band is associated with the formation of I_{bl}.

Figure II-4 shows the RR spectra of P_{bl}, where spectra A and B are obtained for H_2O and D_2O solutions, respectively. Spectra 4A and 4B closely resemble spectra 2C and 2C', respectively, indicating that the component which increases its population under red-light illumination has a chromophore structure similar to P_{bl}. Slight frequency differences between spectra 4A (4B) and 2C (2C') indicate the difference between P_{bl} and I_{bl}. Accordingly, the 1625/1618 and the 1599 cm^{-1} bands in Figure II-2 are reasonably assigned to P_r and I_{bl}, respectively. Note that the most prominent band of P_r shows deuteration shift of -7 cm^{-1}, whereas those of I_{bl} and P_{bl} at 1599 cm^{-1} do not. The deuteration shift of P_r coincides with a previous finding by Fodor et al. that the RR band of oat P_r at 1626 cm^{-1} exhibited a downshift by 5 cm^{-1} in D_2O.

RR spectra of the red-light illuminated phytochrome observed upon excitation at 407 nm are depicted in Figure II-5, and the relative populations of P_r, P_{fr} and I_{bl} are described in the figure caption. Under red light illumination, where the main component is I_{bl} (44% at pH 7.8),[21] two prominent RR bands are observed at 1630 and 1590 cm^{-1}. It is noted that the spectral pattern for the D_2O solution at pD 7.8 (spectrum B) also resembles that of the H_2O solution (spectrum A). These RR spectra cannot be ascribed to P_r because of its negligible population in spectrum (C). It is unreasonable to ascribe these RR spectra to I_{bl} because two prominent bands at 1631 and 1591 cm^{-1} are not observed in Figures II-2C and -2C', where remaining bands in the difference calculation are assigned to I_{bl}. Therefore, we assign the 1631 and 1591 cm^{-1} bands to P_{fr}. Selective enhancement of RR bands of P_{fr} is likely to happen, since the absorbance of P_{fr} at 407 nm is twice larger than those of P_r and P_{bl}[22].

The deuteration shift of Raman band was observed for P_r under 364 nm excitation (see Figure II-2). This fact strongly suggests that the protonation state of C-ring is different in P_{fr} and P_r. No deuteration shift of the Raman band was recognized in I_{bl}

as well as P_{fr}, suggesting that the protonation level of I_{bl} is the same as that of P_{fr}. It was reported previously that there is no net gain and loss of protons between P_r and P_{fr} as a whole molecule of large pea phytochrome, and no net gain and loss of protons suggested that proton release and uptake of phytochrome occurs in the process $P_r \rightarrow I_{bl}$ and $I_{bl} \rightarrow P_{fr}$, respectively.[11] The difference in the protonation level is possibly related to a proton release of the large pea phytochrome during the phototransformation process from P_r to the bleached intermediate[23,24]. Several studies on the photoreaction kinetics of intact oat phytochrome have revealed that proton translocation is not involved in the primary process, *i.e.* $P_r \rightarrow I_{700}$. Therefore, proton migration should occur in the process of $I_{700} \rightarrow I_{bl}$. This result also suggests that an absorption spectral change between I_{700} and I_{bl} detected at low temperatures[28] arises from deprotonation of C-ring. The protonation/deprotonation scheme for pea large phytochrome speculated from this study is drawn in Figure II-6. In order to discuss the chromophore structure, including the protonation structure, a time-resolved RR study is desirable in a further study.

In SERR spectra of phytochrome adsorbed on Ag sol,[15,17] the most intense RR band upon 413.1 nm excitation appears at a lower frequency for P_{fr} (1591 cm^{-1}) than for P_r (1615 cm^{-1}), in a qualitative agreement with the present results. However, since the reported SERR spectra of P_{fr} on the Ag electrode and Ag sol are significantly different with each other and also from the present spectra, discussion on differences in absolute frequencies between the SERR and present spectra would not be fruitful at this moment.

References

(1)   Kendrick, R. E; Kronenberg, G. H. M. Ed. In *Photomorphogenesis in Plants*; M. Nijhoff, Dordrecht, 1986.

(2)   Furuya, M. Ed. In *Phytochrome and Photoregulation in Plants*; Academic Press, Tokyo, 1987.

(3)   Tokutomi, S.; Nakasako, M.; Sakai, J.; Kataoka, M.; Yamamoto, K. T.; Wada, M.; Tokunaga, M.; Furuya, M. *FEBS Lett.* **1987**, *247*, 139-142.

(4)   Grombein, S.; Rüdiger, W.; Zimmermann, H. R. *Z. Physiol. Chem.* **1975**, *356*, 1709-1714.

(5)   Lagarias, J. C.; Rappoport, H. *J. Am. Chem. Soc.* **1975**, *102*, 4821-4828.

(6)   Rüdiger, W.; Thümmler, F.; Cmiel, E.; Schneider, S. *Proc. Natl. Acad. Sci. U.S.A.* **1983**, *80*, 6244-6248.

(7)   Thümmler, F.; Rüdiger, W. *Tetrahedron* **1983**, *39*, 1943-1951.

(8)   Rüdiger, W.; Eilfeld, P.; Thümmler, F. In *Optical Properties and Structure of Tetrapyrroles*; Blauer, G., Sund, H. Eds.; Walter de Gruyter: Berlin, New York, 1985; pp. 349-369.

(9)   Sarkar, H. K.; Song, P.-S. *Biochemistry* **1981**, *20*, 4315-4320.

(10)   Moon, D.-K.; Jeen, G.-S.; Song, P.-S. *Photochem. Photobiol.* **1985**, *42*, 633-641.

(11)   Tokutomi, S.; Yamamoto, K. T.; Furuya, M. *Photochem. Photobiol.* **1988**, *47*, 439-445.

(12)   Spiro, T. G. Ed. In *Biological Applications of Raman Spectroscopy*, Wiley, New York, 1987.

(13)   Fodor, S. P. A.; Lagarias, J. C.; Mathies, R. A. *Photochem. Photobiol.* **1988**, *48*, 129-136.

(14)   Fodor, S. P. A.; Lagarias, J. C.; Mathies, R. A. *Photochem. Photobiol.* **1989**, *49s*, 63s.

(15)   Rospendowski, B. N.; Farrens, D. L.; Cotton, T. M.; Song, P.-S. *FEBS Lett.* **1989**, *258*, 1-4.

(16)   Holt, R. E.; Farrens, D. L.; Song, P.-S.; Cotton, T. M. *J. Am. Chem. Soc.* **1989**, *111*, 9156-9162.

(17)   Farrens, D. L.; Holt, R. E.; Rospendowski, B. N.; Song, P.-S.; Cotton, T. M. *J. Am. Chem. Soc.* **1989**, *111*, 9162-9169.

(18)   Large pea P was prepared from 7 day-old etiolated seedlings of pea (*Pisum sati-*

vum cv. Alaska) as described in Tokutomi, S.; Kataoka, M.; Sakai, J.; Nakasako, M.; Tokunaga, F.; Tasumi, M.; Furuya, M. *Biochim. Biophys. Acta*, **1985**, *953*, 297-305. The specific absorbance ratio (A_{667}/A_{280}) of the present sample was 0.98. Its purity was estimated to be more than 95% as judged from the SDS polyacrylamide gel electrophoresis.

(19) Pratt, L. H. *Photochem. Photobiol.* **1975**, *21*, 99-103.

(20) Yamamoto, K. T.; Smith, W. O., Jr. *Plant Cell Physiol.* **1985**, *22*, 1149-1158.

(21) Tokutomi, S.; Inoue, Y.; Sato, N.; Yamamoto, K. T.; Furuya, M. *Plant Cell Physiol.* **1986**, *27*, 765-773.

(22) The absorption spectra of the large phytochrome measured under double laser illumination can be simulated by digital addition of the spectra of P_r, P_{fr} and I_{bl}. As the spectrum of P_{fr}, the spectrum of oat intact phytochrome calculated by Rüdiger and Eilfeld (in reference 2, p.18) was used by shifting the absorption maximum from 730 to 724 nm. The spectrum of I_{bl} was regarded as the same as that of P_{bl} obtained for an alkaline solution of the pea phytochorme after red light illumination. The relative populations of each component were calculated by solving three simultaneous linear equations set up for the absorptions at three different wavelengths.

(23) Brock, H.; Ruzsicka, B. P.; Arai, T.; Schlamann, W.; Holtzwarth, A. R.; Braslavsky, S. E.; Schaffner, K. *Biochemistry* **1987**, *26*, 1412-1417.

(24) Aramendía, P. F.; Ruzsicska, B. P.; Braslavsky, S. E.; Schattner, K. *Biochemistry* **1987**, *26*, 1418-1422.

(25) (a) Thümmler, F.; Rüdiger, W. *Physiol. Plant.* **1984**, *60*, 376-382. (b) Thümmler, F.; Rüdiger, W. *Physiol. Plant.* **1984**, *60*, 383-388.
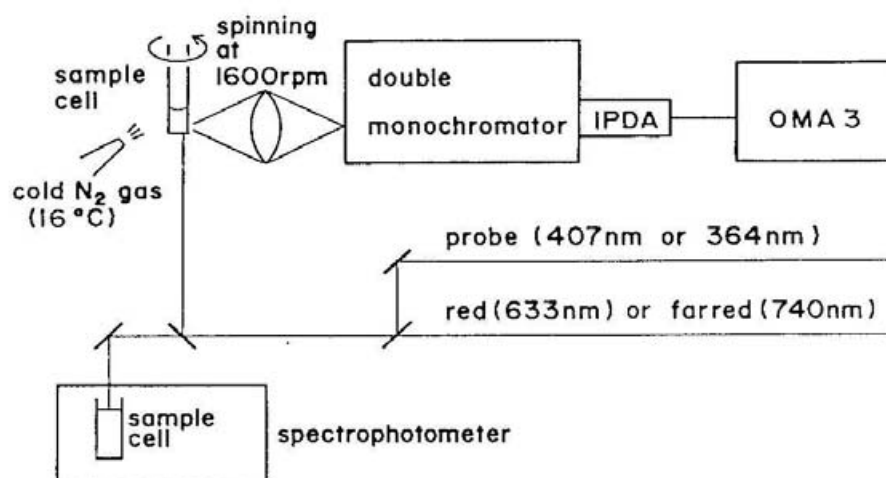
MEASUREMENT SYSTEM

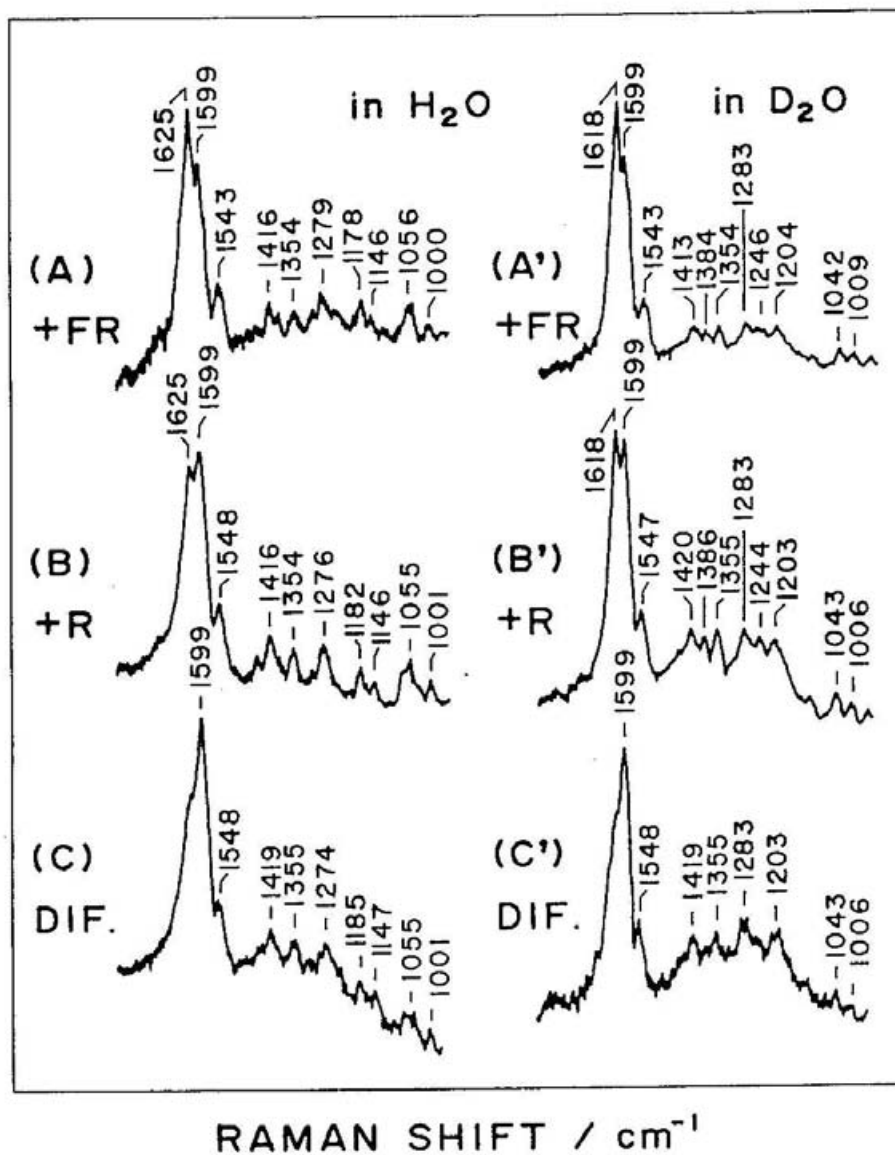**Figure II-1.** Diagram of RR measurement system.

Figure II-2. RR spectra of large pea phytochrome under far-red light illumination (740.0 nm) at pH 7.8 in H$_2$O (left column) and in D$_2$O (right column). Excitaion, 364 nm. Spectra (A) and (A') were obtained under far-red light illumination and spectra (B) and (B') were obtained under red light illumination. Spectra (C) and (C') are differences calculated so as not to generate negative peaks.
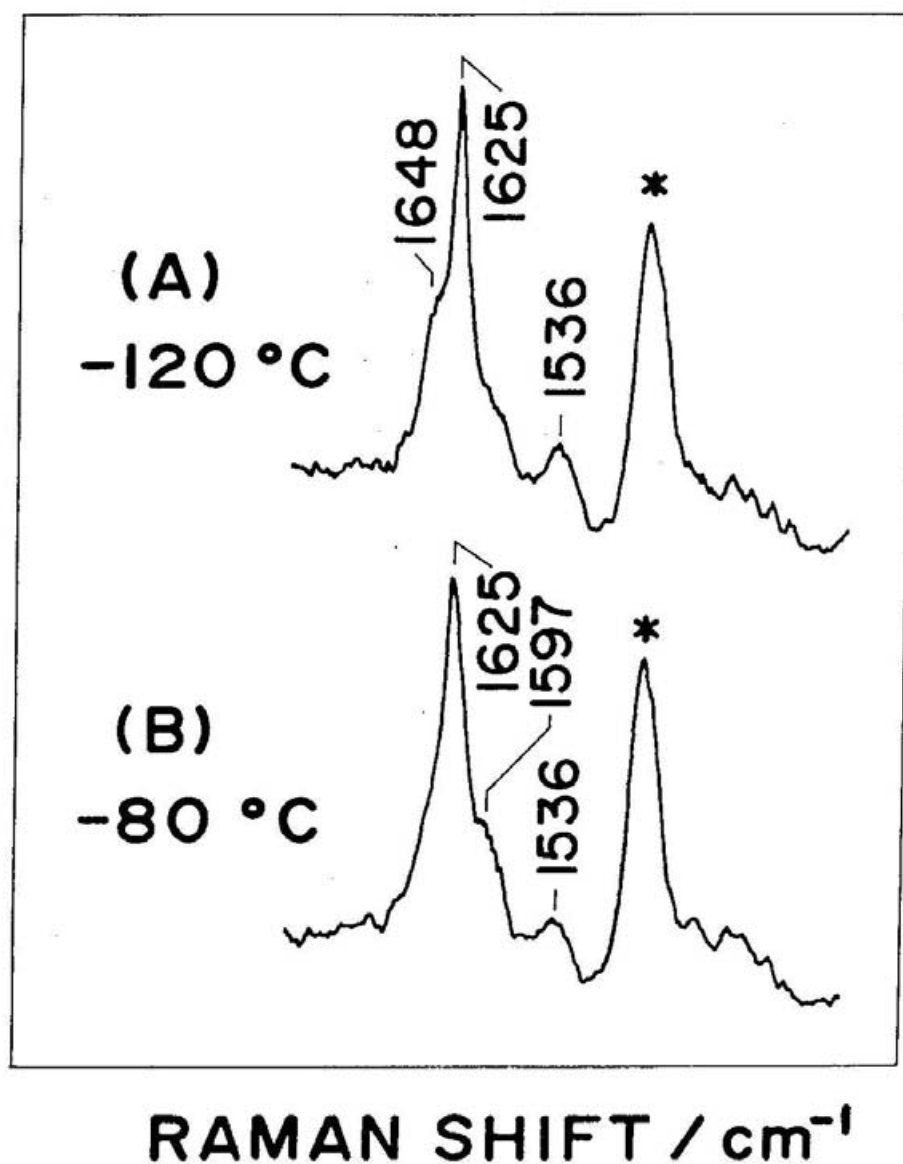
32

Figure II-3. RR spectra of large pea phytochrome under red light illumination (633 nm) at low temperature. (A): -120°C; (B): -80°C. Large pea phytochrome was resuspebded in 50 mM HEPES and 1 mM Na₂EDTA, pH 7.8, diluted with glycerol (final concentration 66% (v/v)). Excitation, 364 nm. The bands marked by asterisk are due to glycerol.
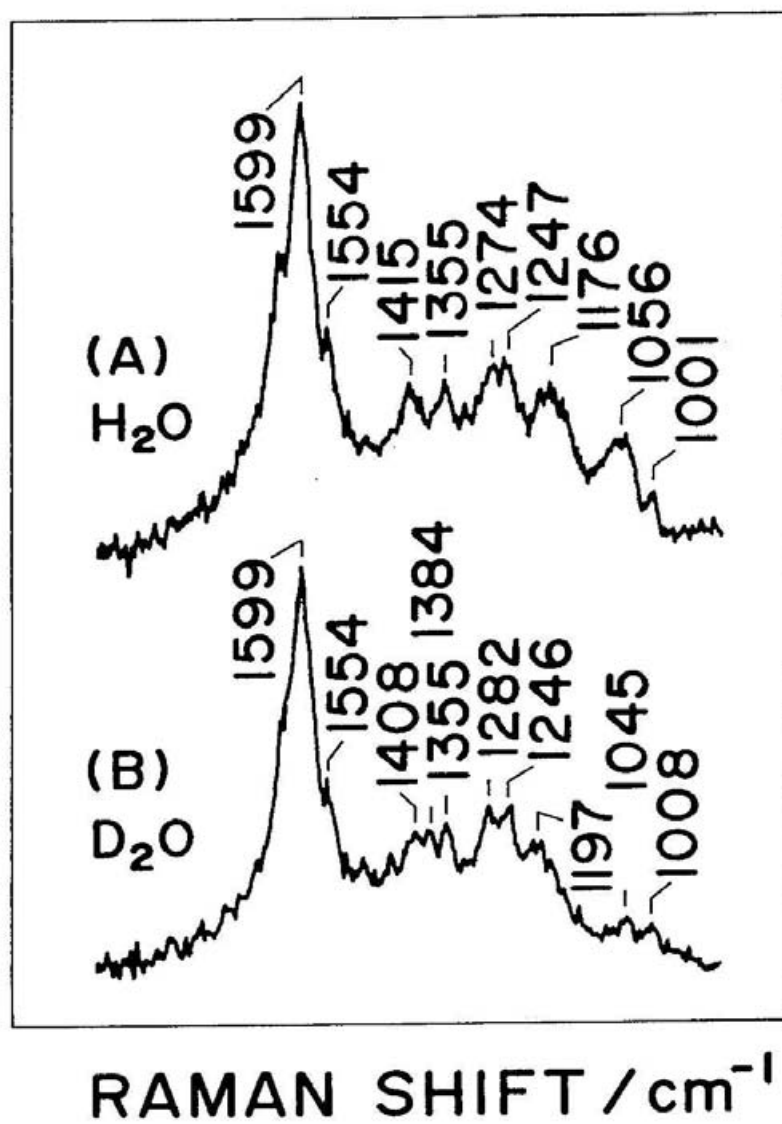
33

Figure II-4. RR spectra of P_{bl} of large pea phytochrome in H_2O solution (A) and D_2O solutions (B). Excitation, 364 nm. Spectra were obtained under red light illumination.

34
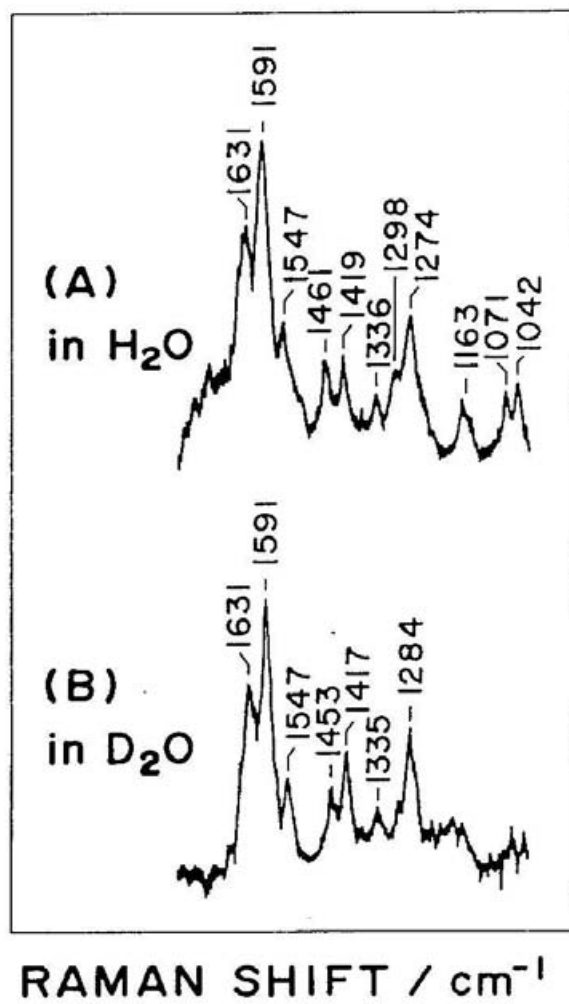
Figure II-5. RR spectra of large pea phytochrome under red light illumination (633 nm) at pH 7.8 in H₂O (A) and at pD 7.8 in D₂O (B). Excitation, 407 nm. Relative populations of P_r, P_{fr} and I_{bl} under individual illumination conditions are as follows; P_r 20%, P_{fr} 36%, I_{bl} 44% for (A); P_r 18%, P_{fr} 32%, I_{bl} 50% for (B).
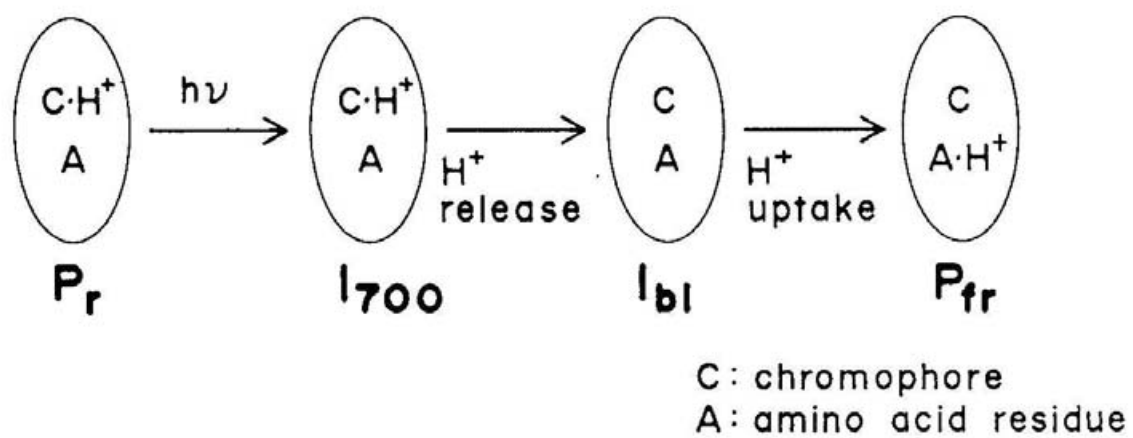
model of the phototransformation

Figure II-6. Proposed model for the phototransformation of phytochrome.

Chapter III

Resonance Raman Studies on Intact Pea Phytochrome
and Its Model Compounds:
Evidence for Proton Migration during the Phototransformation

Abstract

Resonance Raman (RR) scattering from intact pea phytochrome was observed in resonance with the blue band at ambient temperature. The relative populations of the red absorbing form (P_r) and far-red absorbing form (P_{fr}) under laser illumination were estimated from the absorption spectra. The most prominent RR band of P_r obtained by 364-nm excitation under 740-nm pumping exhibited a frequency shift between H_2O and D_2O solutions, but that of P_{fr} obtained by 407-nm excitation under 633-nm pumping did not. The results indicated a distinct difference in a protonation state of their chromophores. Since the protonation level of a whole molecule of intact phytochrome remains unchanged between P_r and P_{fr}, this observation indicates migration of a proton from the chromophore of P_r to the protein moiety of P_{fr}. As model compounds of the chromophore octaethylbiliverdin (OEBV-h_3), its deuterated and ^{15}N derivatives, and their protonated forms were also studied with both RR and ^1H- and ^{15}N-NMR spectroscopies. The RR spectrum of the protonated form, for which the protonation site was determined to be C-ring pyrrole nitrogen by NMR, displayed a deuteration shift similar to that of P_r. This result suggested a similar protonated structure for the pyrrolic rings of P_r. The RR spectral difference between OEBV-h_3 and OEBV-d_3 and that between H_2O and D_2O solutions of P_{fr} suggested that the N-H protons of the A-, B- and D-rings of intact phytochrome are replaced with deuterons in D_2O. A role of the 7 kDa segment of phytochrome is discussed on the basis of RR spectral differences between the intact and large phytochromes.

III-1. Introduction

Phytochrome is a chromoprotein which acts as a photoreceptor for a variety of light-triggered morphogenetic responses in green plants.[1,2] The chromoprotein has two distinct spectral forms called a red absorbing form (P_r) and a far-red absorbing form (P_{fr}), which are interconvertible by illumination with red and far-red light, respectively. The chromoprotein has recently been shown to have two isoforms, named types I and II depending on the light sensitivity of their quantity in tissues.[3] The type I phytochrome used in this study consists of two identical subunits with an N-terminal chromophoric and a C-terminal nonchromophoric domains,[4] the former contains a 2,3-dihydrobiliverdin chromophore[5,6]. The tetrapyrrole chromophore is thought to be deprotonated at C-ring as shown in Figure III-1a, although it has not been established yet.

The type I phytochrome is biosynthesized in the biologically inactive form (= P_r) in the dark, and is transformed to the active form (= P_{fr}) upon red-light illumination, which triggers physiological responses in green plants. The molecular mechanism by which phytochrome regulates a great diversity of morphogenetic responses is still obscure. To understand it, elucidation of the primary process ($P_r \rightarrow P_{fr}$) of the light signal transduction is quite important. So far, the Z,Z,Z to Z,Z,E configurational changes in the tetrapyrrole chromophore[7-10] and/or proton migration[11,12] have been proposed as the chemical event in the P_r to P_{fr} phototransformation. Evidence for a light-induced conformational change in the protein moiety have also been presented by several groups.[13-15] In order to know further details of the photoreaction mechanism, it is requisite to explore the structural differences between P_r and P_{fr} and to relate these changes to the physiological function.

Resonance Raman (RR) spectroscopy is a powerful technique for studying the structure of chromophore in chromoproteins.[16] Since Raman excitation in resonance with the first absorption band of P_r brings about intense fluorescence background, the RR technique had not been successfully applied to phytochrome until Fodor et al.[17] measured the RR spectra of oat intact phytochrome at 77 K by using far-red-light excitation to avoid much of the inherent fluorescence. Song and his coworkers have employed surface enhanced resonance Raman spectroscopy (SERRS) using silver colloids as the adsorbing substrate.[9,18] In both studies, the sample solutions were frozen, which might cause possible changes in its tertiary and/or quaternary structures and moreover, SERRS may be suffered from a possible structural change of the pro-

tein which is induced by the adsorption onto the substrate.

In order to study the structural changes of the chromophore accompanied by phototransformation, it is highly desirable to observe the RR spectra of phytochrome in a natural state at an ambient temperature. Accordingly, we adopted Soret excitation of Raman scattering to avoid the interference by fluorescence and the two-color excitation technique to modulate the population of either P_r or P_{fr} under the photosteady state and successfully measured the RR spectra of the "large" pea phytochrome, which lacks amino acid residues corresponding to 7 kDa from the "intact" form,[19] in a solution at 16 °C for the first time[20].

Recently Siebert et al.[21] applied FT-IR spectroscopy to phytochrome and its model compounds, pointing out that both P_r and P_{fr} are protonated contrary to our results on large phytochrome.[20] Furthermore, Fodor et al.[10] observed far-red-excited RR spectra of P_{fr} at room temperature and concluded that P_{fr} is protonated. Therefore, we examined the protonation problem with intact phytochrome and report here the Soret excited RR spectra of the P_r and P_{fr} forms of intact pea phytochrome at 16 °C, which demonstrates that P_r and P_{fr} have different protonated structures similar to the case of the large pea phytochrome. Based on the present observations and earlier results about the light-induced proton release and uptake by pea phytochromes[12], possible proton migration during the phototransformation is deduced. In addition, we specify the protonation site in the chromophore from the structural studies on the model compounds, octaethylbiliverdin. Its structure and numberings of pyrrole rings and atoms are illustrated in Figure III-1b, where the deprotonated pyrrole ring is tentatively defined as C-ring.

III-2. Experimental Section

Phytochrome Preparation. Intact pea phytochrome consisting of two subunits with M_r of 121 kDa (determined by SDS PAGE) was isolated from 7-day-old etiolated seedlings of pea (*Pisum sativum* cv. Alaska) as described previously.[22] The protein was precipitated by ammonium sulfate [$(ND_4)_2SO_4$ in D_2O for the deuterated preparation] and resuspended in 50 mM HEPES and 1 mM Na_2EDTA, pH 7.8 (D_2O was used for the deuterated preparation). The solution was then dialyzed for complete removal of ammonium sulfate. All the preparation procedures were carried out under dark or dim green light. The specific absorbance ratio (A_{667}/A_{280}) of the present sample was 0.90 and its purity was estimated to be higher than 95% from SDS PAGE.

Synthesis of Model Compounds. Octaethylbiliverdin (OEBV-h_3) and its ^{15}N-derivative (OEBV-$^{15}N_4$-h_3) were synthesized from octaethylporphyrinatoiron(III) chloride [(OEP)Fe^{III}Cl] and its ^{15}N-derivative, respectively, according to the reported method[23,24] with some modifications about reaction temperature, time, and pH, which raised the yield from 5% to 35%. The N-deuterated form of octaethylbiliverdin (OEBV-d_3) was obtained by mixing a small amount D_2O with the $CHCl_3$ solution of OEBV-h_3. Protonation of OEBV-h_3 (or -d_3) was accomplished by adding 1 M HCl (or DCl) to the $CHCl_3$ solution of OEBV-h_3 (or -d_3) according to the procedures described by Margulies and Stockburger.[25]

Measurements of RR Spectra. Fifty microliters of the phytochrome solution with the concentration of 8.0 cm^{-1} in terms of A_{667} in the P_r form, which corresponds to 61 μM on the basis of $\epsilon_M = 1.32 \times 10^5$ cm^{-1} for the intact oat phytochrome,[26] was put into a micro spinning-cell (diameter = 5 mm, 1600 rpm) and kept at 16±3 °C by flushing with cold N_2 gas. RR scattering was excited by the 407 nm line of a Kr$^+$ ion laser (Spectra Physics, Model 2016) or the 364 nm line of an Ar$^+$ ion laser (Spectra Physics, Model 2045), dispersed with a double monochromator (SPEX 1404), and detected with a diode array detector with an image intensifier (PAR 1421HQ). The data were processed with an OMA III system (PAR 1460). The Raman spectra were calibrated with indene for each excitation line, and errors in band positions for well defined peaks are ±2 cm^{-1}. The differences in sensitivity of individual pixels of the diode-array detector were corrected by the white light: the observed spectra were divided by the spectrum of white light. The background due to fluorescence was removed by subtraction of the curve generated by a suitable polinominal function.

The sample solution in the spinning cell was illuminated with either far-red (740 nm) or red (633 nm) light at another spot during the blue light excitation in order to bias the equilibrium of the photo-steady state toward P_r or P_{fr}, respectively. The illuminating spot of the red (or far-red) light was located at the downstream side of the blue-light illuminating spot of the spinning cell and the two spots were placed as close as possible for making the interval after the red (or far-red) light illumination longest in one turn of the cell. The far-red light was generated by a Ti-doped sapphire laser (Spectra Physics, Model 3900) pumped by an Ar$^+$ ion laser (Spectra Physics, Model 164). The red light was generated by a He/Ne laser (NEC GLS5800).

To estimate the relative population of P_r and P_{fr} under the photo-steady state attained by double laser illumination, the absorption spectra of the phytochrome solu-

tions with concentrations from 15 to 23 μM were measured under the same illumination conditions as used for measurements of RR spectra; the two laser beams were introduced to a magnetically stirred sample solution in the cuvette placed in a spectrophotometer (Shimazu, UV240). It was confirmed that the sample preserved its original photoreversibility and gave no degradation or aggregation products in the SDS PAGE patterns after the double laser illumination experiments. The absorption spectrum of P_r was measured after saturating irradiation with far-red light. The spectrum of P_{fr} was determined by subtracting the spectrum of P_r from that observed after saturating irradiation with red light, in which it was assumed that the red light irradiated pea intact phytochrome is composed of 84% of P_{fr} and 16% of P_r based on the method reported by Vierstra and Quail.[27]

Measurements of NMR Spectra. The 400 MHz ^{1}H- and 40.5 MHz proton-decoupled ^{15}N-NMR spectra were observed with a JEOL JNM GX400 pulse Fourier transform NMR spectrometer. The chemical shifts were measured downfield in ppm relative to Si(CH$_3$)$_4$ for ^{1}H nuclei and to 2.9 M ^{15}NH$_4$Cl dissolved in 1M HCl for ^{15}N as a standard.[28] The pulse width and pulse delay were 13 μs and 2s, respectively, for ^{15}N nuclei.

III-3. Results

Since P_r and P_{fr} of the intact pea phytochrome have the second absorption band around 380 and 410 nm, respectively, the excitation of Raman scattering at 364 and 407 nm is expected to selectively enhance the intensity of Raman bands of P_r and P_{fr}, respectively. However, as the wavelength of the probe light of Raman scattering approaches to the absorption maximum, the probe light would increasingly induce the photoreaction, although the light intensity is made as low as possible, and we might observe the photoreacted species after several turns of the spinning cell. In order to circumvent this problem, the sample was illuminated with the second laser (pump beam). The effects of the second laser illumination was examined with the spectra of intact phytochrome excited at 407 nm, as illustrated in Figure III-2, where three spectra were observed under the same conditions except for illumination of the second laser, and are represented in a common scale. Spectrum B was obtained without the pump beam. Upon red-light illumination (spectrum A) the intensity of Raman scattering was enhanced by a factor of 1.3 without a change of the spectral pattern. This is consistent with the population increase of P_{fr} upon red-light illumination in the pho-

42

tosteady state determined by the absorption spectroscopy. Upon far-red-light illumination, on the other hand, those bands became weaker and the relative intensities were slightly altered as shown by spectrum C. Therefore, it is reasonable to assign the bands intensified by red-light illumination to P_{fr}.

Figures III-3 and -4 show the RR spectra of intact pea phytochrome excited at 407 nm under red light (633nm) illumination and at 364 nm under far-red light (740nm) illumination, respectively (A, H_2O solution; B, D_2O solution). The RR spectra of large pea phytochrome in H_2O observed previously under the same conditions as this measurement[12] are also displayed by spectra C for comparison. The RR spectral pattern of the intact phytochrome (A) resembles that of the large phytochrome (C), except for the presence of a band at 1356 cm^{-1} in the spectrum of P_{fr} (Figure III-3A).

The spectra in Figures III-3 and III-4 arise from a photo-steady state mixture of phytochrome generated by two laser illuminations. The visible absorption spectra of the large pea phytochrome observed under the two-color excitation were well simulated by the weighted sum of the spectra of P_r, P_{fr} and I_{bl}, in which I_{bl}, the bleached intermediate, was accumulated under red-light illumination.[20,29] The absorption spectra of the intact pea phytochrome under the two-color excitation, however, can be well reproduced by the weighted sum of the spectra of only P_r and P_{fr}. This coincides with the observation that I_{bl} is hardly accumulated with the pea intact phytochrome under red- light illumination.[29] The relative populations of P_r and P_{fr} under the double laser illumination in this experiment are described in the figure captions. When the sample was illuminated with either red or far-red light in addition to with the blue light, the population of P_{fr} or P_r, respectively, increased 1.3-2 times similarly to the case of the large phytochrome.

Major RR bands of the large phytochrome in Figure III-3C were previously assigned to P_{fr} judging from the relative populations of the three components present under the double laser illumination.[12] This supports to attribute the spectra in Figures III-3A and -3B to P_{fr}. The RR spectrum of large phytochrome shown in Figure III-4C was attributed to the mixture of P_r and I_{bl} and the 1625 and 1599 cm^{-1} bands were ascribed to P_r and I_{bl}, respectively. In a similar way, the 1626/1621 (Figure III-4A) and 1599 cm^{-1} (Figure III-4B) bands can be assigned to P_r and I_{bl}, respectively. Although the relative population of I_{bl} estimated from the absorption spectra under double laser illumination in this experiment is negligible, the bands which are attrib-

43

utable to I_{bl} were observed. Since the diameters of the cell and the laser beam were ca. 5 mm and 100 μm, respectively, the transit time of a given molecule across the laser beam was about 240 μs. Because I_{bl} rises at ca. 20 μs after P_r absorbs light, the observed I_{bl} is considered to be the photoreacted species within the transit time, but it would not be an accumulated one.

In Figure III-4A, the most prominent Raman band of P_r is observed at 1626 cm^{-1} and exhibits a downshift to 1621 cm^{-1} upon deuteration (B). A similar deuteration shift was observed for the large phytochrome at the same excitation conditions as this experiments[12] and for oat phytochrome with far-red excitation at 77K.[17] In contrast, the RR spectra of P_{fr} shown in Figure III-3 give distinct features; although none of double-bond stretching RR bands around 1550-1650 cm^{-1} shows deuteration shift similar to the case of the large phytochrome,[12] the RR bands at 1460 and 1420 cm^{-1} in H_2O downshift to 1453 and 1417 cm^{-1} in D_2O, respectively and the band at 1275 cm^{-1} in H_2O upshifts to 1281 cm^{-1} in D_2. All these observations suggest that the protonation structures of the chromophores of P_r and P_{fr} are different.

Although the 1626/1621 cm^{-1} and 1599 cm^{-1} bands in Figures III-4A and -4B, respectively, are in proximity, the accurate wavenumbers were determined by the deconvolution calculations of these bands. The 1597 cm^{-1} in Figure III-4A, which was attributable to I_{bl}, did not show a deuteration shift. This suggests that the protonation structure of the I_{bl} chromophore is different from P_r but is close to P_{fr}.

Figure III-5 shows the absorption spectra of OEBV-h_3 (solid line) and its protonated form (OEBV-h_4^+) in $CHCl_3$ (broken line). The absorption spectrum of OEBV-h_3 gives a broad and weak band centered at 643 nm and a strong band at 369 nm. Upon addition of 1M HCl, the absorption maximum of the red band shifted to 664 nm with a new band centered at 714 nm and the overall absorption intensity increased. The 369 nm band also slightly shifts to 366 nm. These spectral changes were accompanied by the existence of an isosbestic point at 575 nm, implying that a single protonation to OEBV-h_3 occurs. The protonation site to OEBV-h_3 was determined to be the pyrrole nitrogen of the C-ring by NMR (*vide infra*). These features closely resemble those of BVDE-h_3 reported by Margulies and Stockburger.[25]

The left panel of Figure III-6 shows RR spectra of OEBV-h_3 (A), OEBV-d_3 (B), OEBV-h_4^+ (C) and OEBV-d_4^+ (D). A prominent band is observed at 1617 cm^{-1} in addition to many weak bands in spectrum (A). This pattern is characteristic of the RR spectra of linear C=C conjugated systems like carotenoids. These RR spectra did

44

not change when spinning of the Raman cell was abolished, the laser power was raised, or the sample was cooled to -50°C. Upon N-deuteration of A-, B-, and D-rings, the 1617 and 1467 cm^{-1} bands exhibited downward shifts by -3 and -7 cm^{-1}, respectively, while the bands at 1431 and 1362 cm^{-1} little shifted. From the similar behavior upon the deuterium substitution and proximity of frequencies between the model compound and the intact phytochrome, it is inferred that the bands of OEBV-h_3 at 1467, 1431, and 1362 cm^{-1} correspond to the RR bands of P_{fr} at 1460, 1420, and 1356 cm^{-1}, respectively.

The RR spectrum of OEBV-h_3 changed definitely upon protonation of C-ring as shown by spectrum C. The changes include disappearance of the Raman bands at 1431 and 1405 cm^{-1} and the frequency shifts and intensity changes of the bands around 1700 and 1600 cm^{-1}. The 1699 cm^{-1} band in spectrum A is shifted to higher frequency by 14 cm^{-1} upon protonation and to a slightly lower frequency upon deuteration. Judging from its frequency, this band would arise from the C=O stretching mode of A- and D-rings. The increase in the C=O stretching frequency upon protonation is in agreement with the FT-IR data.[21] Presumably protonation at C-ring appreciably changes the conjugation system and thus all the double bond stretching force constants. These RR spectral changes resemble those of BVDE-h_3.[25]

The most prominent Raman band of the protonated form at 1616 cm^{-1} exhibits deuteration shift of -6 cm^{-1}. This well corresponds to the deuteration shift of the most prominent band of P_r of the intact phytochrome at 1626 cm^{-1} by -5 cm^{-1} (Figures III-4A and -4B) and that of the large phytochrome at 1625 cm^{-1} by -7 cm^{-1} and, accordingly, this observation strongly suggests that the structures of the P_r chromophore in the two kinds of phytochromes are similar to that of OEBV-h_4^+.

The corresponding RR spectra of the ^{15}N-substituted octaethylbiliverdin (OEBV-[15]N_4) are shown in the right panel of Figure III-6. The most prominent band of OEBV-[15]N_4-h_3 appears at 1615 cm^{-1} (1614 cm^{-1} for the protonated form), which is little shifted from that of OEBV-[14]N_4 (although the ^{14}N/^{15}N isotopic frequency shifts are comparable to experimental uncertainty (2 cm^{-1} per one pixel), the frequency shifts were confirmed by three independent measurements and also by difference calculations). If the 1615 cm^{-1} band involved 30% of the C=N stretching character, it would exhibit a frequency shift as large as 8 cm^{-1} on the basis of a simplified diatomic calculation. In fact, the C=N stretching RR band of (OEP)Ni[II] showed the ^{15}N shift of -6 cm^{-1} for the totally symmetric mode at 1383 cm^{-1}[30] which was deduced to contain

ca. 50% of the C=N stretching character and to shift by -9 cm^{-1} through the normal coordinate calculations.[31] Therefore, the 1617 cm^{-1} band of OEBV-h$_3$ in Figure III-6A is not primarily associated with the C=N stretching vibration. However, the 2 cm^{-1} shift due to the ^{15}N substitution implies a small coupling with the C=N stretching mode irrespective of the protonation at C-ring. It is stressed for the 1617 cm^{-1} band that the deuteration shift is fairly large for the protonated form but the ^{15}N shift is small. It is most likely that the 1617 cm^{-1} band has the largest contribution from the methine-bridge C=C stretching vibrations adjacent to C-ring and some contributions from other C=C and the C=N stretching modes.

The highest frequency band (1699 cm^{-1}) in the left panel of Figure III-6A shows little shift upon ^{15}N substitution but an appreciable shift to lower frequencies upon N-deuteration (10-13 cm^{-1}). The shift size is close to the deuteration shift of the amide I band and reasonable to assign it to the C=O stretching mode of the lactam. While most of the RR bands show the ^{15}N frequency shifts smaller than 4 cm^{-1}, the 1405 cm^{-1} band of OEBV-h$_3$ and the 1429 cm^{-1} band of OEBV-d$_3$ exhibit downshifts by 7-12 cm^{-1} upon ^{15}N substitution and seem to disappear upon protonation to C-ring. These may be associated mainly with the C=N stretching mode of C ring.

The 400-MHz ^{1}H NMR spectra of OEBV-h$_3$ in deuterated chloroform (CDCl$_3$) are shown in Figure III-7A. The triplet signals at 1.0-1.3 ppm and the quartet signals at 2.2-2.7 ppm are assigned to methyl and methylene protons of ethyl groups, respectively. The broad band at 1.7 ppm is due to water contaminated in the sample. The singlet peaks at 5.9 and 6.6 ppm are assigned to the methine protons at positions-5 and -15 and to that at position-10, respectively, since the former is strong as twice as the latter. The protons of pyrrole NH are not observed as a result of line broadening.

Upon protonation, while the chemical shifts of ethyl groups are scarcely affected, the methine protons show downfield shift as shown by spectrum B. New signals appear at 10.1 and 13.0 ppm, each corresponding to two protons in intensity. As shown by spectrum C, these signals are weakened when DCl is used instead of HCl. Therefore these protons are exchangeable with the protons in the solvent. With the ^{15}N-enriched compound, the proton signals are split into doublets with an N-H coupling constant of 94 Hz for the 10.1 ppm signal and 93 Hz for the 13.0 ppm signal, which are typical values of one-bond NH couplings and close to that of the ^{15}N enriched OEPH$_4$$^{2+}$ [^1J(^{15}N-H);93 Hz].[34] These coupling constants clearly indicate that the corresponding protons bind to the nitrogen atoms. Probably, the 13.0 and 10.1

ppm signals are assignable to the B- (and C) and the A- (and D) rings, respectively. Since both OEBV and protonated OEBV have C_2 symmetry in the NMR time scale, distinction between B- and C-rings is impossible. A positive charge of OEBV-h_4^+ is delocalized and the downshift of the C_{10}-H proton signal indicates this.

The 40.5-MHz proton-decoupled ^{15}N-NMR spectra of OEBV-^{15}N$_4$-h_3 and its protonated form in CDCl$_3$ at -50°C are shown in Figures III-7E and -7F, respectively. The signal at 107.1 ppm is assignable to the nitrogens of A- and D-rings with the lactam skeleton, because the chemical shift is comparable to that of 2-pyrrolidinone (98.6 ppm), Δ^3-pyrrolin-2-one (98.1 ppm), and Δ^4-pyrrolin-2-one (124.0 ppm).[32] Since the chemical shift of 184.5 ppm is close to that of imidazole (184.5 ppm)[33] and ^{15}N-OEPH$_2$ (160.6 ppm),[34] the signal is assignable to the nitrogens of B- and C-rings. In contrast to ^{15}N-OEPH$_2$, the signal at 184.5 ppm does not collapse into two peaks, even at low temperature (-50°C). This implies that the proton exchange between B- and C-rings is faster than the relaxation of the ^{15}N nuclei.

Upon protonation, while the nitrogen resonance of A- and D-rings is little affected, the nitrogen resonance of B- and C-rings shows a large upfield shift by 51 ppm. It is known that the nitrogen resonance of pyridine shifts to upfield by *ca.* 100 ppm upon protonation.[35] The upfield shift of 51 ppm can be reasonably interpreted as an average of the shifts for the hydrogen-attached B ring- and the protonated C ring-nitrogens. A similar upfield shift was also reported for protonation of OEPH$_2$ to OEPH$_4^{2+}$.[34] This result also evidently shows that protonation occurs on nitrogen of C-ring.

III-4. Discussion

Protonation of the Chromophore. The RR spectra of oat phytochrome in P$_{fr}$ excited at 752 nm were recently reported by Fodor et al.[10] Four RR bands were observed above 1300 cm^{-1} for P$_{fr}$; 1622, 1599, 1552, and 1312 cm^{-1}. Contrary to the present results, all bands exhibited deuteration shifts (to 1618, 1591, 1494 and 1060 cm^{-1}, respectively) and therefore, it was deduced that P$_{fr}$ was protonated similar to P$_r$. The RR bands of P$_{fr}$ at 1460, 1420, and 1356 cm^{-1} in Figure III-3 cannot be seen in the reported RR spectra excited at 752 nm, and other peak frequencies appreciably differ beyond the experimental errors between the two studies. Such discrepancies are also seen for the spectra of P$_r$. However, it is unlikely to attribute the spectral difference to the difference in sources; pea and oat.

47

Linear dichroism measurements of the absorption spectrum[36] determined the angle between the transition dipoles for the near UV and red bands of P_r to be 68°. This would imply that different parts of the chromophore primarily contribute to the two transitions. Accordingly, different kinds of vibrational modes are resonance enhanced upon the near UV and red excitations. If the red excitation preferentially probes vibrations attributed to A-, B- and D-rings, it should exhibit deuteration effects irrespective of protonation to the chromophore, since the three rings have exchangeable protons. Fodor et al.[10] observed a single N-H bending band for three N-H groups of A-, B-, and D-rings and three C=C or C=N stretching bands for P_{fr}. The number of observed bands is much less than the number of modes expected even for the limited part of the molecule. Consequently, the deuteration effects observed similarly for P_r and P_{fr} do not necessarily demonstrate that the chromophore is protonated. In contrast, the present observation revealed a clear difference between the deuteration effects of the C=C stretching modes of P_r and P_{fr}, and this cannot be explained by the idea that both P_r and P_{fr} are protonated unless only the C-ring proton of P_{fr} is nonexchangeable. On the other hand, if the near UV excitation preferentially probes the C-ring moiety, the difference in deuteration shifts between P_r and P_{fr} would be reasonably ascribed to the protonation effects. In fact, the 1617 cm^{-1} band of OEBV-h$_3$ in the near UV excited RR spectrum (Figure III-6) gave -3 cm^{-1} shift for deuteration of three pyrrole rings while the protonated form gave a doubled amount of the deuteration shift (-6 cm^{-1}).

The FT-IR study by Siebert et al.[21] demonstrated that the difference spectrum between P_r and P_{fr} is altered between in H_2O and in D_2O both in positive and negative sides and, therefore, proposed that both P_r and P_{fr} are protonated. As mentioned above, three pyrrole rings are deuterated even for non-protonated form, deuteration effects are not diagnostic unless the absorption bands associated with C ring are specified. This is practically impossible at the present stage since there are too many bands to be assigned. On the other hand, the FTIR difference spectrum between P_r and P_{fr} provided a few difference peaks around 1690-1710 cm^{-1}. Since protonation to C ring causes an upshift of the lactam C=O stretching band (Figure III-6), the FTIR data are not incompatible with a model that the protonation level differs between P_r and P_{fr}.

Song and his coworkers reported SERR spectra of phytochrome adsorbed on colloidal Ag sols at 77K.[18] In the 406.7 nm excited RR spectra of P_{fr} they reported peaks at 1624, 1596, 1458, 1414, and 1354 cm^{-1} for P_{fr} above 1350 cm^{-1}. The relative

peak intensities and frequencies, especially in the single-bond stretching region, are not necessarily coincident with those in Figure III-3. The difference would not be due to the difference in temperature, because Fodor et al.[21] obtained similar spectra for P_r at 77 and 300K upon excitation at 752 nm. Therefore, the discrepancy may be attributed to a plausible phenomenon that adsorption to Ag colloids alters the protein-choromophore interactions.

Photoreaction. Phototransformation of phytochrome is considered to involve the Z,Z,Z to Z,Z,E isomerization of the chromophore[7-11] and/or proton migration[11,12] and is known to proceed via a few intermediates; $P_r \rightarrow I_{700}(= \text{lumi-R}) \rightarrow I_{bl}(= \text{meta-R}) \rightarrow P_{fr}$. It was reported previously that there was no net gain or loss of protons between P_r and P_{fr} as a whole molecule of intact pea phytochrome protonation. However, the present experiments demonstrated that the protonation state of the chromophore was definitely different between P_r and P_{fr} (and I_{bl}). Accordingly, a proton should be transferred from the chromophore to an amino acid residue in the process of phototransformation from P_r to P_{fr}. Several studies on the photoreaction kinetics have revealed that proton translocation is not involved in the photoreaction from P_r to I_{700}.[37,38] Therefore, the proton migration from the chromophore to an amino acid residue should occur in the processes $I_{700} \rightarrow I_{bl}$.

Pea large phytochrome lacks the N-terminal polypeptide of Ser-1 to Ser-51,16-500 compared with pea intact phytochrome. The molecular mass of the N-terminal polypeptide is calculated to be 5.6 kDa, which suggests that the large phytochrome also lacks a C-terminal segment OEP of like oat phytochrome. The 7-kDa segment(s) of the intact phytochrome is reported to be necessary for appearance of the characteristic spectral properties of P_{fr}.[27,19] Without the 7 kDa segment(s), the population ratio of constituents present in the photo-steady state is different between the H_2O and D_2O solutions although with it the D_2O effect is absent[11,42]. Furthermore, the 7 kDa segments prevent the chromophore from reaction with exogenous reagents[43-45]. In the spectra shown in Figure III-3, the 1355 cm^{-1} band of intact phytochrome was shifted to 1336 cm^{-1} with the large phytochrome. Both bands did not exhibit a frequency shift in D_2O. Therefore, they cannot be assigned to the N-H bending mode. It seems to be most plausible to assign them to the methine-bridge C-H in-plane bending mode. If this is the case, the frequency difference between the large and intact P_{fr} implies that the 7 kDa segments interact with the chromophore and induce some structural changes at the methine-bridge moiety. Since the 1460 cm^{-1} band of intact

P_{fr} is shifted to 1453 cm^{-1} in D_2O, bulk water should reach the chromophore even in the presence of the 7 kDa peptides in either P_{fr} or in other intermediates during photocycle. However, with intact phytochrome, the population ratio of constituents present in the photosteady state is hardly affected by bulk pH and I_{bl} is not accumulated in it,[12] suggesting that the 7 kDa peptides have an acceptor/donor residue and behave to have a shield effect for proton translocation between bulk water and the chromophore.

Phycocyanin, the light harvesting component of the photosynthetic apparatus of cyanobacteria (blue-green algi) and of some red algi, contains a chromophore similar to that of phytochrome (the vinyl substituent of the D ring is replaced by an ethyl group in phycocyanin). The protonated structure of its chromophore was recently studied by using an FT-Raman technique[46] and it was found that the C=C stretching RR bands around 1635 cm^{-1} were shifted to lower frequency by 5-6 cm^{-1} in D_2O as in the case of P_r. Its X-ray crystallographic molecular structure at 2.1 Å resolution was revealed by Schirmer;[47] the chromophores arch around aspartate residues and the nitrogens of pyrroles B and C are within the hydrogen-bonding distance of one of the carboxylate oxygens. Since the pK_a value of the cation of the P_r chromophore in an unfolded protein is 5.4,[48] the tetrapyrrole would ordinarily be deprotonated at C-ring at pH 7.8 of the present solution. Therefore, the change in the protonation state of the chromophore in phytochrome must be induced by a change of the unique protein environment as in phycocyanin. It is plausible that the protonation/deprotonation of the chromophore during the phototransformation is switched by the distance between the nitrogen of C-ring and a proton donating (or accepting) amino acid residue(s) like in rhodopsin[49] and bacteriorhodopsin.[50]

The protonation effect on the most prominent Raman band of OEBV-h$_3$ is very small. This shows that the protonation itself little alters the RR spectral feature in the C=C stretching regions. In contrast, the RR spectral features of P_r and P_{fr} around the C=C stretching region are much different with each other in both large and intact phytochromes. As a plausible explanation for it, one may note the presence of specific interactions between the chromophore and the apoprotein for P_{fr}, since the first absorption band of intact P_{fr} is bathochromically shifted in comparison with the absorption band of the P_{fr} chromopeptide.[51] Such interactions may make the Raman spectra of the intact phytochrome different from those of the chromophore without apoprotein. However, it would be unlikely that the specific interactions ceased to exist

in P_r if the structure of the chromophore remained unaltered between P_r and P_{fr}. The photoisomerization from Z,Z,Z to Z,Z,E may bring about a specific interaction between the chromophore and the protein moiety of P_{fr}.

In conclusion, the present RR experiments demonstrated that the protonation state of the chromophore is distinctly different between P_r and P_{fr} of intact pea phytochrome. The model compound study strongly suggests that the binding site of the additional proton in the P_r chromophore is the pyrrole nitrogen of C-ring. Since there is no net gain or loss of protons between intact pea P_r and P_{fr}, the proton released from the chromophore of P_r would be migrated to a protein moiety of P_{fr}.

References

(1)   Lagarias, J. C. *Photochem. Photobiol.* **1985**, *42*, 811-820.

(2)   Furuya, M. In *Phytochrome and Photoregulation in Plants*; Academic Press, Tokyo, 1987.

(3)   Furuya, M. *Advances in Biophysics*, **1989**, *25*, 133-165.

(4)   Tokutomi, S.; Nakasako, M.; Sakai, J.; Kataoka, M.; Yamamoto, K. T.; Wada, M.; Tokunaga, F.; Furuya, M. *FEBS Lett.* **1989**, *247*, 139-142.

(5)   Lagarias, J. C.; Rapoport, H. *J. Am. Chem. Soc.* **1980**, *102*,   4821-4828.

(6)   Rüdiger, W.; Eilfeld, P.; Thümmler, F. In *Optical Properties and Structure of Tetrapyrroles*; Blauer, G., Sund, H. Eds.; Walter de Gryter, Berlin, New York, 1985; pp. 349-366.

(7)   Rüdiger, W.; Thümmler, F.; Cmiel, E.; Schneider, S. *Proc. Natl. Acad. Sci. USA* **1983**, *80*, 6244-6248.

(8)   Thümmler, F.; Rüdiger, W. *Tetrahedron* **1983** *39*, 1943-1951.

(9)   Farrens, D. L.; Holt, R. E.; Rospendowski, B. N.; Song, P.-S.; Cotton, T. M. *J. Am. Chem. Soc.* **1989**, *111*, 9162-9169.

(10)   Fodor, S. P. A.; Lagarias, J. C.; Mathies, R. A. *Biochemistry* **1990**, *29*, 11141-11146.

(11)   Moon, D.-K.; Jeen, G.-S.; Song, P.-S. *Photochem. Photobiol.* **1985**, *42*, 633-641.

(12)   Tokutomi, S.; Yamamoto, K. T.; Furuya, M. *Photochem. Photobiol.* **1988**, *47*, 439-445.

(13)   Wong, Y.-S.; Cheng, H.-C.; Walsh, D. A.; Lagarias, J. C. *J. Biol. Chem.* **1986**, *261*, 12089-12097.

(14)   Chai, Y.-G.; Song, P.-S.; Cordonnier, M.-M.; Pratt. L. H. *Biochemistry* **1987**, *26*, 4947-4952.

(15)   McMicheal, R. W., Jr.; Lagarias, J. C. *Biochemistry* **1990**, *29*, 3872-3878.

(16)   Spiro, T. G. Ed. In *Biological Applications Raman Spectroscopy* **1987**, Wiley, New York.

(17)   Fodor, S. P. A.; Lagarias, J. C.; Mathies, R. A. *Photochem. Photobiol.* **1988**, *48*, 129-136.

(18)   Rospendowski, B. N.; Farrens, D. L.; Cotton, T. M.; Song, P.-S. *FEBS Lett.* **1989**, *258*, 1-4.

(19)   Lumsden, P. J.; Yamamoto, K. T.; Nagatani, A.; Furuya, M. *Plant Cell Physiol.*

1985, *26*, 1313-1322.

(20) Tokutomi, S.; Mizutani, Y.; Anni, H.; Kitagawa, T. *FEBS Lett.* **1990**, *269*, 341-344.

(21) Siebert, F.; Grimm, R.; Rüdiger, W.; Schmidt, G.; Scheer, H. *Eur. J. Biochem.* **1990**, *194*, 921-928.

(22) Tokutomi, S.; Kataoka, M.; Sakai, J.; Nakasako, M.; Tokunaga, F.; Tasumi, M.; Furuya, M. *Biochim. Biophys. Acta* **1988**, *953*, 297-305.

(23) Bonnett, R.; Dimsdale, M. J. *J. Chem. Soc., Perkin Trans. I* **1972**, 2540-2548.

(24) Cavaleiro, J. A. S.; Smith, K. M. *J. Chem. Soc., Perkin Trans. I* **1973**, 2149-2155.

(25) Margulies, L.; Stockburger, M. *J. Am. Chem. Soc.* **1979** *101*, 743-744.

(26) Lagarias, J. C.; Kelly, J. M.; Cyr, K. R.; Smith, W. O. Jr. *Photochem. Photobiol.* **1987**, *46*, 5-13.

(27) Vierstra, R. D.; Quail, P. H. *Plant Physiol.* **1983**, *72*, 264-267.

(28) Srinivasan, P. R.; Lichter, R. L. *J. Mag. Reson.* **1977**, *28*, 227-234.

(29) Tokutomi, S.; Inoue, Y.; Sato, N.; Yamamoto, K. T.; Furuya, M. *Plant Cell Physiol.* **1986**, *27*, 765-773.

(30) Kitagawa, T.; Abe, M.; Kyogoku, Y.; Ogoshi, H.; Sugimoto, H.; Yoshida, Z. *Chem. Phys. Lett.* **1977**, *48*, 55-58.

(31) Abe, M.; Kitagawa, T.; Kyogoku, Y. *J. Chem. Phys.* **1978**, *69*, 4526-4534.

(32) Fronza, G.; Mondelli, R.; Randoll E. W.; Gardini, G.-P. *J. Chem. Soc., Perkin Trans. II* 1746-1749.

(33) Schuster, I. I.; Roberts, J. D. *J. Org. Chem.* **1979**, *44*, 3864-3867.

(34) Kawano, K.; Ozaki, Y.; Kyogoku, Y.; Ogoshi, H.; Sugimoto, H.; Yoshida, Z. *J. Chem. Soc., Perkin Trans. II* **1978**, 1319-1325.

(35) Witanowski, M.; Stefaniak, L.; Szymanski, S.; Januszewski, H. *J. Magn. Reson.* **1977**, *28*, 217-226.

(36) Chae, Q.; Song, P. S. *J. Am. Chem. Soc.* **1075**, *97*, 4176-4179.

(37) Aramendía, P. F.; Ruzsicska, B. P.; Braslavsky, S. E.; Schaffner, K. *Biochemistry* **1987**, *26*, 1418-1422.

(38) Brock, H.; Ruzsicska, B. P.; Arai, T.; Schlamann, W.; Holzwarth, A. R.; Braslavsky, S. E.; Schaffner, K. *Biochemistry* **1987**, *26*, 1412-1417.

(39) Yamamoto, K. T.; Tokutomi, S. *Photochem. Photobiol.* **1989**, *50*, 113-120.

(40) Grimm, R.; Lottspeich, F.; Schneider, H. A. W.; Rüdiger, W. *Z. Naturforsch.* **1986**, *41C*, 993-1000.

53

(41) Vierstra, R. D.; Quail, P. H. *Planta* **1982**, *156*, 158-165.

(42) Sarker, H. K.; Song, P.-S. *Biochemistry* **1981**, *20*, 4315-4320.

(43) Baron, O.; Epel, B. L. *Plant Physiol.* **1983**, *73*, 471-474.

(44) Hahn, T.-R.; Song, P.-S.; Quail, P. H.; Vierstra, R. D. *Plant Physiol.* **1985**, *74*, 755-758.

(45) Thümmler, F.; Eilfeld, P.; Rüdiger, W.; Moon D.-K.; Song, P.-S. *Z. Naturforsch* **1985**, *40c*, 215-218.

(46) Sawatzki, J.; Fischer, R.; Scheer, H.; Siebert, F. *Proc. Natl. Acad. Sci. USA* **1990**, *87*, 5903-5906.

(47) Schirmer, T.; Bode, W.; Huber, R. *J. Mol. Biol.* **1987**, *196*, 677-695.

(48) Grombein, S.; Rüdiger, W.; Zimmermann, H. R. *Z. Physiol. Chem.* **1975**, *356*, 1709-1714.

(49) Sakmar, T. P.; Franke, R. R.; Khorana, H. G. *Proc. Natl. Acad. Sci. USA* **1989** *86*, 8309-8313.

(50) Lin, S. W.; Mathies, R. A. *Biophys. J.* **1989**, *56*, 653-660.

(51) Rüdiger, W. In *Phytochrome and Photoregulation in Plants*; Furuya, M., Ed.; Academic Press, Tokyo, 1987; pp.127-138.
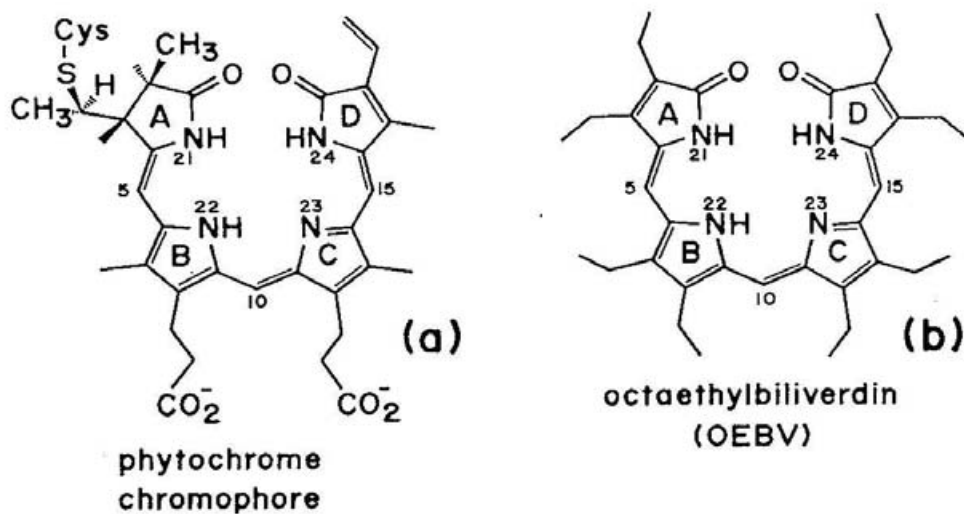
Figure III-1. Structure of phytochrome chromophore (a) and OEBV-h_3 (b). Numbering of pyrrole rings and atoms are denoted in the figure. The deprotonated pyrrole ring is defined as C-ring for OEBV-h_3, although the deprotonated pyrrole ring of phytochrome has not been established yet.
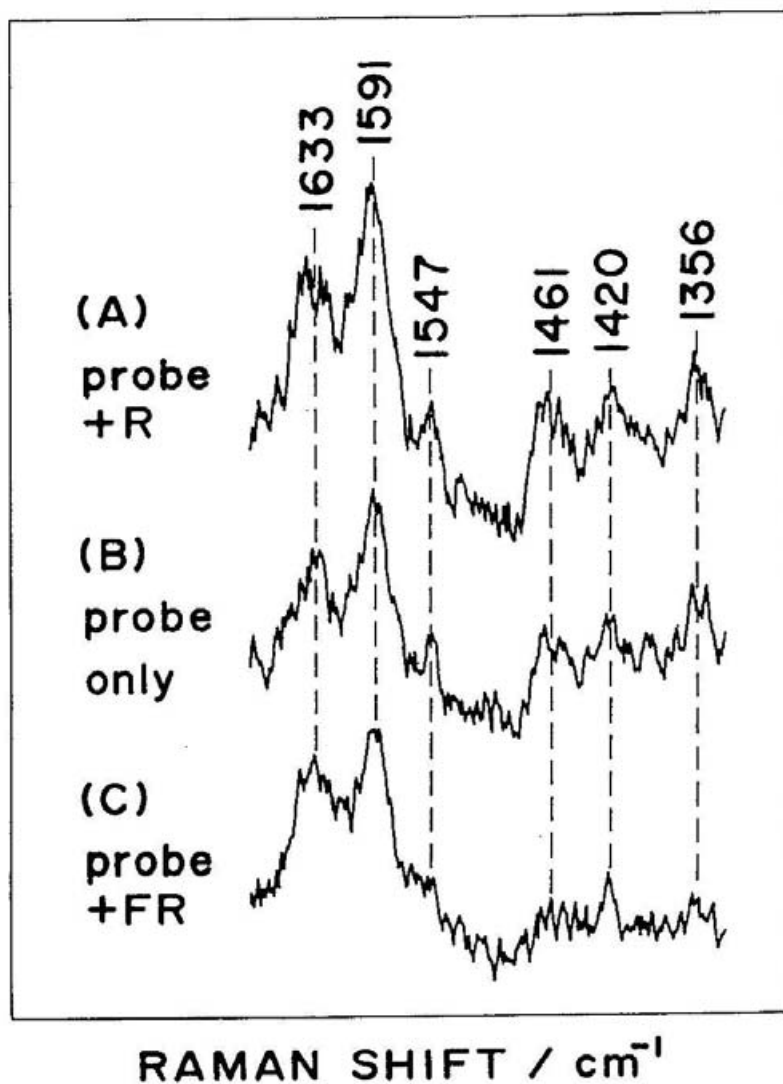
Figure III-2. Effects of red or far-red illumination on RR spectra excited at 407 nm (5 mW). The experimental conditions are common to three spectra except for illumination of red (A, 633 nm, 15 mW) or far-red light (C, 740 nm, 7 mW). Spectrum B was obtained without illumination of the second laser. The three spectra are represented in the same scale.
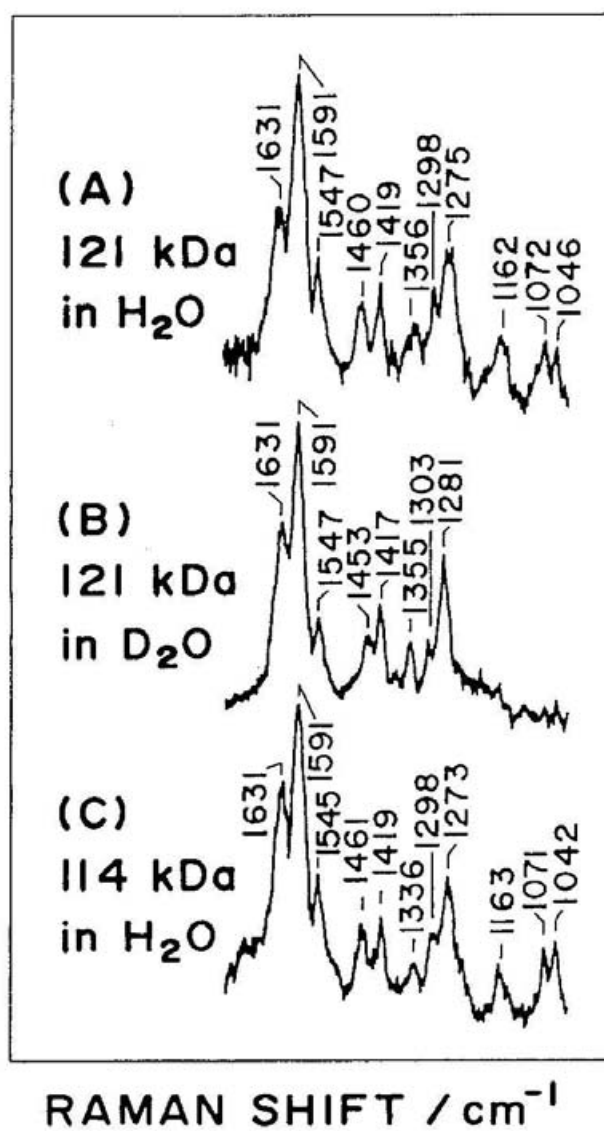
Figure III-3. RR spectra of intact (A and B) and large (C) pea phytochrome excited at 407 nm (5 mW) under red light illumination (633 nm) at pH 7.8. Spectra (A) and (C) are for H_2O solutions and spectrum (B) is for D_2O solution. Accumulation time, 320 sec. Relative population of P_r, P_{fr} and I_{bl} under individual illumination conditions are as follows; P_r 45%, P_{fr} 55% for (A); P_r 40%, P_{fr} 60% for (B); P_r 20%, P_{fr} 36%, I_{bl} 44% for (C).

57
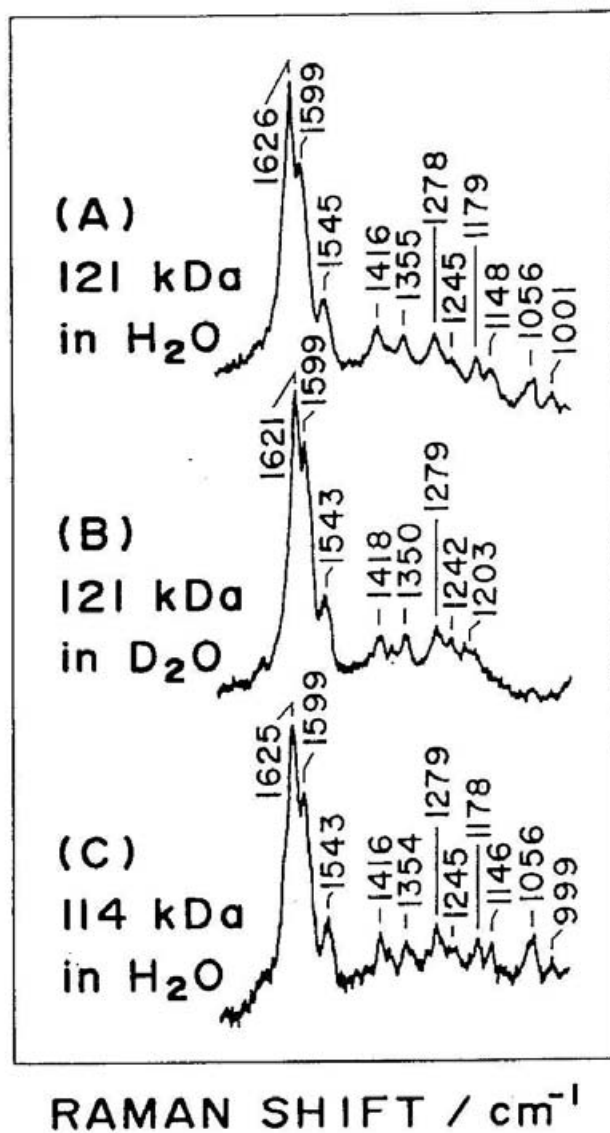
Figure III-4. RR spectra of intact (A and B) and large (C) pea phytochrome excited at 364 nm (5 mW) under far-red light illumination (740 nm) at pH 7.8. Spectra (A) and (C) are for H_2O solutions and spectrum (B) is for D_2O solution. Accumulation time, 320 sec. Relative population of P_r, P_{fr} and I_{bl} under individual illumination conditions are as follows; P_r 55%, P_{fr} 45% for (A); P_r 55%, P_{fr} 45% for (B); P_r 66%, P_{fr} 5%, I_{bl} 29% for (C).

58
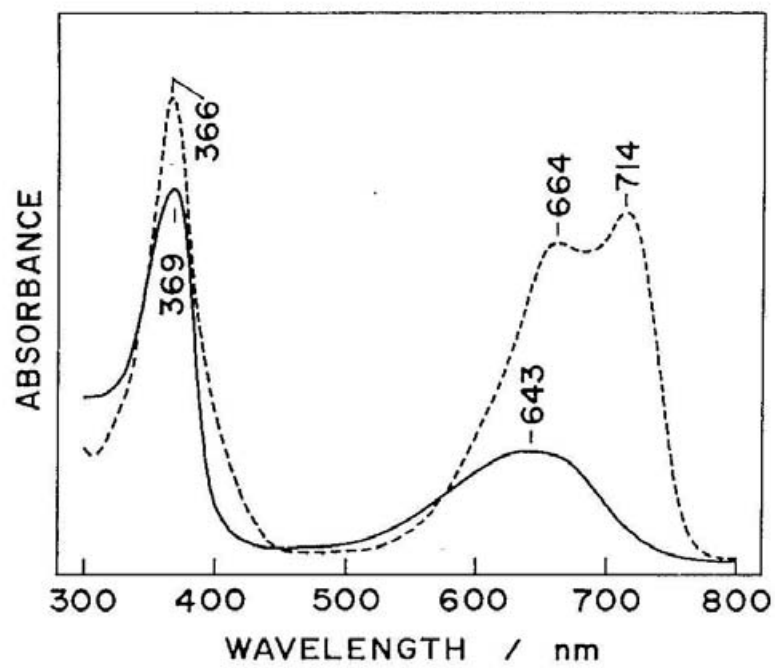
Figure III-5. Absorption spectra of OEBV-h$_3$ (solid line) and its protonated form (OEBV-h$_4^+$, broken line) in chloroform.
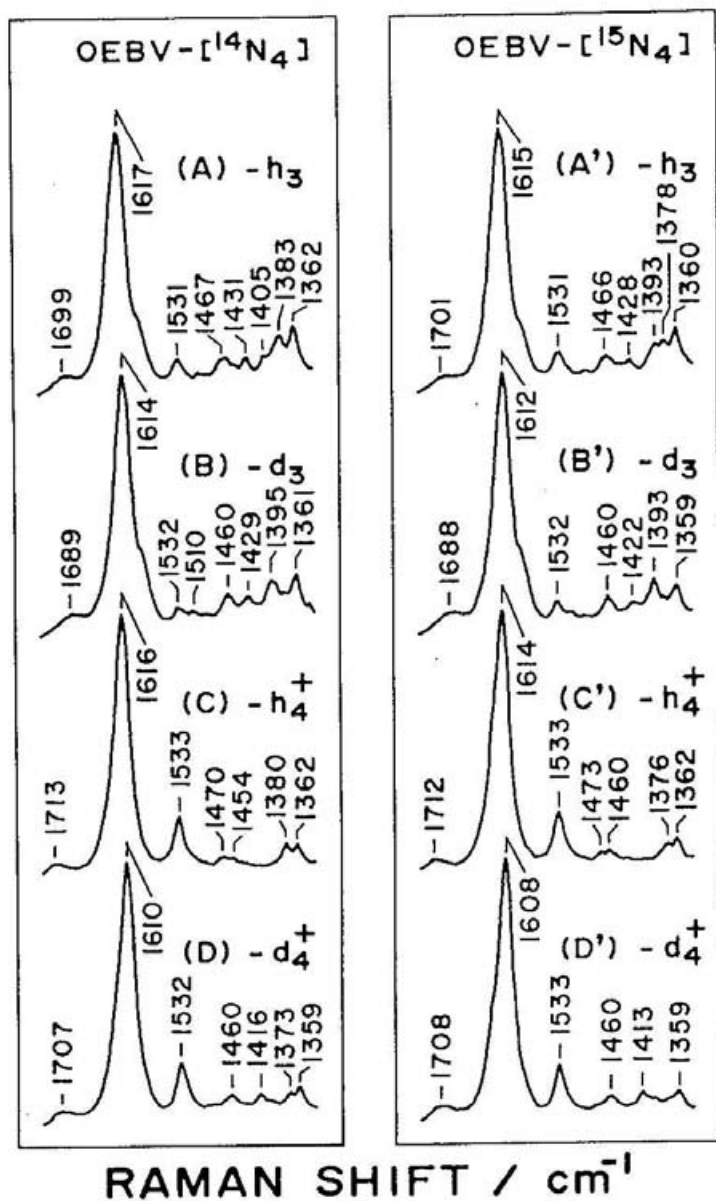
Figure III-6. Left panel: RR spectra of OEBV-h_3 (A) (OEBV-d_3 (B), OEBV-h_4^+ (C) and OEBV-d_4^+ (D) in chloroform. Excitation, 364nm (5mW); Accumulation time, 320 sec. Right panel: RR spectra of OEBV-$^{15}N_4$-h_3 (A), OEBV-$^{15}N_4$-d_3 (B), OEBV-$^{15}N_4$-h_4^+ (C), and OEBV-$^{15}N_4$-d_4^+ (D) in chloroform. Excitation, 364 nm (5 mW), Accumulation time, 320 sec.

60
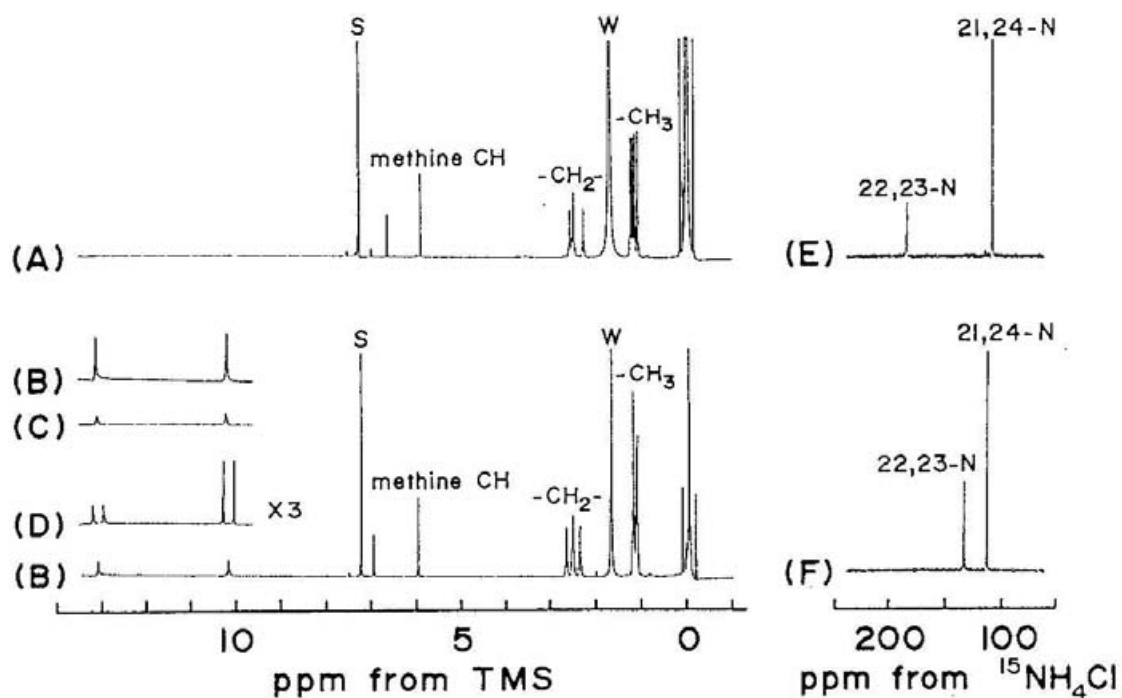
Figure III-7. 400 MHz ^{1}H- (A, B, C and D) and 40.5 MHz proton-decoupled ^{15}N-NMR spectra (E and F) of octaethylbiliverdin and its protonated form in CDCl$_3$. A) OEBV-^{14}N$_4$-h$_3$, B) OEBV-^{14}N$_4$-h$_4^+$, C) OEBV-^{14}N$_4$-d$_4^+$, D) OEBV-^{15}N$_4$-h$_4^+$, E) OEBV-^{15}N$_4$-h$_3$, F) OEBV-^{15}N$_4$-h$_4^+$. The resonances marked by S and W are due to solvent (CHCl$_3$) and water, respectively.

Chapter IV

Resonance Raman Spectra of
Biliverdins and
Their Isotopic Derivatives

Abstract

We have obtained resonance Raman (RR) and IR spectra of octaethylbiliverdin (OEBV) and 1, 2-*trans*-dihydrooctaethylbiliverdin (DHBV) and their protonated forms. Some in-plane skeletal modes observed for OEBV, DHBV and their protonated forms can be reasonably assigned with the aid of the isotopic shifts of ^{15}N, methine-d_3 and methylene-d_{28} isotopomers. The large effects of methylene deuteration on RR spectra for these species indicated that the RR spectra contain several bands which are assignable to the ethyl substituents, on the basis of the reported assignments for $Ni^{II}(OEP)$. The RR spectra of DHBV and protonated DHBV show features common to those of OEBV and protonated OEBV, suggesting that the vibrational modes involving the corresponding C_β-C_β bond do not significantly couple with other modes and that the forms of normal coordinates of DHBV and protonated DHBV bear resemblance to those of OEBV and protonated OEBV, respectively.

IV-1. Introduction

Bile pigments, biliverdins, are porphyrin-related systems released by the liver after metabolic decomposition of heme in animals. During this process, heme is released from its linkage with globin and finally excreted as esterfied bilirubin. The physiological importance of bile pigments is not only related to animal metabolism. They are also structurally related to the chromophoric system of pigments of utmost importance in the plant world. Typical examples are phycocyanin and phycoerythrin, involved in energy-storage and -transfer processes in blue-green algae,[1] and phytochrome, the pigment responsible for plant growth regulation.[2]

Recently, vibrational spectroscopies have been applied to the study of the biliproteins. Fodor et al. obtained resonance Raman spectra of oat phytochrome in a red absorbing (P_r) form at 77 K by using 752 nm-excitation in order to avoid the fluorescence emission of P_r.[3] Qualitatively similar studies were subsequently reported by using coherent anti-Stokes Raman scattering (CARS) spectroscopy.[4] More recently, Fodor et al. reported RR spectra of P_r and a far-red absorbing (P_{fr}) form at ambient temperature.[5] Surface-enhanced resonance Raman (SERR) spectroscopy was also applied to oat phytochrome.[6] Recently, several groups carried out Fourier-transform infrared (FT-IR) studies on phytochrome, making a good use of the advantage that probe light does not induce the photoreaction.[7] We have obtained RR spectra of pea phytochrome at ambient temperature by using UV excitation at 364 nm.[8] On the other hand, RR spectra of phycocyanin excited at 364 nm were reported by Szalontai et al.[9] FT-Raman[10] and CARS spectroscopies[11] were applied to phycocyanin.

The vibrational spectra are generally capable of providing detailed structural information, when band assignments are completed. However, no detailed analysis of the vibrational modes of the pigments has been carried out owing to largeness and low symmetry of biliverdins. In this study, we observed RR and IR spectra of octaethylbiliverdin (OEBV), 1,2-*trans*-dihydro-octaethybiliverdin (DHBV), their protonated forms as model compounds of the chromophore. We discuss mode assignments of their vibrational bands on the basis of isotopic substitutions; pyrrole-^{15}N, methine-d_3 and ethyl-d_{28} for OEBV and pyrrole-^{15}N for DHBV.

IV-2. Experimental Section

Synthesis of Biliverdins. Octaethylbiliverdin (OEBV-h_3) and its ^{15}N-derivative (OEBV-^{15}N$_4$-h_3) were synthesized from octaethylporphyrinato-iron(III) chloride

[(OEP)Fe^{III}Cl][12] and its ^{15}N-derivative, respectively, according to the reported method[13] with some modifications about reaction temperature, time, and pH, which raised the yield from 5% to 35%. The ^{15}N-rich (OEP)Fe^{III}Cl was prepared by using ^{15}N-enriched NaNO$_3$. The methine-d$_3$ derivative was prepared from meso-d$_4$ (OEP)Fe^{III}Cl, which was synthesized by reported method.[14] Ethyl-d$_{28}$ OEBV with ethyl groups alternately substituted by -CD$_2$CD$_3$ and -CD$_2$CH$_3$ was synthesized from ethyl-d$_{28}$ (OEP)Fe^{III}Cl, which was prepared by reported method, but CD$_3$CD$_2$I and NaBD$_4$ were used instead of CH$_3$CH$_2$I and NaBH$_4$, respectively. 1,2-*trans*-Dihydrooctaethylbiliverdin (DHBV-h$_3$) and its ^{15}N-derivative (DHBV-^{15}N$_4$-h$_3$) were synthesized from γ,δ-dideuterio-*trans*-octaethylchrolinatoiron(III) chloride [(OEC)Fe^{III}Cl][15] and its ^{15}N-derivative, respectively, according to the reported method.[16] The N-deuterated form of octaethylbiliverdin (OEBV-d$_3$) was obtained by mixing a small amount of D$_2$O with the CHCl$_3$ solution of OEBV-h$_3$. Protonation of OEBV-h$_3$ (or -d$_3$) was accomplished by adding 1 M HCl (or DCl) to the CHCl$_3$ solution of OEBV-h$_3$ (or -d$_3$) according to the procedures described by Margulies and Stockburger.[17] The N-deuteration and protonation of DHBV were carried out in a similar way to those of OEBV.

Measurements of Vibrational Spectra. RR scattering was excited by the 364 nm line of an Ar$^+$ ion laser (Spectra Physics, Model 2045), dispersed with a double monochromator (SPEX 1404), and detected with a diode array detector with an image intensifier (PAR 1421HQ). The data were processed with an OMA III system (PAR 1460). The RR spectra were observed by using a micro spinning-cell (diameter = 5 mm, 1600 rpm). The Raman spectra were calibrated with indene and errors in band positions for well defined peaks are ±2 cm^{-1}. The infrared spectra in KBr pellets were recorded at room temperature on an FT-IR spectrophotometer (Perkin Elmer, series 1600).

IV-3. Results and Discussion

The structures of OEBV and DHBV are depicted in Figures IV-1A and -B, respectively. The labeling of carbon atoms follows that generally used for porphyrins; the adjacent carbons to pyrrole nitrogens and other two carbons of pyrrole rings are represented by C$_\alpha$ and C$_\beta$, respectively. The methine carbons, bridging between pyrrole rings are represented by C$_m$. The methylene and methyl carbons of ethyl substituents are represented by C$_1$ and C$_2$, respectively. We tentatively assume

DHBV to be deprotonated at C-ring.

The fundamental frequencies of OEBV, DHBV and their protonated forms can be separated into two groups which are approximately vibrationally independent. Because the biliverdin skeleton is nearly planar,[18] we can separately discuss the out-of-plane and in-plane vibrations of the skeleton. In this chapter only in-plane vibrations above 1000 cm^{-1} are discussed.

1. Vibrational Spectra of OEBV and Its Protonated Form.

Figure IV-2 shows IR spectra of OEBV-h_3 in KBr pellet. Figures IV-3, -4, -5 and -6 show RR spectra of OEBV-h_3, OEBV-d_3, OEBV-h_4^+ and OEBV-d_4^+, respectively. In Figures IV-2 - IV-6 spectra (A), (B), (C) and (D) represent unlabeled species, pyrrole-^{15}N-, methine-d_3- and ethyl-d_{28}-derivatives, respectively. The IR spectrum of unlabeled OEBV-h_3 is coincident with the spectrum for a chloroform solution reported by Siebert et al.[7] except for the bands assignable to $C=O$ stretching (*vide infra*), which can be reasonably attributed to the difference in environments of carbonyl groups between in solution state and in solid state, such as hydrogen bonding.

Carbonyl Stretching Modes. The amide I vibration of the *cis* CONH group, to which the $C=O$ stretching mode mainly contributes, is usually observed in 1650-1720 cm^{-1}.[19] In the IR spectra of OEBV in Figure IV-2, two strong bands are observed at 1690 and 1701 cm^{-1}, which are insensitive either to $^{14}N/^{15}N$ substitution, methine deuteration or ethyl deuteration. These two bands can be assigned to the two carbonyl stretching vibrations of A- and D-rings. In the RR spectra in Figure IV-3A, the corresponding band is weakly observed at 1699 cm^{-1}. This band shows a considerable low frequency shift upon N-deuteration, which indicates that this band is not a pure $C=O$ stretching mode but is coupled with the vibration of N-H bending modes (δ(N-H)). Upon protonation, the $C=O$ stretching mode shows upshifts by 11-20 cm^{-1} for unlabeled OEBV-h_4^+ or -d_4^+, and seems to be intensified. The increase in the $C=O$ stretching frequency upon protonation is in agreement with the FT-IR data reported by Siebert et al.

C=C Stretching Modes. In IR spectra five bands can be observed between 1500 and 1650 cm^{-1} where $C=N$ and $C=C$ stretching modes are expected to be observed: weak shoulder bands near 1631 and 1583 cm^{-1}, intense bands at 1620 and 1594 cm^{-1}, and weak band at 1531 cm^{-1}. On the other hand, in RR spectra, three bands are recognized in this region: very intense band at 1617 cm^{-1}, a shoulder near 1590 cm^{-1} and relatively weak band at 1531 cm^{-1}. A weak IR band at 1531 cm^{-1} and an RR band

at 1531 cm^{-1} are not due to an identical mode since they show different ^{15}N and ethyl-d$_{28}$ isotopic frequency shifts. Also the 1617 cm^{-1} band in the RR spectra and the 1620 cm^{-1} band in the IR spectra are not due to identical mode since they show different methine-d$_3$ isotopic shifts (-2 cm^{-1} for 1617 cm^{-1} band (RR) and -7 cm^{-1} for 1620 cm^{-1} band (IR)).

The IR band at 1631 cm^{-1} for unlabeled OEBV-h$_3$ in Figure IV-2A does not show a frequency shift upon ^{14}N/^{15}N substitution, but shows downshift by 3 and 5-8 cm^{-1} upon methine deuteration and ethyl deuteration, respectively, indicating that this mode involves mainly $C_\beta C_\beta$ stretching ($\nu(C_\beta C_\beta)$) and/or $C_\alpha C_\beta$ stretching modes ($\nu(C_\alpha C_\beta)$). The 1620 cm^{-1} band shows a downshift by 7 cm^{-1} upon methine deuteration, while, upon other two isotopic substitutions, it shows no frequency shift. Therefore, this band can be assigned to the mode involving mainly $C_\alpha C_m$ stretching ($\nu(C_\alpha C_m)$) mode. The band at 1594cm^{-1} considerably downshifts upon methine deuteration. This indicates that this mode is due to fairly pure $\nu(C_\alpha C_m)$. The 1583 cm^{-1} band shows frequency shifts by -5 and -6 cm^{-1} upon methine deuteration and ethyl deuteration, respectively. These deuteration shifts indicate that this band involves $\nu(C_\alpha C_m)$ and $\nu(C_\beta C_\beta)$ and/or $\nu(C_\alpha C_\beta)$ characters. The 1531 cm^{-1} band shows frequency shifts by -5, -3 and -5 cm^{-1} upon ^{15}N substitution, methine deuteration and ethyl deuteration, respectively. If we take account of this uniform isotopic shift, this band might be due to out-of-phase stretching mode involving the whole conjugated skeleton because it has scarce resonance Raman activity.

The intense RR band at 1617 cm^{-1} for OEBV-h$_3$ in Figure IV-3A shows frequency shifts by -2, -2 and -3 cm^{-1} in Figures IV-3B, -3C and -3D, respectively. The intensity of this band and its uniform isotopic shifts upon three kinds of isotopic substitutions suggest that this band is due to the in-phase stretching mode involving the whole conjugated skeleton. Upon protonation of OEBV-h$_3$, this band shows slight downshift (0-3 cm^{-1}) in Figure IV-5 but in the case of OEBV-d$_3$ more prominent downshifts (4-8 cm^{-1}) are observed in Figure IV-6. This difference in sensitivities upon protonation is not well explained in the present stage. Because the shoulder band near 1590 cm^{-1} is not well resolved in the spectra, its isotopic shifts are not discussed here. However it should be noted that this shoulder is not seen in the RR spectra of protonated form. While the RR band at 1531 cm^{-1} is insensitive either upon ^{14}N/^{15}N substitution or upon methine deuteration, this band shows downshift upon ethyl deuteration. These features indicate that this band has $\nu(C_\alpha C_\beta)$ and/or

68

$\nu(C_\beta C_\beta)$ characters. The peak position of this band is insensitive to protonation but its intensity becomes large upon protonation.

Ethyl Substituent Modes. Czernuszewicz et al.[20] pointed out that bands assignable to ethyl C-C stretching and C-H bending modes are surprisingly strong in RR spectra. Saturated alkyl substituents are not ordinarily thought to couple electronically to aromatic chromophore, although the influence of inductive and hyperconjugative effects is readily seen in shifts of the electronic transition energies. Their results suggested that the ethyl groups of $Ni^{II}(OEP)$ do significantly delocalize the B_x and/or B_y excited state, presumably by mixing of the ethyl σ character into the porphyrin π^* orbitals. Czernuszewicz et al. observed the RR bands assignable to CH_2 scissoring, CH_2 wagging, CH_2 twisting, CH_2 rocking, and C_1C_2 stretching modes at ~ 1460, ~ 1310, ~ 1260, ~ 770 and ~ 1020 cm^{-1}, respectively. Although the normal modes of OEBV associated with conjugated skeleton is quite different from those of $Ni^{II}(OEP)$, the results for $Ni^{II}(OEP)$ would be useful for the analysis of OEBV as for ethyl substituents modes. Also in the present case, RR bands which can be assigned to ethyl C-C stretching and C-H bending modes seem to be observed. These RR bands are discussed by comparing with those of $Ni^{II}(OEP)$.

The 1305 cm^{-1} RR band does not show a frequency shift upon $^{14}N/^{15}N$ substitution and an upshift to 1311 cm^{-1} upon methine deuteration both for OEBV-h_3 and -d_3. This band disappears upon ethyl deuteration. Therefore, this band can be assigned to the CH_2 wagging mode. When we assume the existence of the C_m-H in-plane bending ($\delta(C_m$-H)) mode around 1330 cm^{-1} which couples to the 1311 cm^{-1} band, the upshift by 6 cm^{-1} upon methine deuteration can be explained by the decoupling to $\delta(C_m$-H).

The RR band at 1018 cm^{-1} in Figure IV-3A and 1011 cm^{-1} in Figure IV-4A do not show an $^{14}N/^{15}N$ isotopic shift and show an upshift upon methine deuteration (11 cm^{-1} for OEBV-h_3; 17 cm^{-1} for OEBV-d_3). These bands disappear upon ethyl deuteration. Accordingly these bands are assignable to C_1C_2 stretching ($\nu(C_1C_2)$). These bands show an upshift upon protonation as shown in Figures IV-5 and -6. Upon N-deuteration new RR bands appear at 1030 cm^{-1} for OEBV-d_3 in Figure IV-4A and at 1034 cm^{-1} for OEBV-d_4^+ in Figure IV-6A, which can be assigned to $\delta(N$-D).

Thus ethyl C-C stretching and C-H bending modes are also observed in OEBV and protonated OEBV and strongly couple to $\delta(C_m$-H). The present results are fairly instructive for the normal mode analysis to be carried out because it indicates that we

69

cannot regard the methylene groups as single dynamical units and that, at least, they should be included explicitly for the ethyl groups in normal mode calculations.

C_m-H In-plane Bending Modes. The RR bands at 1275 and 1230 cm^{-1} of unlabeled OEBV-h$_3$ are slightly affected by pyrrole ^{14}N/^{15}N substitution and disappear for methine-d$_3$ isotopomer. For the ethyl-d$_{28}$ isotopomer there is only one RR band at 1241 cm^{-1} instead of two bands in this region. A similar feature is observed for OEBV-d$_3$ derivatives although the two RR bands of OEBV-d$_3$ are narrower and more intensified than those of OEBV-h$_3$. The peak intensity ratio between the higher and the lower bands is changed upon N-deuteration. While the peak positions of two RR bands of unlabeled species and ^{15}N derivative are not affected by N-deuteration, the RR band of ethyl-d$_{28}$ derivative upshifts by 10 cm^{-1} upon it. The disappearance of the RR bands upon methine deuteration suggests that these RR bands are mainly due to $\delta(C_m$-H).

On the analogy of the RR spectra of Ni^{II}(OEP), the CH$_2$ wagging mode is considered to locate at 1250-1260 cm^{-1}. The present result is well understandable when we consider that unperturbed $\delta(C_m$-H) locates at 1241 cm^{-1} for OEBV-h$_3$ and 1251 cm^{-1} for OEBV-d$_3$ and that $\delta(C_m$-H) mode significantly couples to the CH$_2$ wagging mode of ethyl substituents and splits to the doublet. Since the $\delta(C_m$-H) locates in the lower frequency side of the CH$_2$ wagging mode for OEBV-h$_3$, the lower band of the doublet is more intense than the higher one. For OEBV-d$_3$, since $\delta(C_m$-H) approaches to the CH$_2$ wagging mode, the band intensities of the doublet become even. The relation between the intensity ratio of the doublet and the location of unperturbed band is consistent with above interpretation. For OEBV-h$_4^+$, the feature upon isotopic substitution is common to OEBV-h$_3$; the two RR bands observed at 1241 and 1280 cm^{-1} in Figure IV-5A disappear upon methine substitution and, for ethyl deuterated derivative, one RR band at 1260 cm^{-1} is observed instead of them.

Other Skeletal Stretching Modes. The RR band at 1124cm^{-1} in Figure IV-3A does not show a prominent frequency shift either upon pyrrole ^{14}N/^{15}N substitution or methine deuteration and disappears upon ethyl deuteration. For Ni^{II}(OEP) the RR band which involves mainly $\nu(C_\alpha C_\beta)$ and $\nu(C_\beta C_1)$ modes is observed at 1138 cm^{-1}. It does not show an isotopic shift upon methine deuteration and downshifts to 1068 cm^{-1} with an intensity decrease upon ethyl deuteration. For the ethyl deuterated OEBV, the corresponding RR bands are observed at 1068 or 1045 cm^{-1} in Figure IV-3D and 1048 cm^{-1} in Figure IV-4D. While ν_5 of the Ni^{II}(OEP) band shows an ^{14}N/^{15}N isotop-

70

ic shift by -7 cm^{-1} because it slightly involves $C_\alpha NC_\alpha$ bending ($\delta(C_\alpha NC_\alpha)$), the band of OEBV does not show such an isotopic shift. This may be due to the difference in the state of pyrrole nitrogens of the OEBV and Ni^{II}(OEP); while four nitrogens coordinate to nickel ion for Ni^{II}(OEP) and three nitrogens bind to hydrogen for OEBV. Accordingly the most plausible assignment for this band is that this is mainly due to $\nu(C_\alpha C_\beta)$ and $\nu(C_\beta C_1)$ modes. The corresponding bands for protonated OEBV are observed at 1122 and 1121 cm^{-1} in Figures IV-5A and -6A, respectively.

The 1171 and 1101 cm^{-1} RR bands of unlabeled OEBV-h$_3$ are assignable to $C_\alpha N$ stretching, $\nu(C_\alpha N)$, on the basis of their isotopic shift upon $^{14}N/^{15}N$ substitution (Figure IV-3B). Also the 1147 cm^{-1} shows a little $^{14}N/^{15}N$ isotopic shift. The frequency shift suggests that this band also has a $\nu(C_\alpha N)$ character. The 1101-cm^{-1} band in Figure IV-3A and the 1104-cm^{-1} band are not due to an identical mode since they show different ^{15}N isotopic frequency shift. The 1171 cm^{-1} band upshifts to 1180 cm^{-1} upon N-deuteration, while other two RR bands disappear. This may indicate strong coupling of these bands to $\delta(N-D)$. Upon protonation the peak position of the 1147-cm^{-1} RR band is not affected (Figure IV-5A). But for other two bands, the correlation of RR bands between unprotonated and protonated species is complicated.

The RR band at 1467 cm^{-1} of OEBV-h$_3$ in Figure IV-3A does not show frequency shift in Figures IV-1B, -1C and -1D. This insensitivity is also observed for the corresponding band for OEBV-d$_3$ at 1460 cm^{-1} in Figure IV-4A. But this band downshifts upon N-deuteration. The downshift suggests that this band couples to $\delta(N-H)$. The 1431 cm^{-1} band in Figure IV-1A shows frequency shifts by -3, -5 and 0 cm^{-1} in Figures IV-1B, -1C and -1D, respectively, while the corresponding band at 1429 cm^{-1} in Figure IV-2A shows frequency shift by -7, -6 and -7 cm^{-1} in Figures IV-2B, -2C and -2D. The downshift of this band upon $^{14}N/^{15}N$ substitution and methine deuteration suggests that this band involves $\nu(C_\alpha N)$ and $\nu(C_\alpha C_m)$. But the difference in the frequency shift upon ethyl deuteration between for OEBV-h$_3$ and for OEBV-d$_3$ cannot be well explained at the present stage.

While two RR bands are observed at 1383 and 1405 cm^{-1} for OEBV-h$_3$ in Figure IV-3A, only one RR band is observed for OEBV-d$_3$, OEBV-h$_4$$^+$ and OEBV-d$_4$$^+$ in the region of 1370-1400 cm^{-1}. It is plausible that the vibration around 1380 cm^{-1} couples to $\delta(N-H)$ and that the coupling vanishes upon protonation. However the pattern of isotopic shifts is too complicated to be reasonably explained at the present stage. The RR band at 1362 cm^{-1} for OEBV-h$_3$ in Figure IV-3A slightly shifts

upon $^{14}N/^{15}N$ substitution, but remarkably shifts upon methine and ethyl deuteration. These features indicate that this vibration has $\nu(C_\alpha C_m)$ and $\nu(C_\beta C_\beta)$ and/or $\nu(C_\alpha C_\beta)$ characters.

2. RR spectra of DHBV and Its Protonated Form.

Figures IV-7 and -8 show RR spectra of DHBV and protonated DHBV, respectively. In each Figure spectra (A), (B), (C) and (D) represent unlabeled-h_3, pyrrole-^{15}N-h_3, unlabeled-d_3 and pyrrole-^{15}N-d_3, respectively. The observed bands for DHBV and its protonated form have good correlations with those of OEBV and its protonated form, respectively, except for several additional bands of DHBV and its protonated form. This good correlation between the two systems implies that the vibrations involving the bond $C_\beta = C_\beta$ of A-ring do not significantly couple to other vibrations. However, the relative intensities of the observed bands fairly change upon the A-ring reduction. It suggests that the molecular structure in B_x and/or B_y excited states in the OEBV and DHBV systems is different. The correlations of RR band frequencies OEBV, DHBV and their protonated forms and their possible assignments are summarized in Tables IV-I and -II.

IV-4. Conclusion

The in-plane skeletal modes observed for OEBV, DHBV and their protonated forms can be reasonably assigned with the aid of the isotopic shifts of ^{15}N, methine-d_3 and methylene-d_{28} isotopomers. The large effects of methylene deuteration on the RR spectra for these species indicated that the RR spectra contain several bands due to modes which are assignable to the ethyl substituents. This feature was previously pointed out for $Ni^{II}(OEP)$. The RR spectra of DHBV and protonated DHBV show features common to those of OEBV and protonated OEBV, respectively. This commonness suggests that the vibrational modes involving the $C_\beta = C_\beta$ bond of A-ring do not significantly couple with other Raman active modes.

72

References

(1)   Gantt, E. *Ann. Rev. Plant Physiol.* **1981**, *32*, 327-347.

(2)   (a) Furuya, M. Ed. In *Phytochrome and Photoregulation in Plants*; Academic Press, Tokyo, 1987. (b) Lagarias, J. C. *Photochem. Photobiol.* **1985**, *42*, 811-820. (b) Song, P.-S. *J. Photochem. Photobiol.* **1988**, *48*, 833-841. (c) Cordonnier, M.-M. *Photochem. Photobiol.* **1989**, *49*, 821-831.

(3)   Fodor, S. P.; Lagarias, J. C.; Mathies, R. A. *Photochem. Photobiol.* **1988**, *48*, 129-136.

(4)   Hermann, G.; Muller, E.; Werncke, W.; Pfeiffer, M.; Kim, M.; Lau, A. *Biochem. Physiol. Pflanzen* **1990**, *186*, 135-143.

(5)   Fodor, S. P.; Lagarias, J. C.; Mathies, R. A. *Biochemistry* **1990**, *29*, 11141-11146.

(6)   (a) Rospendowski, B. N.; Farrens, D. L.; Cotton, T. M.; Song, P.-S. *FEBS Lett.* **1989**, *258*, 1-4. (b) Farrens, D. L.; Holt, R. E.; Rospendowski, B. N.; Song, P.-S. *J. Am. Chem. Soc.* **1990**, *111*, 9162-9169.

(7)   (a)Siebert, F.; Grimm, R.; Rüdiger, W.; Schmidt, G.; Scheer, H. *Eur. J. Biochem.* **1990**, *194*, 921-928.

(8)   (a) Tokutomi, S.; Mizutani, Y.; Anni, H.; Kitagawa, T. *FEBS Lett.* **1990**, *269*, 341-344. (b) Mizutani, Y.; Tokutomi, S.; Aoyagi, K.; Horitsu, K.; Kitagawa, T. *Biochemistry* **1991**, *30*, 10693-10722.

(9)   Szalontai, B.; Gombos, Z.; Csizmadia, V.; Lutz, M. *Biochim. Biophys. Acta* **1987**, *893*, 296-304.

(10)   Swatzki, J.; Fischer, R.; Scheer, H.; Siebert, F. *Proc. Natl. Acad. Sci. U.S.A.* **1990**, *87*, 5903-5906.

(11)   Schneider, S.; Baumann, F.; Klüter, U. *Z. Naturforsch* **1987**, *42C*, 1269-1274.

(12)   Inhoffen, H. H.; Fuhrhop, J.-H.; Voigt, H.; Brockmann, H., Jr. *Ann. Chem.* **1966**, *695*, 133-138.

(13)   Bonnett, R.; Dimsdale, M. J. *J. Chem. Soc., Perkin Trans. I* **1972**, 2540-2544.

(14)   Bonnett, R.; Gale, I. A. D.; Stephenson, G. F. *J. Chem. Soc. C* **1967**, 1169-1171.

(15)   Whitlock, H. W. Jr.; Hanauer, R.; Oestrer, M. Y.; Bower, B. Y. *J. Am. Chem. Soc.* **1969**, *91*, 7485-7489.

(16)   Cavaleiro, J. A. S.; Smith, K. M. *J. Chem. Soc. Perkin Trans. I* **1973**, 2149-2155.

(17)   Margulies, L.; Stockburger, M. *J. Am. Chem. Soc.* **1979**, *101*, 743-744.

(18)   Sheldrick, W. S. *J. Chem. Soc. Perkin Trans. II* **1976**, 1457-1463.

(19) Miyazawa, T. *J. Mol. Spectrosc.* **1960**, *23*, 865-871.

(20) Li, X.-Y.; Czernuszewicz, R. S.; Kincaid, J. R.; Stein, P.; Spiro, T. G. *J. Phys. Chem.* **1990**, *94*, 47-61.

Table IV-I. The correlation of RR bands between OEBV-h$_3$ and DHBV-h$_3$ and their posible assignments.

OEBV-h$_3$	DHBV-h$_3$	assignments
1699	1706	$\nu(C=O)$
1617	1619	in-phase skeletal stretch
1531	1537	$\nu(C_\alpha C_\beta), \nu(C_\beta C_\beta)$
1467	1470	
1431		$\nu(C_\alpha N), \nu(C_\alpha C_m)$
1405	1411	
1383	1381	
1362	1362	$\nu(C_\alpha C_\beta), \nu(C_\beta C_\beta), \nu(C_\alpha C_m)$
	1331	
1305	1311	CH$_2$ wagging
1275	1280	$\delta(C_m\text{-H})$
1256	1261	
1230	1234	$\delta(C_m\text{-H})$
1171		$\nu(C_\alpha N)$
1147	1148	$\nu(C_\alpha N)$
1124	1125	$\nu(C_\alpha C_\beta), \nu(C_\beta C_1)$
1101	1101	$\nu(C_\alpha N)$
1018	1019	$\nu(C_1 C_2)$

75

Table IV-II. The correlation of RR bands between OEBV-h_4^+ and DHBV-h_4^+ and their posible assignments.

OEBV-h_4^+	DHBV-h_4^+	assignments
1713	1706	$\nu(C=O)$
1616	1619	in-phase skeletal stretch
1533	1540	$\nu(C_\alpha C_\beta)$, $\nu(C_\beta C_\beta)$
1470	1475	
1380	1380	
1362	1365	$\nu(C_\alpha C_\beta)$, $\nu(C_\beta C_\beta)$, $\nu(C_\alpha C_m)$
	1337	
1309	1312	CH_2 wagging
1280	1282	$\delta(C_m\text{-}H)$
1262	1264	
1241	1241	$\delta(C_m\text{-}H)$
1171		
1147	1149	
1122	1125	$\nu(C_\alpha C_\beta)$, $\nu(C_\beta C_1)$
1105		
1094	1098	$\nu(C_\alpha N)$
1022	1023	$\nu(C_1 C_2)$
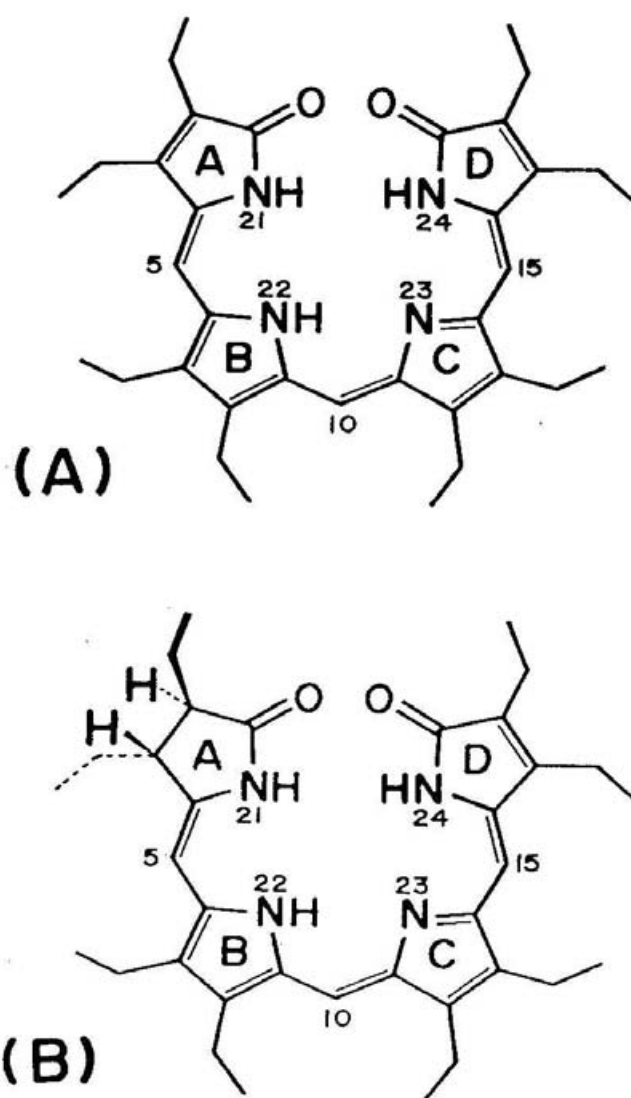
Figure IV-1. Molecular structures of OEBV (A) and DHBV (B).

77
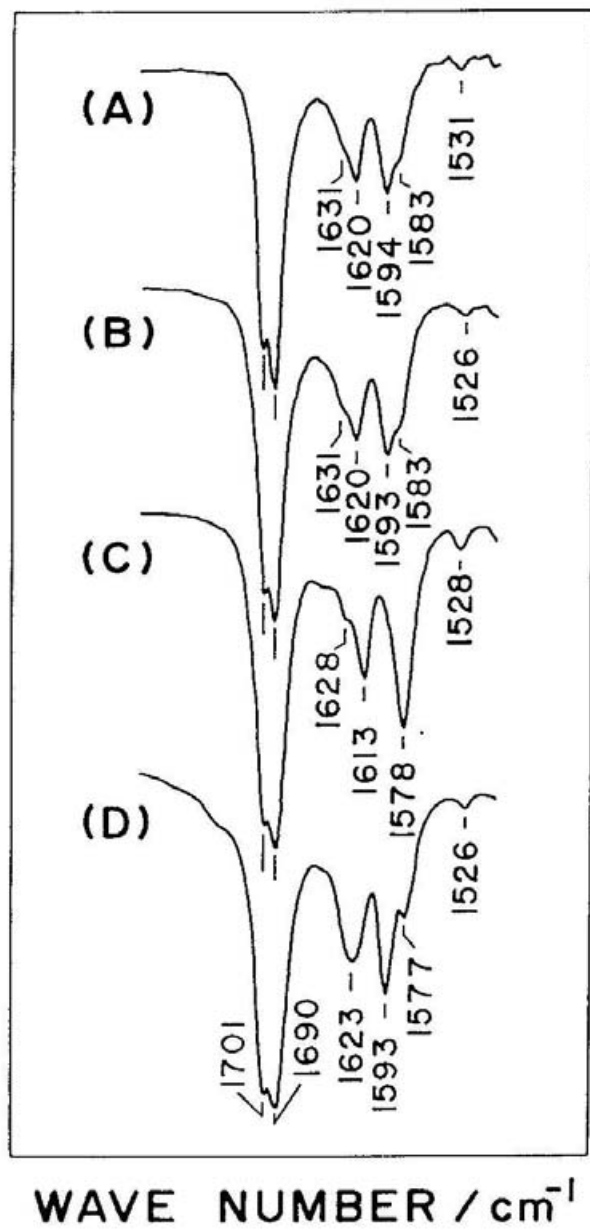
Figure IV-2. IR spectra of OEBV in KBr Pellet; unlabeled OEBV; (A): pyrrole-^{15}N; (B): methine-d_3; (C): ethyl-d_{28} derivatives (D).
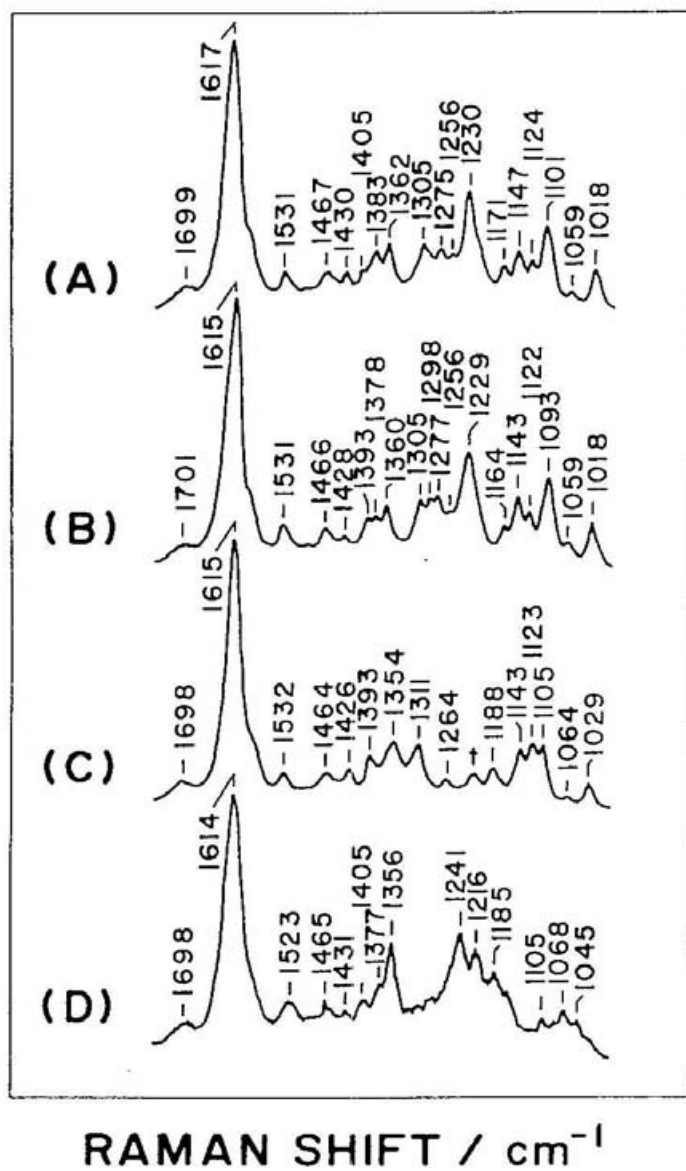
Figure IV-3. RR spectra of OEBV-h$_3$ in chloroform solution; unlabeled OEBV; (A): pyrrole-^{15}N; (B): methine-d$_3$; (C): ethyl-d$_{28}$ derivatives (D).

79
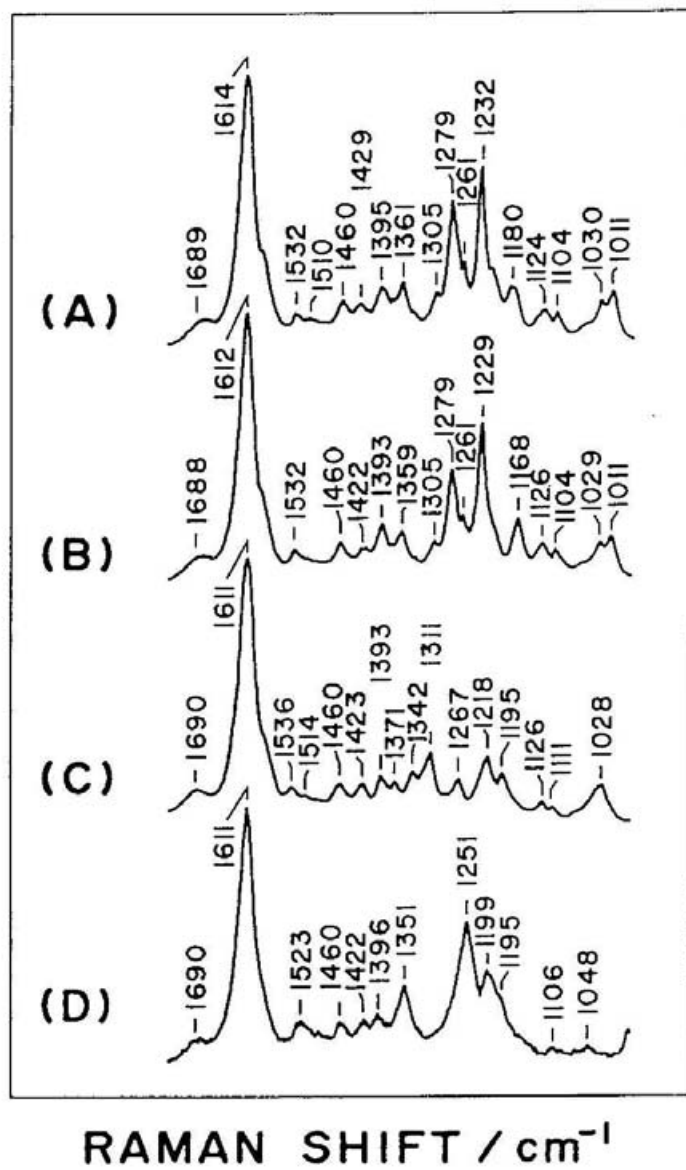
Figure IV-4. RR spectra of OEBV-d$_3$ in chloroform solution; unlabeled OEBV; (A): pyrrole-^{15}N; (B): methine-d$_3$; (C): ethyl-d$_{28}$ derivatives (D).
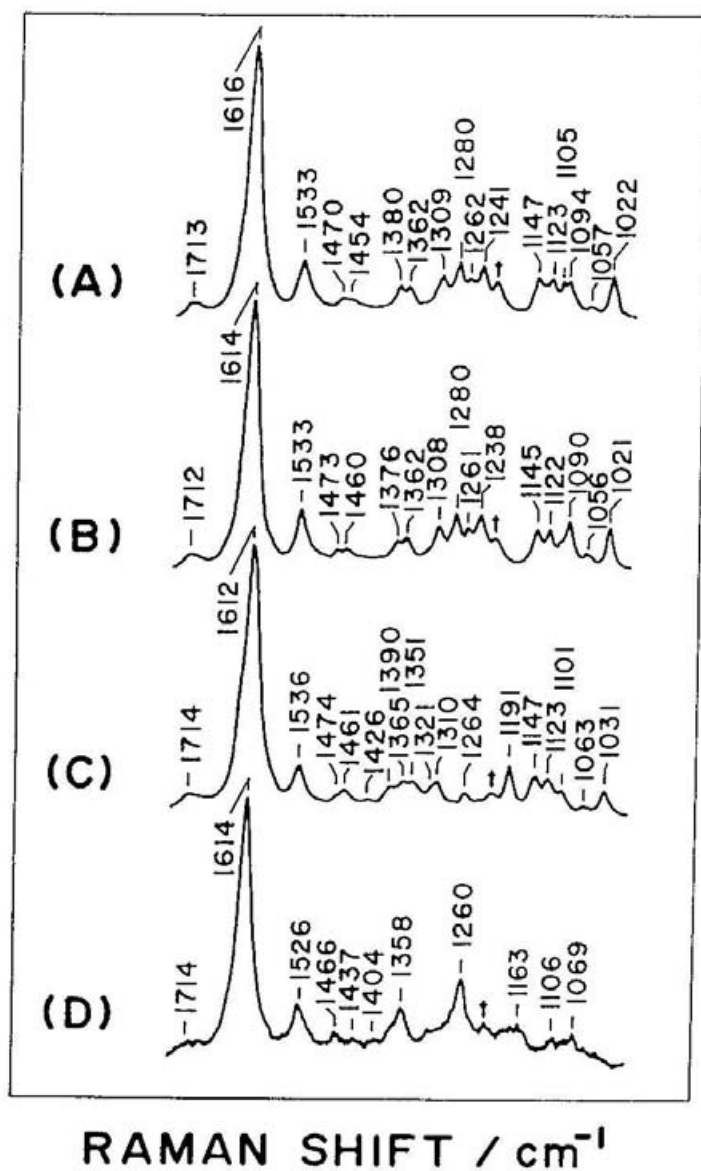
Figure IV-5. RR spectra of OEBV-h_4^+ in chloroform solution; unlabeled OEBV; (A): pyrrole-^{15}N; (B): methine-d_3; (C): ethyl-d_{28} derivatives (D).

81
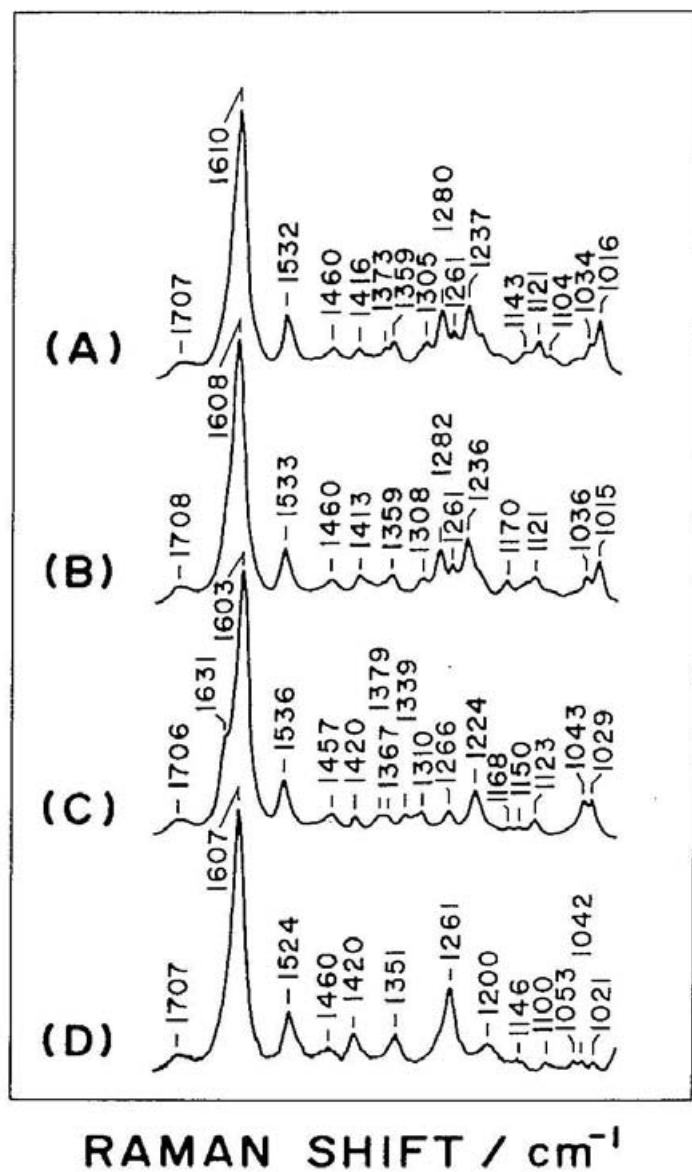
Figure IV-6. RR spectra of OEBV-d$_4$$^+$ in chloroform solution; unlabeled OEBV; (A): pyrrole-^{15}N; (B): methine-d$_3$; (C): ethyl-d$_{28}$ derivatives (D).

82

Figure IV-7. RR spectra of DHBV in chloroform solution; unlabeled-h$_3$; (A): pyrrole-^{15}N-h$_3$; (B): unlabeled-d$_3$; (C): pyrrole-^{15}N-d$_3$ derivatives (D).

Figure IV-8. RR spectra of protonated DHBV in chloroform solution; unlabeled-h$_4$$^+$; (A): pyrrole-^{15}N-h$_4$$^+$; (B): unlabeled-d$_4$$^+$; (C): pyrrole-^{15}N-d$_4$$^+$ derivatives (D).
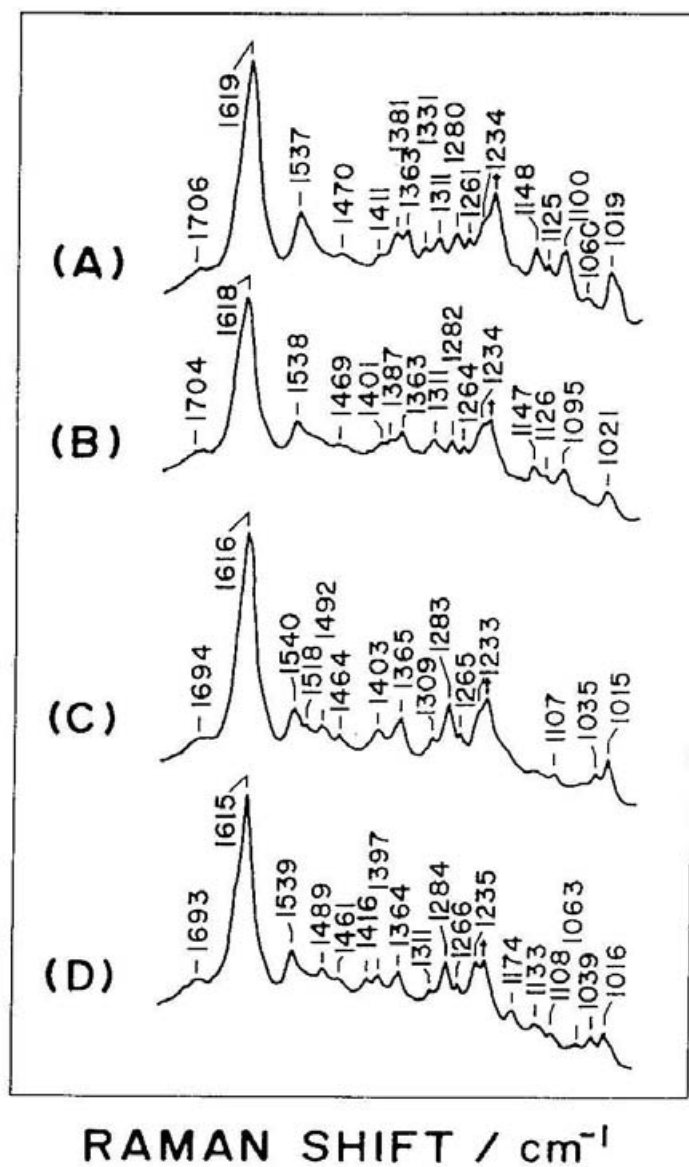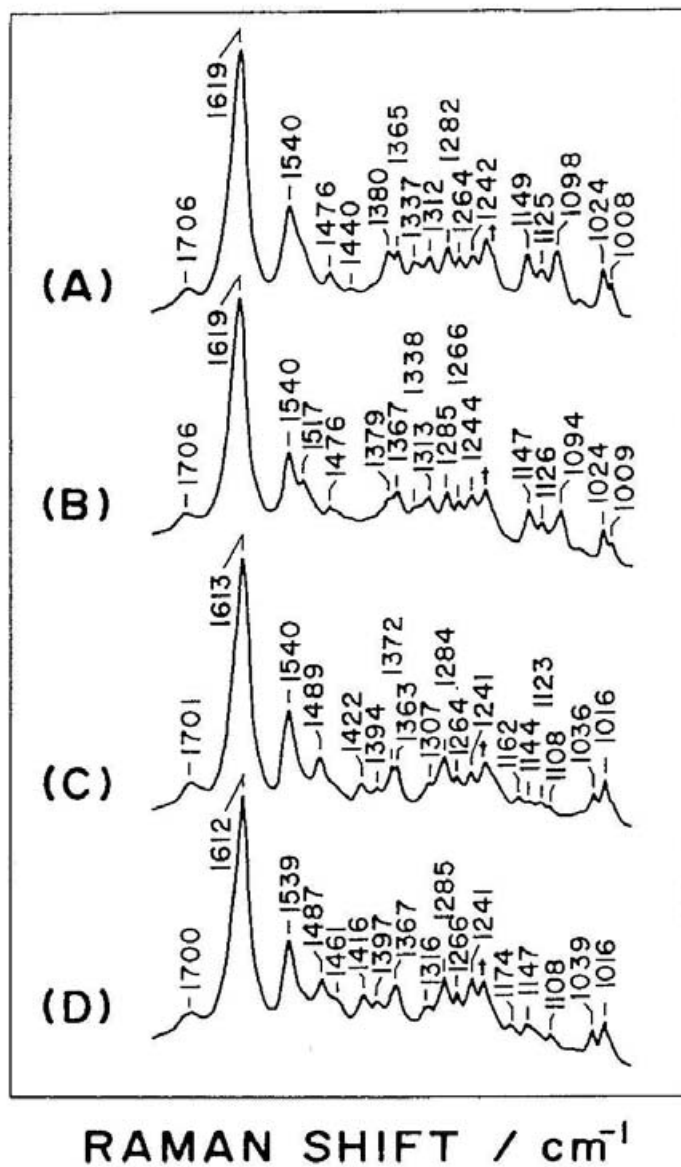
84

Chapter V

Ultraviolet Resonance Raman Spectra of Pea Phytochrome: A Difference Molecular Topography of the Red and Far-red Absorbing Forms

Abstract

Ultraviolet resonance Raman spectra excited at 244 nm by a CW laser were observed for pea intact and large phytochromes. At this excitation wavelength the spectra at pH 7.8 were dominated by bands assignable to tryptophan (Trp) and tyrosine (Tyr) residues and those at pH 9.0 were dominated by tyrosinate (Tyr⁻) residues besides them. The Trp W1 band of the protein was relatively weaker than that of stoichiometrically equivalent mixture of aromatic amino acids. This suggested that some Trp residues interact with tetrapyrrolic chromophore and/or other aromatic amino acids and that its B_b and/or L_a-L_b excited state was altered. The peak intensity ratio of Trp W7 doublet, $I(1360)/I(1340)$, of the red absorbing form (P_r) of both large and intact phytochromes was almost the same as that of aqueous amino acids solutions, while this ratio increased under red light illumination. The change in the ratio showed that most of the Trp residues are exposed on the surface in the P_r and that some of them locate in interior hydrophobic sites of the protein in the far-red absorbing form (P_{fr}) and in the bleached intermediate (I_{bl}). The Tyr⁻ contribution to the protein spectra was not as large as that in the amino acid solution. The small Tyr⁻ contribution indicated that the pK_a values of Tyr are raised by matrix effects, such as hydrogen bonding with surrounding amino acid residues and/or shielding from bulk environment.

V-1. Introduction

The photoreversible red/far-red light regulation of plant growth and development by phytochrome is the most extensively studied features among the photomorphogenetic receptor systems of plants.[1,2] In contrast to the accumulated knowledge about phototransformation between red absorbing (P_r) and far-red absorbing forms (P_{fr}) which initiates many photomorphogenetic responses in plant tissue, understanding about phytochrome-dependent signal transduction pathways is still poor. One approach to this problem has entailed identification and characterization of light-induced changes in the phytochrome molecule. The rationale for such experiments is that some of these active parts of the photoreceptor are likely to participate in the interaction with regulatory molecules and/or with components of the signal transduction pathway. Experiments with chemical modification reagents, monoclonal antibodies and protein-modifying enzymes have provided direct evidence for light-induced changes in phytochrome conformation. Although the chromophore structure of phytochrome has been widely investigated and the information about it has been accumulated,[3-6] much less is known about the protein moiety which would play a specific role in its function.

Ultraviolet resonance Raman (UVRR) spectroscopy has recently been shown to be a powerful technique for the investigation of the structural studies of proteins.[7-11] It has been reported that some resonant modes of aromatic amino acid residues are significantly altered by the protein microenvironment. Therefore, UVRR spectra of the aromatic residues allow us to probe the structural changes which occur in the protein under different physicochemical conditions. So far, studies of UV Raman spectra have been carried out by using pulsed UV light obtained from an Nd-YAG laser. However, in the pulse excitation the photon density per unit time of the excitation light is so high that molecule might be damaged by the laser irradiation. In contrast, the photon density in a light from a continuous wave (CW) laser is extremely low if it is compared with the pulse laser at the same average power. In this chapter, we report UVRR spectra of pea large and intact phytochromes obtained by the 244 nm line of a CW laser and will discuss a differential protein topography of P_r and P_{fr}.

V-2. Experimental Section

Phytochrome Preparation. Pea intact phytochrome (subunit molecular mass 121kDa) and pea large phytochrome (subunit molecular mass 114kDa) were isolated

from 7-day-old etiolated seedlings of pea (*Pisum sativum* cv. Alaska) as described previously.[12] The protein was precipitated by adding ammonium sulfate and resuspended in a 50 mM potassium phosphate and 1 mM Na_2EDTA buffer, pH 7.8 or a 50 mM CHES and 1 mM Na_2EDTA buffer, pH 9.0. The solution was dialyzed for complete removal of ammonium sulfate. This procedure was indispensable to prevent the sample from aggregation during Raman measurements. All the preparation procedures were carried out under dark or dim green light. The specific absorbance ratio (A_{667}/A_{280}) of the present sample was 0.90 for intact phytochrome and 0.98 for large phytochrome and its purity was estimated to be higher than 95% from SDS PAGE. The amino acids were purchased from Wako Pure Chemical Industries, Ltd. and used without further purification.

Measurements of UVRR spectra. Figure V-1 shows the CW UVRR measurement system. The 488 nm line (6-7W) of a high power Ar^+ ion laser (Spectra Physics, 2045) was focused on a β-BaB_2O_4 crystal to generate the second harmonic. The angle of the crystal against the laser axis was adjusted for phase matching. The 244 nm light was led to the sample point after it was separated from fundamental line by a Pellin Broca prism. The 244 nm light was focused by two cylindrical lenses on the sample. Fifty microliters of the phytochrome solution with the concentration of 8.0 cm^{-1} in terms of A_{667} in the P_r form, which corresponded to 61 μM on the basis of $\epsilon_M = 1.32 \times 10^5$ cm^{-1} for the intact oat phytochrome, was put into an ESR tube (diameter = 5 mm), span at 1600 rpm and kept at 16±3 °C by flushing with cold N_2 gas. The sample solution in the spinning cell was illuminated with either far-red light (740 nm) or red (660nm) light during UV light irradiation in order to bias the equilibrium of the photo-steady state toward P_r or P_{fr}, respectively. Farred or red light was obtained by passing the radiation from a 300 W tungsten lamp through a 660 or a 740 nm interference filter and ca. 10 mm path of water. Raman scattered light was dispersed by a double monochromator (Spex 1403) and detected with an intensified photodiode array (PAR, 1421HQ). The data were processed with an OMA system (PAR 1460). Raman shifts were calibrated with cyclohexane.

V-3. Results

Figure V-2 shows UVRR spectra of pea intact phytochrome at pH 7.8. The spectra A and B are obtained under far-red and red light illuminations, respectively. Under far-red illumination, most of the phytochrome is considered to be in the P_r

form, although UV probe light slightly induces phototransformation.[13] On the other hand, under red light illumination, the sample is a mixture of P_r and P_{fr}.

Figures V-3 and -4 show UVRR spectra of aqueous solutions of Trp, Tyr and Phe and their mixture at pH 7.8 and 9.0, respectively. Concentrations of each amino acid are different in accord with those of the protein, but the ordinate scales of three spectra are common. The amounts of these aromatic residues per monomer were estimated from the reported amino acid sequence[14] and the peptide map deduced from partial proteolysis[15] to be 10 Trp, 21 Tyr and 36 Phe for intact phytochrome and 10 Trp, 20 Tyr and 35 Phe for large phytochrome. The concentrations of each amino acid in the mixture are stoichiometrically equivalent to 61 μM solution of pea intact phytochrome. At pH 7.8, the spectrum of the amino acid mixture is dominated by bands of Trp and Tyr, but, at pH 9.0, an intense band at 1603 cm^{-1} due to Tyr$^-$ appears in the spectrum 4D, because Tyr$^-$ has a higher molar absorptivity than Trp, Tyr, Phe at 244 nm and is thus a better Raman scatterer at this excitation wavelength.[7c] A pair of Trp bands around 1360 cm^{-1} and 1340 cm^{-1} are known to arise from the Fermi resonance between one skeletal stretching fundamental and one or two combinations of the indole ring, and the intensity ratio $I(1360)/I(1340)$ is sensitive to the ring environment[11a,b]: the intensity ratio increases as the hydrophobicity around the indole ring increases. At pH 9.0, the band widths of the doublet broaden.

All the major features in Figure V-2 except for the amide I band around 1660 cm^{-1} derive from Trp and Tyr. From the comparison of the spectra of phytochrome with those of the corresponding amino acid solutions, it is evident that the intensity of the 1621 cm^{-1} band is relatively weak in the spectra of the protein. This can be ascribed to the intensity decrease in the Trp W1 band relative to other bands. Trp has absorption maxima at ca. 280, 220 and 195 nm. The 280 and 220 nm bands are considered to be derived from two overlapping $\pi \rightarrow \pi^*$ transitions to the L_a and L_b excited states and to the B_b excited state, respectively.[16] The UVRR spectra in resonance with the B_b excited state give a weaker W1 band than those in resonance with the L_a-L_b excited states. Therefore, the decrease in the peak intensity ratio of W1 to W3, $I(W1)/I(W3)$, upon excitation at 244 nm indicates a redshift of the B_b absorption and/or L_a-L_b absorption of Trp. P_r is phototransformed to P_{fr} by the 290-nm excitation. This is due to an energy transfer from Trp* to the tetrapyrrole.[13a] From this fact, it is deduced that some Trp residues interact with the tetrapyrrolic chromophore. Accordingly, the decrease in the $I(W1)/I(W3)$ intensity ratio can be ascribed to the

interaction between Trp and tetrapyrrole chromophore in part.

Recently, a relation between the Trp W3 frequency near 1550 cm^{-1} and the absolute value of the torsional angle $|\chi^{2,1}|$ around the C_β-C_3 bond has been established;[11c] its frequency increases monotonously from 1542 cm^{-1} for the angle of 61° to 1557 cm^{-1} for 117°. The W3 frequency and the band width are not affected by phototransformation. This indicates that the average of each $|\chi^{2,1}|$ is around ±102° in the P_r and remains practically unchanged in the P_{fr} even though the environment of some Trp is altered.

The W7 doublet of Trp sensitively reflects the ring environment.[11a] The ratio $I(1360)/I(1340)$ in Figure V-3A is almost the same as that for the aqueous Trp solution, which indicates the environments of most Trp side chains in P_r are hydrophilic. The ratio slightly increases upon the phototransformation. The increase in the ratio indicates that the conformational change makes the environments of some Trp side chains hydrophobic.

Figure V-5 shows UVRR spectra of pea large phytochrome, which lacks 6-kDa N-terminal polypeptide from Ser-1 to Ser-51 compared with the intact phytochrome.[15] Under red light illumination, the accumulation of the bleached intermediate, I_{bl}, besides P_r and P_{fr}, is observed in the photo-steady state for pea large phytochrome, especially at alkaline pH.[17] The characteristics of W1, W3 and W7 bands described above are unaltered between the spectra of large and intact phytochromes. The ratio, $I(1360)/I(1340)$, in Figure V-5B is similar to that in Figure V-2B, although the sample solution contains I_{bl} for large phytochrome under red light illumination. This suggests that the environmental change of indole rings already occurs in I_{bl} on P_r to P_{fr} phototransformation.

UVRR spectra of pea large phytochrome at pH 9.0 are shown in Figures V-5C and 5D. The contribution of the Tyr⁻ band at 1600 cm^{-1} is not so significant in Figure V-5 compared to that in Figure V-4D. Tyr in the protein has their pK_a value elevated significantly from the value found in aqueous solution. This suggests that most Tyr's locate in the interior of the protein both in the P_r, I_{bl} and the P_{fr}. In contrast to Tyr, the Trp W7 band of the protein shows a pH dependence as same as that of amino acid solutions. This also suggests that most Trp locates on the surface of the protein and contacts with bulk water and is consistent with the result that the environments of Trp side chains in the P_r are hydrophilic.

V-4. Discussion

There are some clearly recognizable conformational changes in the phototransformation of phytochrome. A 3% increase in α-helix is detected by CD measurement upon photoconversion of intact phytochrome to P_{fr}, which is not observed for large phytochrome.[18] cAMP-dependent protein kinase was also used to probe the differentially accessible sites on oat phytochrome.[19]

The present result of the Trp W7 doublet shows that most Trp residues are exposed on the surface in P_r and that some of them are placed in interior hydrophobic site of the protein in P_{fr}. Song and his coworkers have investigated Trp fluorescence quenching of oat phytochrome.[15] They reported that Trp residue(s) in P_{fr} are more accessible to the cationic quencher than those in the P_r. From this result, they deduced that a photoreversible alternation in the folding of the protein occurs in such a way that either the fluorescent Trp residues become more exposed to the surface or the environment around the Trp residues become more negatively charged, or both. The present result of the Trp W7 doublet seems to be incompatible with their interpretation, at least, the former of the two.

Peptide maps for intact pea and oat phytochromes show that the protein has one small and two large domains: the N-terminal domain of about 6 kDa, the chromophore domain of about 62 kDa and the C-terminal side domain of about 53 kDa, while it was deduced from partial proteolysis. It turned out that the N-terminal sequence on the chromophore domain is extremely susceptive to proteolysis in P_r but not in P_{fr}. Since the N-terminal 6kDa polypeptide does not involve Trp,[14] the spectral change of Trp upon the phototransformation is not due to the conformational change of the segment. The conformational changes are reported for the chromophoric and C-terminal domains, which contain 6 and 4 Trp's, respectively. The environmental changes, detected by quenching of the Trp fluorescence, appear to be in the chromophoric domain,[13] while it is suggested that the C-terminal hydrophobic domain is responsible for the photo-induced increase in hydrophobicity.[20] At the present stage, we can not say anything which conformational change is associated with the environmental change of Trp upon phototransformation. It is desirable to compare the results of small phytochrome, which has the only chromophoric domain, in order to specify the Trp whose environments are altered.

In conclusion, the data presented above provide new informations about the environments of amino acids residues which are summerized as follows. (i) While

91

almost Trp's are on the surface of the protein in P_r, some of them are in the interior in P_{fr}. (ii) Most of the Tyr residues in either P_r or P_{fr} or I_{bl} are in the interior and are not significantly affected by bulk pH. This insensitivity indicates that they have pK_a values elevated from the values in aqueous solutions.

References

(1)   Furuya, M., Ed. In *Phytochrome and Photoregulation in Plants*; Academic Press: New York, 1987.

(2)   (a) Lagarias, J. C. *Photochem. Photobiol.* **1985**, *42*, 811-820. (b) Song, P.-S. *Photochem.Photobiol.* **1988**, *48*, 833-841. (c) Cordonnier, M.-M. *Photochem.Photobiol.* **1989**, *49*, 821-831.

(3)   Lagarias, J. C.; Rapoport, H. *J. Am. Chem. Soc.* **1980**, *102*, 4821-4828.

(4)   (a) Fodor, S. P.; Lagarias, J. C.; Mathies, R. A. *Photochem. Photobiol.* **1988**, *48*, 129-136. (b) Fodor, S. P.; Lagarias, J. C.; Mathies, R. A. *Biochemistry* **1990**, *29*, 11141-11146.

(5)   Siebert, F.; Grimm, R.; Rüdiger, W.; Schmidt, G.; Scheer, H. *Eur. J. Biochem.* **1990**, *194*, 921-928.

(6)   (a) Tokutomi, S.; Mizutani, Y.; Anni, H.; Kitagawa, T. *FEBS Lett.* **1990**, *269*, 341-344. (b) Mizutani, Y.; Tokutomi, S.; Aoyagi, K.; Horitsu, K.; Kitagawa, T. *Biochemistry* **1991**, *30*, 10693-10722.

(7)   (a) Rava, R. P.; Spiro, T. G. *J. Am. Chem. Soc.* **1984**, *106*, 4062-4064. (b) Rava, R. P.; Spiro, T. G. *Biochemistry* **1985**, *24*, 1861-1865. (c) Rava, R. P.; Spiro, T. G. *J. Phys. Chem.* **1985**, *89*, 1856-1861.

(8)   (a) Johnson, C. R.; Ludwig, M.; O'Donnell, S.;Asher, S. A. *J. Am. Chem. Soc.* **1984**, *106*, 5008-5010. (b) Asher, S. A.; Ludwig, M.; Johnson, C. R. *J. Am. Chem. Soc.* **1986**, *108*, 3186-3197.

(9)   Bajdor, K.; Peticolas, W. L.; Wharton, C. W.; Hester, R. E. *J. Raman Spectrosc.* **1987**, *18*, 211-217.

(10)   Mayne, L.; Hudson, B. *J. Phys. Chem.* **1987**, *91*, 4438-4440.

(11)   (a) Harada, I.; Miura, T.; Takeuchi, H. *Spectrochim. Acta, Part A* **1986**, *42*, 307-312. (b) Miura, T.; Takeuchi, H.; Harada, I. *Biochemistry* **1988**, *27*, 88-94. (c) Miura, T.; Takeuchi, H.; Harada, I. *J. Raman Spectrosc.* **1989**, *20*, 667-671.

(12)   Tokutomi, S.; Kataoka, M.; Sakai, J.; Nakasako, M.; Tokunaga, F.; Tasumi, M.; Furuya, M. *Biochim. Biophys. Acta* **1988**, *953*, 297-305.

(13)   Yamamoto, K. T.; Tokutomi, S. *Photochem. Photobiol.* **1989**, *50*, 113-120.

(14)   (a) Sarkar, H. K.; Song, P.-S. *Biochemistry* **1982**, *21*, 1967-1972. (b) Singh, B. R.; Chai, Y. G.; Song, P.-S.; Lee, J.; Robinson, G. W. *Biochim. Biophys. Acta* **1988**, *936*, 395-405.

(15) Sato, N. *Plant Mol. Biol.* **1988**, *11*, 697-710.

(16) Yamamoto, Y.; Tanaka, J. *Bull. Chem. Soc. Jpn.* **1972**, *45*, 1362-1366.

(17) Tokutomi, S.; Inoue, Y.; Sato, N.; Yamamoto, K. T.; Furuya, M. *Plant Cell Physiol.* **1986**, *27*, 765-773.

(18) (a) Vierstra, R. D.; Hahn, T.-R.; Song, P.-S. *Photochem. Photobiol.* **1987**, *45*, 429-432. (b) Tobin, E. M.; Briggs, W. R. *Photochem. Photobiol.* **1973**, *18*, 487-495.

(19) (a) Wong, Y.-S.; Cheng, H.-C.; Walsh, D. A.; Lagarias, J. C. *J. Biol. Chem.*, **1986**, *261*, 12089-12097. (b) McMichael, R. W., Jr.; Lagarias, J. C. *Biochemistry* **1990**, *29*, 3872-3878.

(20) Tokutomi, S.; Yamamoto, K. T.; Furuya, M. *FEBS Lett.*, **1981**, *134*, 159-162.
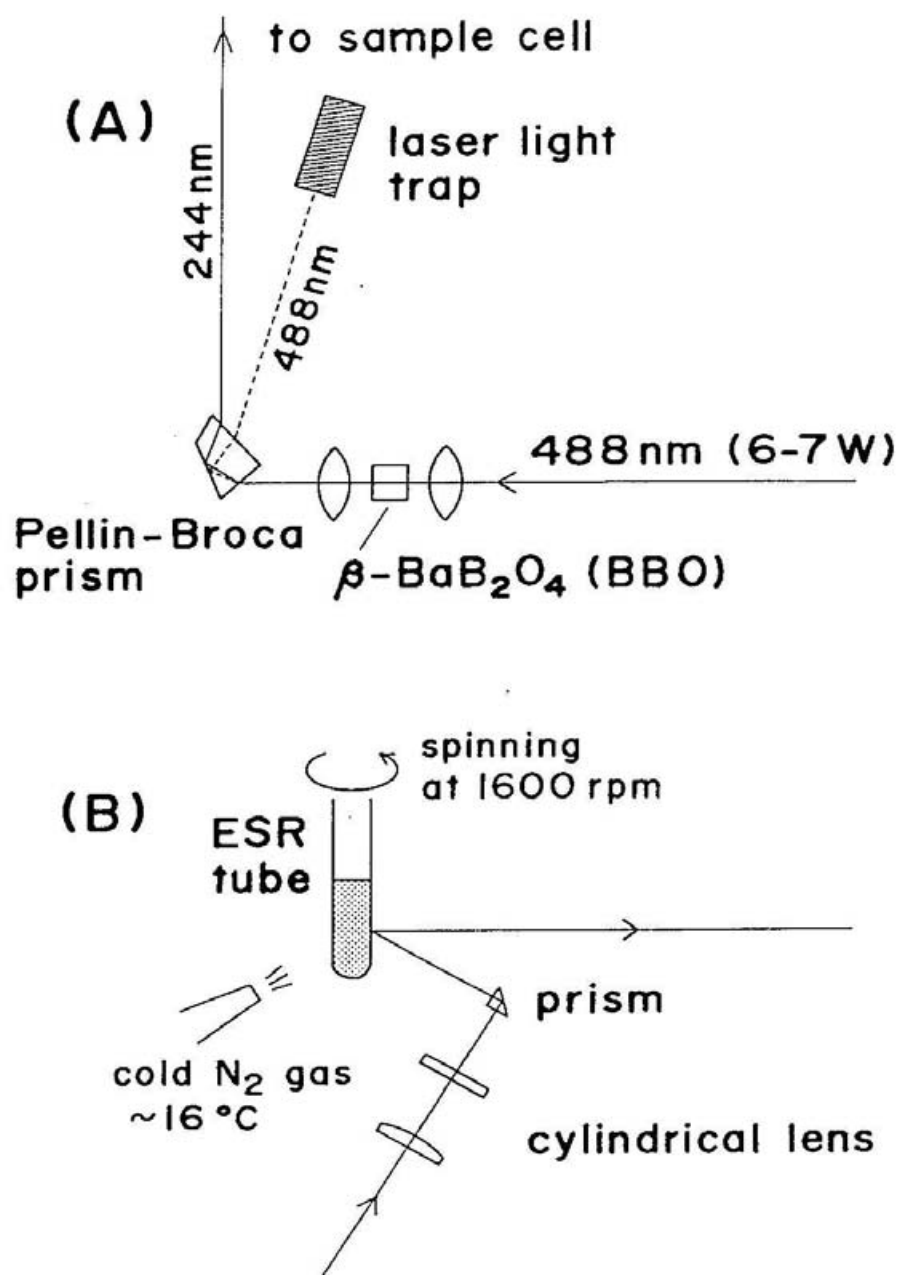
Figure V-1. Diagrams of the measurement system for CW-UV-laser-excited RR spectra. (A): Generation of second harmonic (244 nm) and separation from fundamental line (488 nm); (B) sample cell and laser-light irradiating geometry.
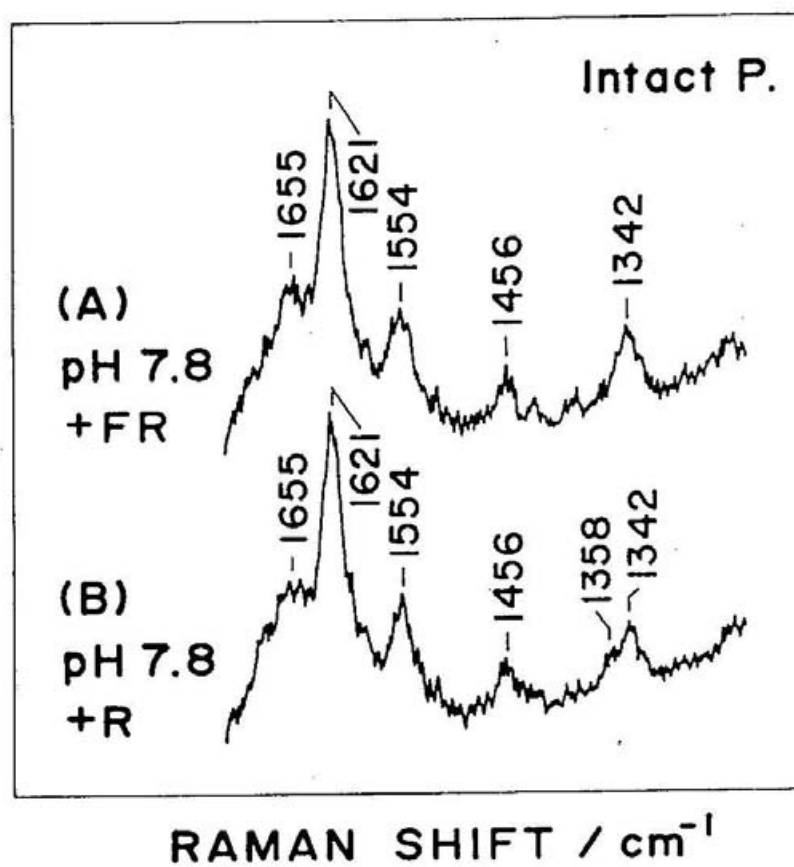
Figure V-2. UVRR spectra of intact pea phytochrome at pH 7.8. Spectra (A) and (B) are obtained under far-red and red light illumination, respectively.
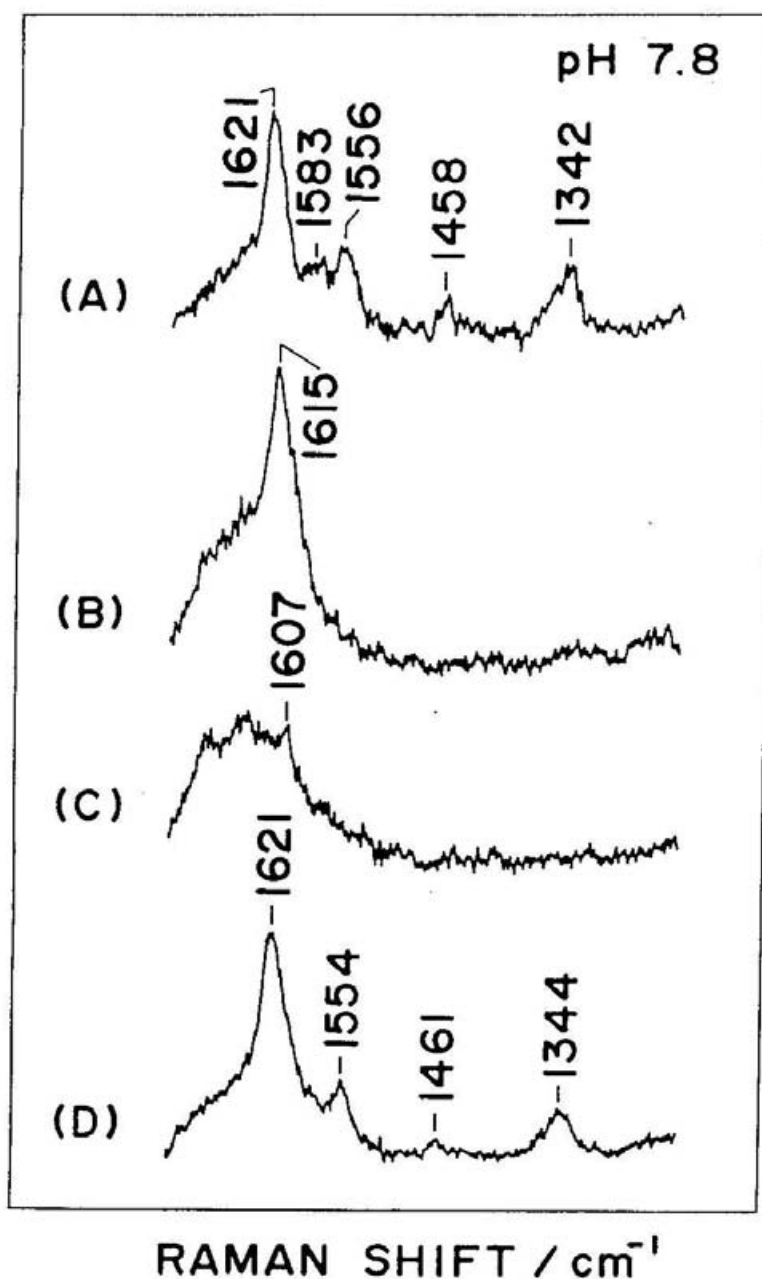
Figure V-3. UVRR spectra of aqueous solution of aromatic amino acids at pH 7.8: Trp (A), Tyr (B), Phe (C) and their mixture (D). The concentrations of each amino acids are 0.61, 1.32 and 2.20 mM for Trp, Tyr and Phe, respectively. The concentrations are stoichiometrically equivalent to that of 61 μM solution of pea intact phytochrome. Spectra (A-C) are represented in common scale.

97
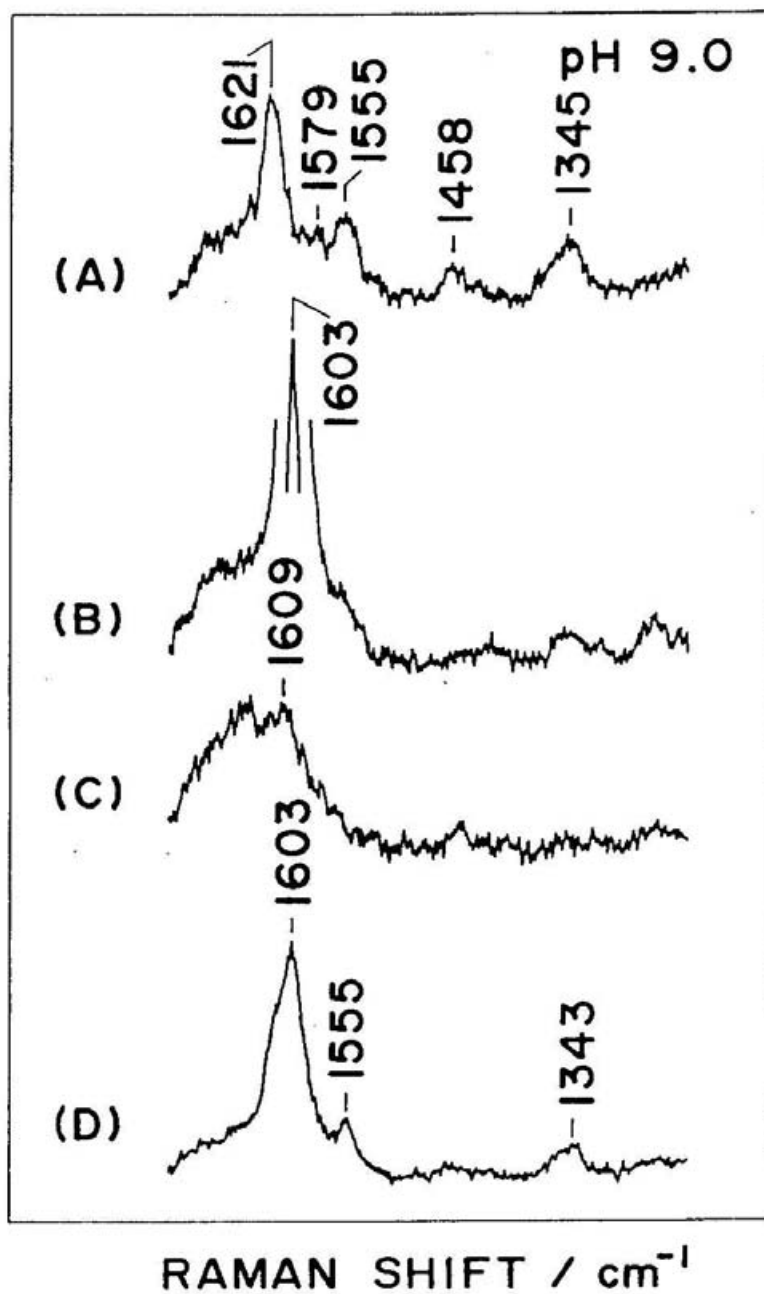
Figure V-4. UVRR spectra of aqueous solution of aromatic amino acids at pH 9.0: Trp (A), Tyr (B), Phe (C) and their mixture (D). The concentration of each amino acids are same as Figure V-2. Spectra (A-C) are represented in common scale.

98
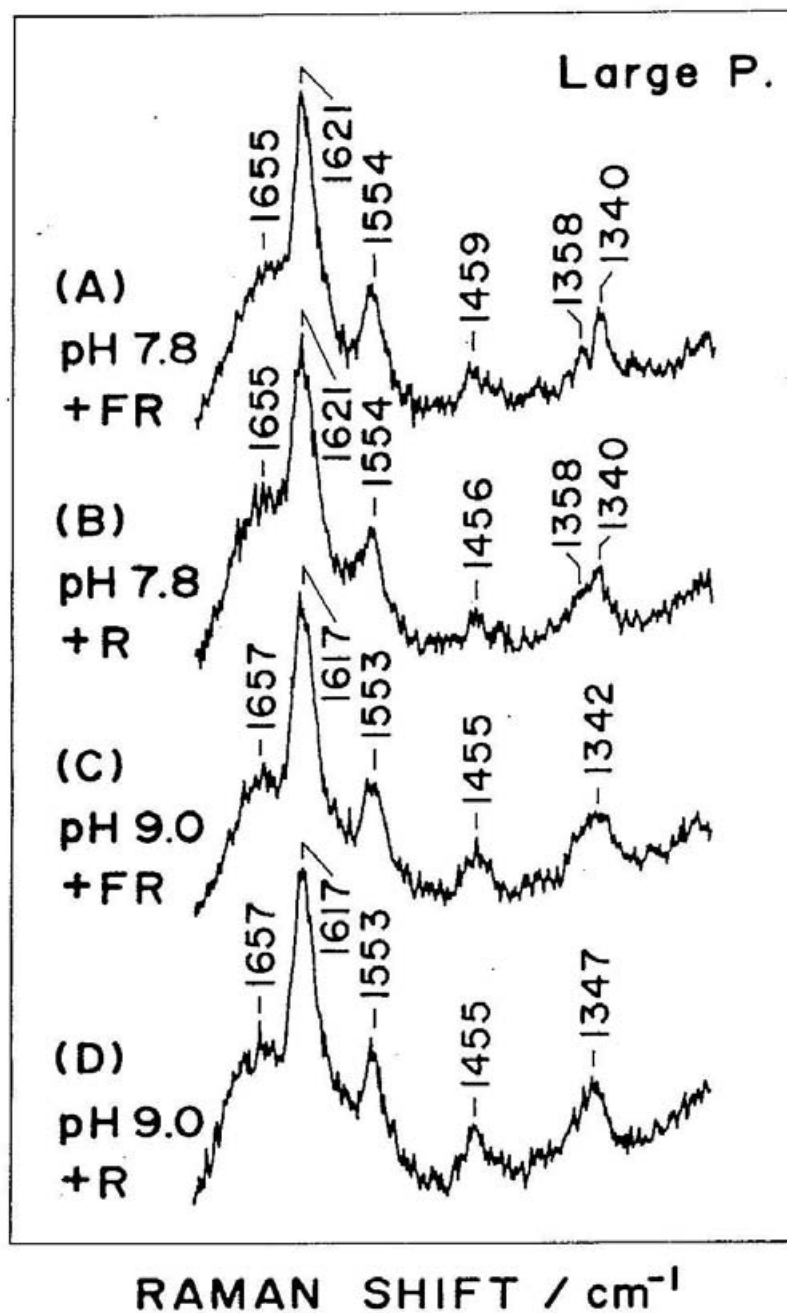
Figure V-5. UVRR spectra of large phytochrome at pH 7.8 (A and B) and at pH 9.0 (C and D). Spectra (A) and (C) are obtained under far-red illumination, and spectra (B) and (D) are obtained under red light illumination.

Part II

Resonance Raman Studies on Iron Porphyrins
in Higher Oxidation States

Chapter I

Overview: Resonance Raman Studies on Metalloporphyrins

I-1. Resonance Raman Spectra of Metalloporphyrins

The resonance Raman (RR) scattering from metalloporphyrins has inspired intense research activity over the past two decades.[1] Biochemical interest has stimulated much of this work, and indeed the first metalloporphyrin spectra were obtained for heme proteins.[2,3] These studies revealed novel spectroscopic phenomena which were of considerable theoretical interest. Structured excitation profiles were discovered and some RR bands were found to exhibit the anomalous polarization.[4]

One of the significance of RR studies on metalloporphyrins is related to hemeprotein biochemistry, where an axiom is that molecular structure determines how these proteins work. Chemical curiosity is stimulated by the heme group in common with these proteins despite of a variety of chemistry involved. When iron porphyrin moieties are captured by different polypeptides, a variety of redox reactions can be performed in various biological systems. Special attention is given to hemoglobin (Hb), an oxygen carrier, particularly because of its cooperative oxygen binding. The electron-carrying cytochrome c has also been intensively studied. Oxygen utilization by enzymes such as cytochrome P-450 (organic substrate oxygenation) and cytochrome c oxidase (reduction of oxygen to water coupled with proton pumping) is also very important.

The earlier heme protein studies revealed vibrational frequency shifts associated with the ligation chemistry of the heme group.[5-7] Subsequent works have uncovered useful structure-spectra correlations, including sensitivities of specific band frequencies to the porphyrin core size,[8-10] and to the ligation, oxidation and spin state of the central metal ion.[1c] In physiological reactions of heme proteins, porphyrins in higher oxidation states such as oxyferrous and oxoferryl species, and π cation radicals are particularly important. In order to investigate these complexes by RR spectroscopy, the iron-oxygen and oxygen-oxygen stretching bands and porphyrin in-plane stretching bands reflecting the radical character may serve as key bands to provide us new insights into porphyrin chemistry. In this chapter, RR studies on metalloporphyrins in higher oxidation states, that is, oxyferrous and oxoferryl species and π cation radicals, are reviewed with special attention to possible key bands.

I-2. Oxygenated Complexes of Iron-porphyrins

Elucidation of the molecular mechanism of biological dioxygen activation by heme proteins has been the focus of sustained attention.[11] The most intensely investi-

gated dioxygen complexes are oxyhemoglobin (HbO_2) and oxymyoglobin (MbO_2). Dioxygen adducts have also been found as intermediates in the catalytic cycles of cytochrome c oxidase[12] and cytochrome P-450.[13]

Considerable interest has been centered also on dioxygen adducts of iron porphyrins without proteins. Many model complexes that reversibly bind O_2 have been synthesized to understand the influence of the steric, electronic and environmental factors on dioxygen binding in heme proteins. In general, oxyferrous porphyrins are unstable at room temperature and easily autoxidized to ferric species. Since "protected" porphyrins[11a,14] such as picket-fence and capped porphyrins were found to bind O_2 reversibly at room temperature, many spectroscopic techniques have been applied to oxygenated complexes of these protected iron-porphyrins.

The applicability of resonance Raman spectroscopy to study dioxygen binding to heme proteins and their model compounds has been demonstrated by many investigators.[15] In a favorable case, where a charge-transfer band between oxygen and iron ion is present in the wavelength region accessible by available laser lines, it facilitates the direct observation of the resonantly enhanced vibrational modes associated with the metal-dioxygen linkage. Thus, spectral features associated with $\nu(O_2)$ and $\nu(Fe^{II}\text{-}O_2)$ vibrations have been identified in RR spectra and definitive assignments of these key modes have been established with the aid of isotopically labeled compounds. Historically, the first observation of the $\nu(Fe^{II}\text{-}O_2)$ band was made for HbO_2 at 567 cm^{-1} by Brunner.[16] Burke et al.[17] obtained a virtually identical frequency in the RR spectrum of the oxy iron "picket-fence" porphyrin imidazole complex. However, this assignment was questioned by Benko and Yu[18] on the basis of the "isotopic zigzag pattern", which was similar to that obtained for the $\delta(Fe^{II}\text{-}CO)$ band of HbCO. These researchers preferred to assign it to the $\delta(Fe^{II}OO)$ band rather than to the $\nu(Fe^{II}\text{-}O_2)$ band. However, Bajdor et al.[19] have shown that the original assignment of the $\nu(Fe^{II}\text{-}O_2)$ by Brunner is correct since $Fe(Pc)O_2$ (Pc, phthalocyanato dianion) shows $\nu(Fe^{II}\text{-}O_2)$ and $\delta(FeOO)$ at 488 and 279 cm^{-1}, respectively. On the other hand, attempts to observe the $\nu(O_2)$ band of heme proteins by RR spectroscopy have not been successful except for those of oxygenated cytochrome P-450[13] and its model compounds containing axial thiolate ligands.[20] Very recently, Nakamoto and coworkers[21] have succeeded in simultaneous observation of the $\nu(O_2)$ and $\nu(Fe^{II}\text{-}O_2)$ bands of $Fe(TPP)O_2$ (TPP, tetraphenylporphyrin dianion) at 1195 and 509 cm^{-1}, respectively, for an O_2 matrix at ~30 K with Soret excitation (the structures of metalloporphyrins treated in this chap-

ter are depicted in Figure I-1).

I-3. Oxoferryl Complexes

The presence of oxoferryl porphyrins as a transient unstable species has been confirmed or postulated in the enzymatic cycles of peroxidase,[22] cytochrome c oxidase,[23] and cytochrome P-450.[11c] The electronic structures of oxoferryl compounds have been studied extensively by using various spectroscopic techniques. Mössbauer studies on peroxidase compound-I and compound-II showed that these compounds have low-spin ($S = 1$) iron (IV).[24]

In the last decade, efforts have been made to detect the $\nu(Fe^{IV}=O)$ RR band of oxoferryl species. The main difficulty in detecting this mode arises from thermally unstable and photolabile properties of the oxoferryl complexes. The pioneering work was carried out by Nakamoto and coworkers;[25] they first succeeded in the observation and characterization of the $\nu(Fe^{IV}=O)$ band (852 cm^{-1}) of (TPP)$Fe^{IV}=O$, (OEP)$Fe^{IV}=O$ (OEP, octaethylporphyrin dianion), and (Salen)$Fe^{IV}=O$ (salen, N,N'-ethylenebis(salicylideneiminato)), which were formed by laser photolysis of the corresponding dioxygen adducts in O_2 matrices at ~15 K. Since then several groups observed the $\nu(Fe^{IV}=O)$ RR band of oxoferryl porphyrin in heme proteins and their model complexes. In the case of horseradish peroxidase (HRP) compound I (see I-4), however, RR data presented by different researchers were inconsistent due to its inherent reactivity and photolability, and this has prevented unambiguous characterization of its π cation radical complex.[26-30]

I-4. Metalloporphyrin Cation Radicals

One electron oxidation of the porphyrin ring produces reasonably stable radical cations. The theory of porphyrin optical spectra developed by Gouterman and coworkers[31] indicates that the two HOMOs with the a_{1u} and a_{2u} symmetries are almost degenerate in the neutral species. Therefore, the π cation radical produced by electron abstraction from one or the other of these orbitals would lead to either an $^2A_{1u}$ or $^2A_{2u}$ ground state. As illustrated in Figure I-2, the nodal patterns and atomic coefficients are very different for these orbitals, and quite different radical properties can be expected, depending on which orbital contains the unpaired electron.

Metalloporphyrin π cation radicals have long been interested, particularly as models for intermediate states of redox-active heme proteins and of the reaction

center of photosynthetic organisms.[32] Especially, much attention is being devoted to catalases (CAT) and peroxidases (which are typified by horseradish peroxidase (HRP)). These two kinds of enzymes have some similarity; the resting enzymes contain the ferric iron and are oxidized by hydrogen peroxide. The primary greenish intermediate observed spectroscopically during this oxidation is so-called compound I, which has two electrons less than the parent ferrihemeprotein. One-electron reduction of compound I forms the brown-red second intermediate, compound II. While the first step in the catalytic cycle of these two enzymes is the same, *i.e.*, a two-electron oxidation, by hydrogen peroxide, to their compound I, the two enzymes then perform different functions. The Co^{III} OEP π cation radical was found to exhibit two different types of optical spectra which had been assigned to two different ground states of a_{1u} and a_{2u}, depending on the axial ligand.[33] Comparison of the optical spectra of HRP compound I and CAT compound I with those of the cobalt π cation radicals suggested that HRP compound I is typical of an $a_{2u}\pi$ cation radical state, whereas CAT compound I is in an a_{1u} state. Recent studies, however, suggested that optical spectra may not serve as a diagnosis to determine the electronic ground states of porphyrin π cation radicals.[34] More recently, it was demonstrated that the ground states of both Co^{III} OEPs are predominantly $^2A_{1u}$ based on the magnitudes of the meso proton hyperfine constants.[35]

RR spectroscopy has been applied to the cation radicals as well as magnetic resonance and absorption spectroscopies. Yamaguchi et al.[36] reported RR spectra of metalloporphyrin π cation radicals for the first time, which were electrochemically prepared from (TPP)Ms. This work, however, is not strictly relevant owing to the strong vibronic coupling and the altered substituent pattern of TPP which reduces its significance as a biological model for RR studies. Kim et al.[37] measured RR spectra of (OEP$^{+\cdot}$)M and reported an unexpected but interesting result that the shift direction of the ν_2 and ν_4 bands upon radical formation are opposite to those expected from simple orbital symmetry arguments. Babcock and his coworkers[38] discovered, however, that the reported a_{1u}-type MOEP$^{+\cdot}$. RR spectra were actually attributed to porphyrin diacid, which was produced as an impurity during radical preparation. In the subsequent paper Oertling et al.[39] obtained authentic RR spectra for (OEP$^{+\cdot}$)M species. The relationship between the shift directions of ν_2 and ν_4 and radical character is established by the most extensive study by Czernuszewicz et al.[40] The frequency shifts upon radical formation differ for OEP and TPP: in particular, ν_2 shifts up for the

OEP but down for the TPP complexes. These shift directions of ν_2 are consistent with those expected from MO descriptions, if the TPP radicals have an a_{2u} character, as generally accepted,[41] but the OEP radicals have an a_{1u} character. The attribution of some OEP radicals to a_{2u}, particularly Ni^{II}, Cu^{II}, and Co^{III} perchlorate adducts, was based on differences in optical absorption spectra.[42] But recently it is revealed that optical spectra are unlikely to be a reliable indicators of radical types as mentioned above. Czernuszewicz et al. also pointed out interesting characteristics of radical RR spectra; 1) π cation radicals show similar RR spectra with violet and yellow excitations contrary to nonradical porphyrins, 2) anomalously polarized bands appear in the ~ 1000-cm^{-1} region upon excitation near the Soret electronic transitions.

I-5. Problems to be Solved and Summary of Studies in Part II

We have the limited knowledge concerning $\nu(Fe^{II}\text{-}O_2)$, $\nu(O_2)$ and $\nu(Fe^{IV}=O)$ as described above. Especially there is no report for these bands of five-coordinated species in the solution state, which is indispensable to discuss the trans ligand effect on these bands. Moreover, the RR data for oxoferryl species are important to discuss the effect of ring oxidation on $\nu(Fe^{IV}=O)$ by comparing them with the data of the corresponding oxoferryl π cation radical (*vide infra*). Accordingly, we attempted to observe the vibrational bands of such five-coordinated species. The results are described in Chapter II. We make use of autoxidation of ferrous porphyrin at low temperatures to prepare oxyferrous and oxoferryl species, because we can obtain oxyferrous, oxoferryl species and other reaction intermediates sequentially by raising temperature. We used tetramesitylporphyrinatoiron complex ((TMP)Fe), which has bulky substituents and stabilizes oxyferrous and oxoferryl species. The autoxidation of (TMP)Fe was studied in detail by Balch et al[43] with NMR spectroscopy. In order to prepare the five-coordinated species, it is necessary to prepare a four-coordinated ferrous complex as starting material. Therefore, we adopted the sodium-contact reduction method, since it is otherwise hard to obtain pure trans-ligand-free ferrous porphyrin. We simultaneously observed $\nu(Fe^{II}\text{-}O_2)$ and $\nu(O_2)$ Raman bands at 1171 and 522 cm^{-1}, respectively, for $(TMP)Fe^{II}O_2$ in a toluene solution at -100°C and discussed a linear inverse correlation between $\nu(Fe^{II}\text{-}O_2)$ and $\nu(O_2)$ frequencies similar to that between $\nu(Fe^{II}\text{-}CO)$ and $\nu(CO)$. As for oxoferryl complex, the $\nu(Fe^{IV}=O)$ RR band was observed at 843 cm^{-1} and the trans-ligand effect on its frequency was discussed. Also, we revealed the photolability of the μ-peroxo complex, $(TMP)Fe^{III}OOFe^{III}(TMP)$.

108

We pointed out the abstraction of a hydrogen atom from solvent by oxoferryl species in the decay process of oxoferryl species.

The RR spectra of HRP compound I including the $\nu(Fe^{IV}=O)$ RR band has been controversial due to its photolability. Therefore, it is quite important to establish with a model system how RR spectra are altered by further oxidation of the $Fe^{IV}=O$ porphyrin and how the $Fe^{IV}=O$ band is affected by it. The effect on $\nu(Fe^{IV}=O)$ remains to be elucidated, although RR spectra of metalloporphyrins π cation radicals were reported for (TPP)M and (OEP)M complexes in which M = Co^{II}, Cu^{II}, Zn^{II}, Ni^{II}, Co^{III} and $V^{IV}=O$, and the RR spectral differences between a_{1u} and a_{2u} radicals have been established.[40] Since metalloporphyrin π cation radicals so far studied were electrochemically prepared, it was difficult to prepare oxoferryl π cation radicals. Accordingly, we prepared oxoferryl π cation radicals by chemical oxidation according to Groves et al.[44] The results are described in Chapter III. Before investigation of unstable oxoferryl π cation radicals, we studied nonradical ferric complexes and ferric π cation radicals as reference. First, we investigated ferric nonradical porphyrins and their isotopic derivatives in order to characterize the vibrational properties of some marker bands to be used in this study. Second, we studied ferric π cation radicals, because they are photostable and also thermally stable even at room temperature and their vibrational properties are instructive for the vibrational analysis for unstable oxoferryl π cation radicals. For this radical, large downshifts of the ν_2 and ν_4 bands were observed, which are consistent with the a_{2u} character of this cation radical. On the basis of the data of ferric nonradical and radical complexes, we studied RR spectra of oxoferryl π cation radicals. Also for these radicals, significant frequency shifts of ν_2 and ν_4 were observed, which are consistent with the a_{2u} character of this radical. The controversy about the $\nu(Fe^{IV}=O)$ band of oxoferryl radicals was interpreted reasonably in terms of the effect of the trans ligand. It is suggested that the $\nu(Fe^{IV}=O)$ band upshifts by ~10 cm^{-1} upon the oxidation of the macrocycle if we take account of the effect of the trans ligand.
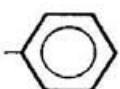
References

(1)   (a) Spiro, T. G., Ed. In *Biological Application of Raman Spectroscopy*; Wiley, New York, 1987; Vol. 3. (b) Kitagawa, T.; Ozaki, Y. *Struct. Bonding (Berlin)* **1987**, *64*, 71-114. (c) Spiro, T. G. *Adv. Protein Chem.* **1985**, *37*, 111-159.

(2)   (a) Strekas, T. C.; Spiro, T.G. *Biophys. Biochim. Acta* **1972**, *263*, 830-833. (b) Strekas, T. C.; Spiro, T.G. *Biophys. Biochim. Acta* **1972**, *278*, 188-192.

(3)   Brunner, H.; Mayer, A.; Sussner, H. *J. Mol. Biol.* **1972**, *70*, 153-156.

(4)   Strekas, T. C.; Spiro, T.G. *Proc. Natl. Acad. Sci. U.S.A.* **1972**, *69*, 2622-2626.

(5)   Yamamoto, T.; Palmer, G.; Gill, D.; Salmeen, I. T.; Rimai, L. *J. Biol. Chem.* **1973**, *248*, 5211-5213.

(6)   (a) Spiro, T.G.; Strekas, T. C. *J. Am. Chem. Soc.* **1974**, *96*, 338-345. (b) Spiro, T.G.; Burke, J. M. *J. Am. Chem. Soc.* **1976**, *98*, 5482-5409.

(7)   Spaulding, L. D.; Cheng, C. C.; Yu, N.-T.; Felton, R. H. *J. Am. Chem. Soc.* **1975**, *97*, 2517-2525.

(8)   Spiro, T.G.; Stong, J. D.; Stein, P. *J. Am. Chem. Soc.* **1979**, *101*, 2648-2655.

(9)   Choi, S.; Spiro, T.G.; Langry, K. C.; Smith, K. M.; Budd, L. D.; LaMar, G. N. *J. Am. Chem. Soc.* **1982**, *104*, 4345-4351.

(10)   Parthasarathi, N.; Hansen, C.; Yamaguchi, S.; Spiro, T. G. *J. Am. Chem. Soc.* **1987**, *109*, 3865-3871.

(11)   (a) Collman, J. P.; Halpert, T. R.; Suslick, K. S. In *Metal Ion Activation of Dioxygen* Spiro, T. G., Ed.; Wiley, New York, 1980; pp 1-72. (b) Ortiz de Montellano, P., Ed. In *Cytochrome P-450: Structure and Biochemistry* Plenum Press: New York, 1986.

(12)   (a) Varotsis, C.; Woodruff, W. H.; Babcock, G. T. *J. Am. Chem. Soc.* **1989**, *111*, 6439-6440. (b) Ogura, T.; Takahashi, S.; Shinzawa-Itoh, K.; Yoshikawa, S.; Kitagawa, T. *J. Am. Chem. Soc.* **1990**, *112*, 5630-5631. (c) Han, S.; Ching, Y.; Rousseau, D. L. *Biochemistry* **1990**, *29*, 1380-1384.

(13)   (a) Bangcharoenpaurpong, O.; Rizos, A. K.; Champion, P. M. *J. Biol. Chem.* **1986**, 261, 8089-8092. (c) Egawa, T.; Ogura, T.; Makino, R.; Ishimura, Y.; Kitagawa, T. *J. Biol. Chem.* **1991**, *266*, 10246-10248.

(14)   Morgan, M.; Dolphin, D. *Struct. Bonding (Berlin)* **1987**, *64*, 116-203.

(15)   Nakamoto, K. *Coord. Chem. Rev.* **1990**, *100*, 363-402, and references cited therein.

(16)   Brunner, H. *Naturwiss.* **1974**, *61*, 71.

(17)   Burke, J. M.; Kincaid, J. R.; Peters, S.; Gagne, R. R.; Collman, J. P.; Spiro, T. G. *J. Am. Chem. Soc.* **1978**, *100*, 6083-6088.

(18)   Benko, B.; Yu, N.-T. *Proc. Natl. Acad. Sci. U.S.A.* **1983**, *80*, 7042-7046.

(19)   Bajdor, K.; Oshio, H.; Nakamoto, K. *J. Am. Chem. Soc.* **1984**, *106*, 7273-7274.

(20)   Chottard, G.; Schappacher, M.; Richard, L.; Weiss, R. *Inorg. Chem.* **1984**, *23*, 4557-4561.

(21)   Wagner, W-D.; Paeng, I. R.; Nakamoto, K. *J. Am. Chem. Soc.* **1988**, *110*, 5565-5567.

(22)   (a) Terner, J.; Sitter, A. J.; Reczek;, C. M. *Biochim. Biophys. Acta* **1985**, *828*, 73-80. (b) Hashimoto, S.; Tatsuno, Y.; Kitagawa, T. *Proc. Jpn. Acad.* **1984**, Ser B, *60*, 345-348. (c) Hashimoto, S.; Tatsuno, Y.; Kitagawa, T. *Proc. Natl. Acad. Sci. U.S.A.* **1986**, *83*, 2417-2421. d) Sitter, A. J.; Reczek, C. M.; Terner, J. *J. Biol. Chem.* **1985**, *260*, 7515-7522. (e) Hashimoto, S.; Nakajima, R.; Yamazaki, I.; Tatsuno, Y.; Kitagawa, T. *FEBS Lett.* **1986**, *208*, 305-307. (f) Hashimoto, S.; Teraoka, J.; Inubushi, T.; Yonetani, T.; Kitagawa, T. *J. Biol. Chem.* **1986**, *261*, 11110-11118.

(23)   (a) Han, S.; Ching, Y.-C.; Rousseau, D. L. *Nature* **1990**, *348*, 89-90. (b) Varotsis, C.; Babcock, G. T. *Biochemistry* **1990**, *29*, 7357-7362.

(24)   (a) Maeda, Y.; Morita, Y. *Biochem. Biophys. Res. Commun.* **1967**, *29*, 680-685. (b) Moss, T. H.; Ehrenberg, A.; Bearden, A. J. *Biochemistry*, **1969**, *8*, 4159-4162. (c) Harami, T.; Maeda, Y.; Morita, Y.; Trautwein, A.; Gonser, U. *J. Chem. Phys.* **1977**, *67*, 1164-1169.

(25)   Proniewicz, L. M.; Bajdor, K.; Nakamoto, K. *J. Phys. Chem.* **1986**, *90*, 1760-1766.

(26)   Ogura, T.; Kitagawa, T. *J. Am. Chem. Soc.* **1987**, *109*, 2177-2179.

(27)   (a) Oertling, W. A.; Babcock, G. T. *J. Am. Chem. Soc.* **1985**, *107*, 6406-6407. (b) Oertling, W. A.; Babcock, G. T. *Biochemsitry* **1988**, *27*, 3331-3338.

(28)   Paeng, K. J.; Kincaid, J. R. *J. Am. Chem. Soc.* **1988**, *110*, 7913-7915.

(29)   Van Wart, H. E.; Zimmer, J. *J. Am. Chem. Soc.* **1985**, *107*, 3379-3381.

(30)   Palaniappan, V; Terner, J. *J. Biol. Chem.* **1989**, *264*, 16046-16053.

(31)   Gouterman, M. In *The Porphyrins* **1978**, Dolphin, D. Ed.; Academic Press, New York Vol. 3, Chapter 1.

(32)   Dolphin, D.; Felton, R. H. *Acc. Chem. Res.* **1974**, *7*, 26-32.

(33)   Dolphin, D.; Forman, A.; Borg, D. C.; Fajer, J.; Felton, R. H. *Proc. Natl. Acad. Sci. U.S.A.* **1971**, *68*, 614-618.

111

(34)   (a) Morishima, I.; Takamuki, Y.; Shiro, Y. *J. Am. Chem. Soc.* **1984**, *106*, 7666-7672. (b) Godziela, G. M.; Goff, H. M. *J. Am. Chem. Soc.* **1986**, *108*, 2237-2243.

(35)   Sandusky, P. O.; Salehi, A.; Chang, C. K.; Babcock, G. T. *J. Am. Chem. Soc.* **1989**, *111*, 6437-6439.

(36)   Yamaguchi, H.; Nakano, M.; Itoh, K. *Chem. Lett.* **1982**, 1397-1400.

(37)   Kim, D.; Miller, L. A.; Rakhit, G.; Spiro, T. G. *J. Phys. Chem.* **1986**, *90*, 3320-3325.

(38)   (a) Salehi, A.; Oertling, W. A.; Babcock, G. T.; Chang, C. K. *J. Am. Chem. Soc.* **1986**, 108, 5630-5631.

(39) Oertling, W. A.; Salehi, A.; Chang, C. K.; Babcock, G. T. *J. Phys. Chem.* **1987**, *91*, 3114-3116.

(40)   Czernuszewicz, R. S.; Macor, K. A.; Li, X. Y.; Kincaid, J. R.; Spiro, T. G. *J. Am. Chem. Soc.* **1989**, *111*, 3860-3869.

(41)   Fajor, J.; Borg, D. C.; Forman, A.; Dolphin, D.; Felton, R. H. *J. Am. Chem. Soc.* **1970**, *92*, 3451-3459.

(42)   Dolphin, D.; Muljiani, Z.; Rousseau, K.; Borg, D. C.; Fajor, J.; Felton, R. H. *Ann. N.Y. Acad. Sci.* **1973**, *206*, 349-364.

(43)   Balch, A. L.; Chan, Y. -W.; Cheng, R.-J.; LaMar, G. N.; Latos-Grazynski, L.; Renner, M. W. *J. Am. Chem. Soc.* **1984**, *106*, 7779-7785.

(44)   Groves, J. T.; Quinn, R.; McMurry, T. J.; Nakamura, M.; Lang, G.; Boso, B. *J. Am. Chem. Soc.* **1985**, *107*, 354-360.

(45)   Kashiwagi, H.; Obara, S. *Int. J. Quantum Chem.* **1981**, *20*, 843-859.

112
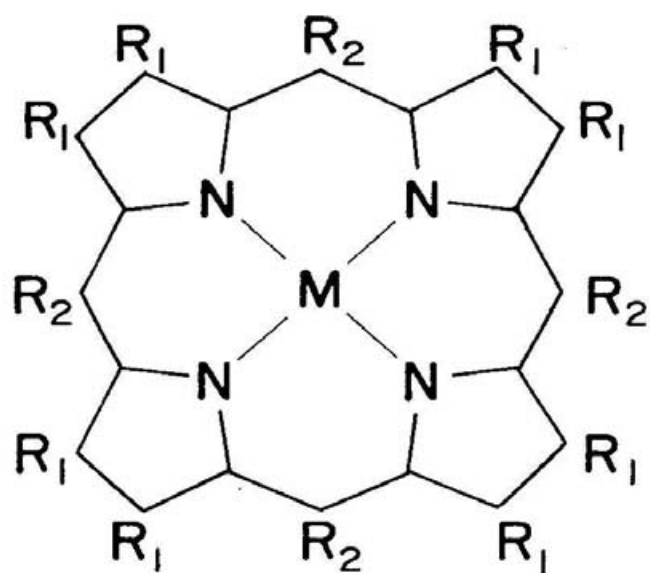
OEP: R_1 = Et, R_2 = H

TPP: R_1 = H, R_2 = ⬡

TMP: R_1 = H, R_2 = (mesityl with Me, Me, Me)
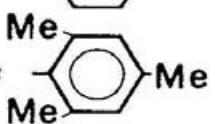
Figure I-1. Molecular structures of metalloporphyrins.

113
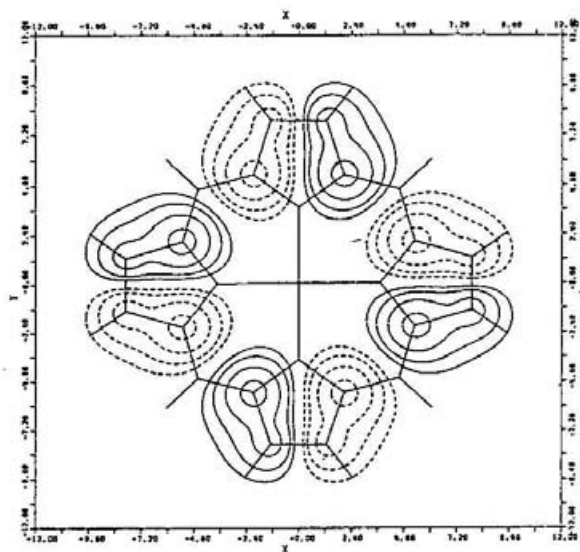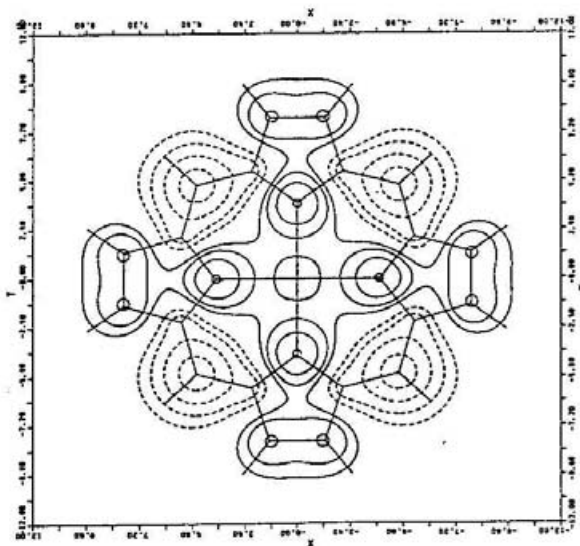
Figure I-2. Contour maps of the MO's, a_{1u} (A) and a_{2u} (B), in a plane 1.0 a.u. above the molecular plane. Solid and broken lines are contours of positive and negative values, respectively. Their values are ±0.01, ±0.02, ±0.04, ±0.08 and ±0.16 (from ref. 45).

114

Chapter II

Resonance Raman Pursuit of the Change from Fe^{II}-O_2 to Fe^{III}-OH via Fe^{IV}=O in Autoxidation of Ferrous Iron-porphyrin

Abstract

Resonance Raman (RR) and visible absorption spectra were observed for autoxidation intermediates of ferrous tetramesitylporphyrin [(TMP)Fe^{II}] to the ferric hydroxy derivative [(TMP)Fe^{III}OH] via (TMP)Fe^{II}-O$_2$, (TMP)Fe^{III}-O-O-Fe^{III}(TMP), and (TMP)Fe^{IV}=O. The O-O stretching [$\nu(O_2)$] and Fe^{II}-O$_2$ stretching [$\nu(Fe^{II}-O_2)$] Raman bands were simultaneously observed at 1171 and 522 cm^{-1}, respectively, for the (TMP)Fe^{II}-O$_2$ complex in a toluene solution at -100°C for the first time. The present data together with the reported IR data for the solution samples indicate a linear inverse correlation between $\nu(O_2)$ and $\nu(Fe^{II}-O_2)$ frequencies similar to that between $\nu(CO)$ and $\nu(Fe^{II}-CO)$, but the data from heme proteins fall off the line. Upon raising the sample temperature to -70°C, formation of (TMP)Fe^{III}-O-O-Fe^{III}(TMP) was confirmed by ^{1}H NMR and its visible absorption spectrum was determined. However the peroxo-bridged dimer was so photolabile that it was decomposed into (TMP)Fe^{IV}=O by laser illumination even at -70°C and, therefore, no oxygen isotope-sensitive RR band assignable to (TMP)Fe^{III}-O-O-Fe^{III}(TMP) was identified. (TMP)Fe^{IV}=O was also photolabile and yielded the photoproduct, the same as the case of thermal decomposition, but (TMP)Fe^{IV}=O gave the Fe^{IV}=O stretching [$\nu(Fe^{IV}=O)$] Raman band at 843 cm^{-1}, which is agreement with the value reported for the five coordinate oxoferryl complex. The reduction rate of (TMP)Fe^{IV}=O to (TMP)Fe^{III}-OH was different between the toluene-h$_8$ and -d$_8$ solutions, suggesting that it proceeds via hydrogen abstraction from toluene. Presumably, the Fe^{IV}=O bond has a partial radical character, which increases upon electronic excitation, and this is the reason why decomposition of (TMP)Fe^{IV}=O is accelerated by laser illumination.

II-1. Introduction

A mechanism of dioxygen activation by iron(II) porphyrin has attracted chemists' attention in relevance to elucidation of catalytic mechanisms of various heme enzymes.[1,2] The presence of the oxy-ferrous form (PFe^{II}-O_2; P denotes a porphyrin dianion) was revealed spectroscopically for cytochrome P-450[3] and cytochrome oxidase[4] as well as for hemoglobin (Hb) and myoglobin (Mb), although structures of the successive reaction intermediates such as the oxoferryl form ($PFe^{IV}=O$) have not been well documented yet. Physicochemical properties of $PFe^{IV}=O$ in peroxidases have been extensively investigated with Mössbauer,[5] NMR,[6] ENDOR[7], EXAFS,[8] and resonance Raman (RR) techniques[9] and are compared with those of model $PFe^{IV}=O$ complexes.[10-12] It was also pointed out for horseradish peroxidase compound II that the bound oxygen atom of $PFe^{IV}=O$ is exchanged with the oxygen atom of bulk water only when the bound oxygen atom is hydrogen-bonded to a particular distal residue.[9c] Elucidation of the effective environmental factors which determine the reactivity of $PFe^{IV}=O$ toward oxygenation or oxidation is a topic of current biochemical studies using site-directed mutagenesis.[13]

The autoxidation mechanism of Fe^{II}-porphyrin has been revealed through observations of NMR spectra of the peroxo- (PFe^{III}-O-O-Fe^{III}P) and oxoferryl intermediates.[14] The reaction is considered to proceed in the following way;

$$PFe^{II} + O_2 \rightarrow PFe^{II}\text{-}O_2\,(1) \qquad\qquad (1)$$
$$2PFe^{II}\text{-}O_2 \rightarrow PFe^{III}\text{-O-O-}Fe^{III}P\,(2) + O_2 \qquad\qquad (2)$$
$$PFe^{III}\text{-O-O-}Fe^{III}P \rightarrow 2PFe^{IV}=O\,(3) \qquad\qquad (3)$$
$$PFe^{IV}=O + H \rightarrow PFe^{III}\text{-OH}\,(4) \qquad\qquad (4)$$
$$PFe^{IV}=O + PFe^{II} \rightarrow PFe^{III}\text{-O-}Fe^{III}P\,(5) \qquad\qquad (5)$$
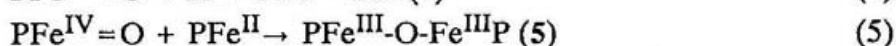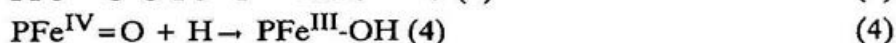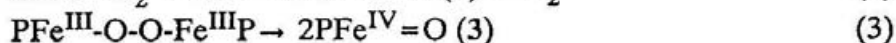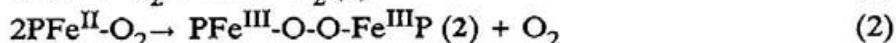
Although reaction (5) is a general route, Balch et al.[14c] pointed out from their NMR study that when bulky substituents are bound to the periphery of porphyrin, decomposition of $PFe^{IV}=O$ via Eq. (5) is unfavorable.

Resonance Raman spectroscopy is a powerful technique for this kind of study since it enables us to detect the $Fe^{IV}=O$ stretching [$\nu(Fe^{IV}=O)$], Fe^{II}-O_2 stretching [$\nu(Fe^{II}\text{-}O_2)$], and O-O stretching [$\nu(O_2)$] vibrations for heme proteins[9] as well as for the corresponding model compounds,[15] allowing discussion about delocalization of electrons among the axial ligand, the iron ion and the porphyrin macrocycle. The $\nu(Fe^{IV}=O)$ RR band was first identified for the O_2 matrix of (TPP)Fe^{II} (TPP: tetraphenylporphyrin dianion)[16] and later for low temperature solutions of

$(T_{piv}PP)Fe^{IV}=O$ [$T_{piv}PP$: *meso*-tetra($\alpha,\alpha,\alpha,\alpha$-o-pivalamidophenyl)porphyrin dianion][17] and $(TMP)Fe^{IV}=O$ (TMP: 5,10,15,20-tetramesitylporphyrin dianion).[18] Recently, Nakamoto and coworkers observed the $\nu(Fe^{II}\text{-}O_2)$ and $\nu(O_2)$ RR bands for the O_2 matrix of $(TPP)Fe^{II}$ at 25 K[19] and also the symmetric Fe-O stretching mode of the PFe-O-O-FeP dimer in toluene at -78°C.[20] On the other hand, we succeeded in simultaneous observation of the $\nu(O_2)$ and $\nu(Fe\text{-}O_2)$ RR bands for a solution sample of $(TMP)Fe^{II}\text{-}O_2$ at -100°C. In this chapter we describe the RR spectral changes in each step of Eqs. (1)-(4) with a particular emphasis on temperature dependence of intensity of the $\nu(O_2), \nu(Fe^{II}\text{-}O_2)$ and $\nu(Fe^{IV}=O)$ RR bands.

II-2. Experimental Section

$(TMP)Fe^{III}Cl$ and its ^{54}Fe-substituted derivative [$(TMP)^{54}Fe^{III}Cl$] were obtained from the reaction of the corresponding ferrous sulfate with $(TMP)H_2$ in *N, N*-dimethylformamide (DMF), followed by the 3M HCl treatment according to Kobayashi et al.[21] $(TMP)Fe^{III}OH$ was prepared by treatment of $(TMP)Fe^{III}Cl$ with NaOH.[22] Toluene-h_8 (Dojin Chemicals) and toluene-d_8 (Aldrich) were dried with solid sodium and degassed by repeated freeze-pump-thaw cycles. $(TMP)Fe^{II}$ was obtained from sodium mirror contact reduction of $(TMP)Fe^{III}Cl$ in toluene as described previously[23] and confirmed by visible absorption spectra. Autoxidation of $(TMP)Fe^{II}$ was initiated by incorporating O_2 into the toluene solution of $(TMP)Fe^{II}$ at -100 °C, and the subsequent reactions were monitored by visible absorption and NMR spectroscopy. Although the absorption spectra were observed for the path-length of 1 mm with a known amount of the starting material, we failed to determine the extinction coefficients of individual intermediates, since their precise concentrations were indeterminable.

Raman scattering was excited by the 406.7 nm line of a Kr^+ ion laser (Spectra Physics, model 264) and detected with a photo-diode array (PAR 1420) attached to a Spex 1404 double monochromator. Accumulation time for one measurement is ca. 5 min. Raman shifts were calibrated with indene and accuracy of frequencies of well defined Raman bands are ±1 cm^{-1}. All Raman measurements were performed with a cuvette with path-length of 1 mm, with which Raman and absorption spectra were measured for an identical preparation, or a spinning cell (1800 rpm) which can be spun in a cryostat containing cooled ethanol.

II-3. Results

Figure II-1 illustrates the change of visible absorption spectra for each step of Eqs. (1)-(2). The sodium mirror contact reduction of (TMP)Fe^{III}Cl in toluene yielded the split Soret bands at 418 and 445 nm and the α band at 538 nm as shown by the solid line. Since several isosbestic points were observed between this and the spectrum of (TMP)Fe^{III}Cl, this should correspond to the one electron reduced state, that is, (TMP)Fe^{II}. This species would have no axial ligand and is, therefore, considered to adopt the intermediate spin state.[24] Depth of the valley between the two peaks at 418 and 445 nm serves as a diagnostic marker for good preparation; when coordinating impurities are present, the 445 nm band becomes weaker.

Upon incorporation of O_2 into the (TMP)Fe^{II} solution at -100°C, the 445 nm band disappeared while the 418 and 538 nm bands were shifted to 416 and 526 nm, respectively, as shown by a broken line in Figure II-1. This curve is considered to be the absorption spectrum of 1, although there has been no report about it. When the temperature of the solution was raised to -70°C, the absorption spectrum drawn by a dotted line was obtained and its NMR spectrum (not shown) exhibited the characteristic features of the μ-peroxo dimer reported.[14c] Therefore, the dotted curve is inferred to be the absorption spectrum of 2 with the purity higher than 95%. When the same experiments were carried out with (TPP)Fe^{III}Cl, incorporation of O_2 at -100°C immediately yielded the spectrum similar to the dotted curve. It indicates instability of the Fe^{II}-O_2 structure in the absence of protecting groups such as methyl groups.

Figure II-2 shows the RR spectra in the $\nu(O_2)$ and $\nu(Fe^{II}-O_2)$ regions of (TMP)Fe^{II} and 1 in toluene at -100°C. As shown by spectra (A) and (A'), (TMP)Fe^{II} exhibits no prominent RR band in these frequency regions. When $^{16}O_2$ was incorporated into the cell, a trough between two solvent bands at 1158 and 1179 cm^{-1} became noticeably shallow (B) and in addition a new band appeared at 522 cm^{-1} (B'). On the other hand, when $^{18}O_2$ was incorporated, the trough between the two solvent bands remained unchanged compared with spectrum (A) but a new band and a shoulder appeared at 1107 cm^{-1} (C) and 498 cm^{-1} (C'), respectively. The difference spectra between the $^{16}O_2$ and $^{18}O_2$ derivatives, which are shown by traces (D) [= (B) - (C)] and (D') [= (B') - (C')], clearly indicate that the 1171 and 522 cm^{-1} bands of $^{16}O_2$ derivative are shifted to 1107 and 498 cm^{-1}, respectively, for the $^{18}O_2$ derivative. The magnitude of the observed isotopic frequency shifts (64 and 24 cm^{-1}, respectively) are in reasonable agreement with the expected values for the $\nu(O_2)$ ($\Delta\nu = 67$ cm^{-1}) and

119

$\nu(Fe^{II}\text{-}O_2)$ ($\Delta\nu = 19$ cm^{-1}) modes in the diatomic harmonic approximation. Consequently the RR bands of the $^{16}O_2$ derivative of 1 at 1171 and 522 cm^{-1} are assigned to the O-O and Fe-O$_2$ stretching vibrations, respectively. This is the first simultaneous observation of the $\nu(O_2)$ and $\nu(Fe^{II}\text{-}O_2)$ modes for PFe^{II}-O$_2$ in solution and strongly supports the idea that the solid line in Figure II-1 stands for the absorption spectrum of 1. Spectra (E) and (E') in Figure II-2 show the RR spectra of the $^{18}O_2$ and $^{16}O_2$ derivatives at -70°C, respectively, which were observed for the same samples as used for obtaining Figures II-2C and -2B', respectively. The $\nu(O_2)$ and $\nu(Fe^{II}\text{-}O_2)$ RR bands disappear upon warming to -70°C.

Figure II-3 shows the RR spectrum of 1 in toluene-d$_8$ at -100°C (A) and -70°C (B and C). The RR bands of 1 at 1569 and 1367 cm^{-1} are assignable to ν_2 and ν_4 modes, respectively.[25] The ν_4 frequency of 1 is higher than that of (TMP)Fe^{III}Cl (1364 cm^{-1}) in consonance with the results for hemeproteins such as Hb and Mb for which the ν_4 frequency is higher for the oxy-form than for the met form.[26,27] When temperature of the solution was raised to -70 °C and its RR spectrum was measured with a very low laser power, a new band was recognized at 843 cm^{-1} as shown by spectrum (B). When the laser power was raised to 20 mW without changing the temperature of the sample, the bands at 1570, 1368 and 843 cm^{-1} became weaker. Although these measurements were performed with the cuvette, the same results were obtained with the spinning cell. In order to understand the implication of these spectral changes, the RR spectra in the 1000-600 cm^{-1} region were examined in detail.

Spectra (A) and (B) in Figure II-4 were obtained at -70 °C for the $^{16}O_2$ derivative in toluene-h$_8$ and the $^{18}O_2$ derivative in toluene-d$_8$, respectively. A new band appeared at 810 cm^{-1} in spectrum (B). When $^{16}O_2$ was used in toluene-d$_8$, the 810 cm^{-1} band disappeared and the band at 843 cm^{-1} was relatively intensified as shown by spectrum (C), indicating that a solute band was overlapped with a solvent band at 841 cm^{-1}. Accordingly, the 843 and 810 cm^{-1} bands should be associated with vibrations involving motions of ^{16}O and ^{18}O, respectively. If the species observed were 2, the oxygen isotope-sensitive band would be the O-O stretching mode of the peroxo-bridged dimer, and if the species observed were 3, it would be the $\nu(Fe^{IV}=O)$ mode. To determine the alternative, the same experiment was carried out for the ^{54}Fe derivative, and the results are shown by spectrum (D). Comparison of spectrum (D) with spectrum (A) indicates that the 843 cm^{-1} mode is ^{54}Fe isotope-sensitive and, therefore, should significantly involve the Fe-O stretching character. The magnitudes of the

observed frequency shifts (33 cm^{-1} for $^{16}O/^{18}O$ and 4 cm^{-1} for $^{56}Fe/^{54}Fe$) are closer to those expected for a Fe-O diatomic oscillator ($\Delta\nu$ = 37 cm^{-1} for $^{16}O/^{18}O$ and 3.4 cm^{-1} for $^{56}Fe/^{54}Fe$) than that for an O-O diatomic oscillator ($\Delta\nu$ = 48 cm^{-1}). Furthermore, the observed shifts are in good agreement with the corresponding data for the five coordinate $Fe^{IV}=O$ porphyrin obtained in an O_2 matrix at 15 K ($\Delta\nu$ = 34 cm^{-1} for $^{16}O/^{18}O$ and 4 cm^{-1} for $^{56}Fe/^{54}Fe$).[16a,b] Consequently, we assign the 843 cm^{-1} band to the $\nu(Fe^{IV}=O)$ mode and the spectrum shown by Figure II-3B to the $Fe^{IV}=O$ complex (3) rather than to the PFe-O-O-FeP dimer (2) contrary to the fact that Balch et al.[14c] assigned the complex at -70°C to 2. It seems to be most likely that 2 is extremely photolabile and is immediately converted to 3 when the sample is brought into the laser beam. Probably, the absorption spectrum at -70 °C in Figure II-1 reflects 2 but the RR spectrum at -70 °C primarily reflects 3. Since the laser power dependence of intensity of the bands at 1570 and 1368 cm^{-1} [Figure II-3B] were nearly parallel with that of the 843 cm^{-1} band, they are assigned to the ν_2 and ν_4 modes of 3, respectively. The ν_2 and ν_4 frequencies of 3 are apparently very close to those of the Fe^{II}-O_2 complex, but when spectrum (C) was subtracted from spectrum (B), the ν_4 band appeared at 1371 cm^{-1} which is slightly higher than that of 2 and distinctly higher than that of the Fe^{III}-OH complex (*vide infra*).

When temperature of the sample used for the measurement of spectrum (A) in Figure II-4 was raised to -30 °C and cooled to -70 °C again, spectrum (E) was obtained. This spectrum is practically the same as the spectrum of authentic (TMP)Fe^{III}OH shown by spectrum (F). It implies that (TMP)$Fe^{IV}=O$ is reduced to (TMP)Fe^{III}OH at -30 °C according to Eq. (4), in agreement with the results from NMR studies.[14a-c] The spectral change from Figure II-4A to -4E was pursued in detail and the results are illustrated in Figure II-5.

Spectrum (A) in Figure II-5 was observed for (TMP)$Fe^{IV}=O$ in toluene-h_8 at -70°C. When the sample was kept at -30°C for 10, 20, 50, and 110 min, spectra (B), (C), (D) and (E), respectively, were observed. The 843 cm^{-1} bands became weaker as lapse of time. The inset of Figure II-5 displays the plot of the relative intensity of the 843 cm^{-1} band to a solvent band versus the period kept at -30°C. The open and closed circles denote the data obtained from the toluene-h_8 and -d_8 solutions, respectively. The ordinate is scaled with regard to the value at 0 min of each series.

The increase of intensity during initial 50 min of the toluene-d_8 solution means the increase of 3. Since the formation of 3 from 2 runs in parallel with reduction of 3

to **4**, the accumulation of **3** can be recognized when the latter reaction is relatively slower. In fact, such a feature can be simulated when the formation and decay rates of **3** are of similar magnitude. Consequently, the results shown in the inset of Figure II-5 implies that the decay of the $Fe^{IV}=O$ species is faster in toluene-h_8 than in toluene-d_8. This is consistent with the recent report that the oxoferryl porphyrin π cation radical, whose reduction to neutral oxoferryl porphyrin is considered to involve hydrogen abstraction from solvent, is more stable in CD_2Cl_2 than in CH_2Cl_2.[28]

We note that the RR spectrum finally obtained at -30 °C (Figure II-5E) is coincident with the spectrum obtained at -70 °C with a higher laser power [not shown, but the corresponding spectrum in toluene-d_8 is shown by Figure II-3C]. This means that reduction from **3** to **4** is also promoted by laser illumination. Therefore, it is quite important to use a lower laser power to observe RR spectra of the peroxo-bridged and oxoferryl porphyrins.

II-4. Discussion

In the ^{1}H NMR study on autoxidation of (TMP)Fe^{II} by Balch et al.[14c] the first intermediate observed upon incorporation of O_2 to (TMP)Fe^{II} was the peroxo-bridged dimer, although O_2 was incorporated at -70°C and the presence of some precursor was anticipated. The observation of $\nu(O_2)$ in the present study demonstrated that the first intermediate is the Fe^{II}-O_2 type complex and relatively photostable. The NMR study with more sterically crowded porphyrins[29] also yielded evidence for the formation of diamagnetic PFe^{II}-O_2 complex at -70°C as the primary compound. The $\nu(O_2)$ and $\nu(Fe^{II}$-$O_2)$ vibrations of oxygenated iron porphyrins have been investigated by several groups and their results are summarized in Table II-1. The $\nu(O_2)$ mode has been detected only by IR spectroscopy[30a,b,31] for the oxy-form of iron porphyrins and heme proteins[15a] until recently Wagner et al.[19] succeeded in observing the $\nu(O_2)$ and $\nu(Fe^{II}$-$O_2)$ RR bands for (TPP)Fe^{II}-O_2 in the dioxygen matrix at 25 K. The present experiment also provided the first simultaneous observation of the $\nu(O_2)$ and $\nu(Fe^{II}$-$O_2)$ RR bands for a solution state. Since the $\nu(O_2)$ frequency for the side-on geometry is distinctly low,[30a] the present $\nu(O_2)$ frequency suggests that the O_2 molecule in **1** adopts the end-on geometry.

The $\nu(O_2)$ frequencies are plotted against $\nu(Fe^{II}$-$O_2)$ frequencies in Figure II-6. The $\nu(Fe^{II}$-$O_2)$ frequencies are higher for six coordinate complexes than for the five coordinate complexes[12,17,18,30,32] in contrast to the $\nu(Fe^{IV}=O)$ frequencies of the

122

$Fe^{IV}=O$ porphyrins. The $\nu(O_2)$ frequencies decrease as $\nu(Fe^{II}\text{-}O_2)$ frequencies increase in consonance with the relation of $\nu(CO)$ vs. $\nu(Fe^{II}\text{-}CO)$.[33] The data from solutions fall on a straight line drawn in Figure II-6, which is represented by

$$\nu(O_2) = -0.264 \cdot \nu(Fe^{II}\text{-}O_2) + 1309$$

but those from $(TPP)Fe^{II}\text{-}O_2$ in the dioxygen matrix at $25K^{[19]}$ and proteins deviate significantly from the line. One may argue against this to point out that $(TPP)Fe^{II}\text{-}O_2$, $(TMP)Fe^{II}\text{-}O_2$, HbO_2, and MbO_2 form a straight line and that the six-coordinate porphyrins in the solution fall off the line. If such a line was drawn, it would be given by

$$\nu(O_2) = -1.306 \cdot \nu(Fe^{II}\text{-}O_2) + 1853.$$

For the limit of $\nu(Fe^{II}\text{-}O_2) = 0$ cm^{-1}, the extrapolated $\nu(O_2)$ frequency with the former equation is closer to the gas phase value (1551 cm^{-1}, it would be lower than this in an aqueous solution) than that with the latter equation. Furthermore, when we think about some regularity between the two kinds of frequencies, it is more reasonable to contain all solution data in a group rather than to involve the data from the solid matrix at 25 K at the expense of a part of solution data.

The deviations of the protein data from the straight line shown in Figure II-6 imply that π back donation from $d_{yz}(Fe)$ and $d_{xz}(Fe)$ orbitals, which leads to lower the $\nu(O_2)$ frequency and to raise the $\nu(Fe^{II}\text{-}O_2)$ frequency, is sensitively affected by surroundings or that the $\nu(O_2)$ frequency is very sensitive to interactions of bound O_2 with distal residues in the protein as suggested by Oertling et al.[12] The difference in π back donation would alter polarization of the $Fe^{II}\text{-}O_2$ bond and thus reactivity of oxygen. Another possibility is that the hydrogen bonding between O_2 and protein residues little alters the $\nu(O_2)$ and $\nu(Fe^{II}\text{-}O_2)$ frequencies but changes the Fe-O-O bond angle, which results in a large change of $\nu(O_2)$ and $\nu(Fe^{II}\text{-}O_2)$ frequencies. The compounds which fall off the straight line in Figure II-6 may have different Fe-O-O bond angles.

It is fairly confident that the absorption spectrum obtained at -70°C (Figure II-1) reflects **2**, since the ^1H NMR spectrum reproduced that of **2** reported[14c] and the amount of impurity like **3** is deduced to be less than 5%. The absorption spectral

changes in reactions (1)-(3) were reported by Paeng et al.[20] The relative absorbances at 418 and 445 nm of (TMP)Fe^{II} are significantly different between the reported [Figure II-2A in Ref. 20] and the solid line in Figure II-1, and the reported curve could be reproduced when reduction by the sodium mirror was incomplete and/or the solution was contaminated by impurities. Paeng et al.[20] observed an oxygen isotope-sensitive band at 574 cm^{-1} upon incorporation of $^{16}O_2$ to (TMP)Fe^{II} at -78°C and assigned it to the symmetric Fe-O stretching mode of the Fe-O-O-Fe dimer. Although we failed to detect the 574 cm^{-1} band, we expected to recognize it in the spectra shown in Figure II-2, if present. Presumably the peroxo-bridged dimer is a poor Raman scatterer at this excitation wavelength and undergoes rapid homolytic cleavage upon laser illumination, leading to formation of the oxoferryl complex, while the rate-limiting step in reduction of the oxoferryl complex is hydrogen abstraction from solvent molecules.

The reported absorption spectrum [Figure II-2B in Ref. 20] is also different from any in Figure II-1. Therefore, the interpretation by Paeng et al.[20] might be correct, but judging from their absorption spectrum of PFe^{II} we cannot rule out the possibility that the 574 cm^{-1} band arised from a six coordinate PFe^{II}-O_2. However, in this case, it is puzzling why upon warming to -46°C the ν(Fe^{IV}=O) band appear at 845 cm^{-1}, namely, in the frequency region of the five coordinate PFe^{IV}=O complexes.

Judging from the ν(Fe^{IV}=O) frequency and chemical species coexistent in the solution, 3 in this experiment is considered to adopt the five coordinate structure. The ν(Fe^{IV}=O) frequency of the five coordinate (TPP)Fe^{IV}=O in the dioxygen matrix at 15 K (852 cm^{-1})[16a] is slightly higher than the present value. This would not be due to the difference in a type of porphyrin, because the ν(Fe^{IV}=O) frequencies of (TPP)Fe^{IV}=O, (OEP)Fe^{IV}=O and (Salen)Fe^{IV}=O [Salen: N, N'-ethylenebis(salicylideneiminato)] in the dioxygen matrix are the same.[16b] The ν(Fe^{IV}=O) frequency is expected to decrease for six coordinate complexes (841-807 cm^{-1})[12] than for five coordinate complexes (852-843 cm^{-1}) due to σ donation from a trans ligand to the antibonding orbital of the Fe^{IV}=O bond.[12,34] The ν(Fe^{IV}=O) frequencies reported for hemeproteins (797-767 cm^{-1}) are still lower than those of the six-coordinate PFe^{IV}=O complexes presumably due to hydrogen bonding to a distal residue and/or to protein effects on bond polarization.

It is quite important to establish the RR spectrum of 3 for comparison with that of oxoferryl porphyrin π cation radical in the future. Spectrum (B) in Figure II-3 con-

tained an appreciable contribution from **4** and we failed to isolate **3**. On the basis of the parallel behavior of intensities among the bands at 1570, 1368, and 843 cm^{-1}, we assigned the 1570 and 1368 cm^{-1} bands to ν_2 and ν_4 of (TMP)Fe^{IV}=O, respectively. The ν_2 and ν_4 bands have not been reported yet for this complex, while ν(Fe^{IV}=O) frequency is in agreement with that reported.[20]

The reduction mechanism of **3** to **4** has not been discussed in a previous NMR study.[14c] A large difference in the reduction rate between the toluene-h$_8$ and -d$_8$ solutions, which was noticed in this study for the first time, evidently indicated that a reductant is solvent toluene and the hydrogen (or deuterium) abstraction brings about a mass effect of the transferred reducing equivalent on the reaction from **3** to **4**.

Chemistry of the oxoferryl porphyrin has been extensively investigated in relation to intermediates of the oxygenation reaction by cytochrome P-450.[2a,b] Presumably the oxoferryl oxygen has an appreciable radical character, which leads to hydrogen abstraction by **3**, and the radical character of the Fe^{IV}=O bond is promoted by electronic excitation. Therefore, the reaction from **3** to **4** seemed to be accelerated by laser illumination as well as by thermal excitation.

In conclusion, resonance Raman spectra for autoxidation intermediates of ferrous porphyrin were obtained and they are consistent with Eqs. (1)-(4) deduced from NMR spectroscopy.[14c] Some additional new information obtained here demonstrated the presence of the Fe^{II}-O$_2$ complex at -100°C and the Fe^{IV}=O complex at -70°C, although they are photolabile, and suggested that reduction of the Fe^{IV}=O porphyrin proceeds via hydrogen abstraction from solvent (toluene).

References

(1)   Collman, J. P.; Halpert, T. R.; Suslick, K. S. In *Metal Ion Activation of Dioxygen*; Spiro, T. G. Ed.; Wiley: New York, 1980; pp 1-72.

(2)   Groves, J. T. In *Cytochrome P-450: Structure and Biochemistry*; Ortiz de Montellano, P. Ed.; Plenum Press: New York, 1986; Chapter 1.

(3)   (a) Ishimura, Y.; Ullrich, V.; Peterson, J. A. *Biochem. Biophys. Res. Commun* **1971**, *42*, 140-146. (b) Peterson, J. A.; Ishimura, Y.; Griffin, B. W. *Arch. Biochem. Biophys.* **1972**, *149*, 197-208. (c) Bangcharoenpaurpong, O.; Rizos, A. K.; Champion, P. M. *J. Biol. Chem.* **1986**, *261*, 8089-8092.

(4)   (a) Chance, B.; Saronio, C.; Leigh, J. S. Jr. *J. Biol. Chem.* **1975**, *250*, 9226-9237. (b) Varotsis, C.; Woodruff, W. H.; Babcock, G. T. *J. Am. Chem. Soc.* **1989**, *111*, 6439-6440. (c) Orii, Y.; *Ann. N.Y. Acad. Sci.* **1988**, *550*, 105-117.

(5)   (a) Maeda, Y.; Morita, Y. *Biochem. Biophys. Res. Commun.* **1967**, *29*, 680-685. (b) Moss, T. H.; Ehrenberg, A.; Bearden, A. J. *Biochemistry*, **1969**, *8*, 4159-4162. (c) Harami, T.; Maeda, Y.; Morita, Y.; Trautwein, A.; Gonser, U. *J. Chem. Phys.* **1977**, *67*, 1164-1169.

(6)   La Mar, G. N.; deRopp, J. S.; Latos-Grazynski, L.; Balch, A. L.; Johnson, R. B.; Smith, K. M.; Parish, D. W.; Cheng, R.-J. *J. Am. Chem. Soc.* **1983**, *105*, 782-787.

(7)   Roberts, J. E.; Hoffman, B. M.; Rutter, R.; Hager, L. P. *J. Am. Chem. Soc.* **1981**, *103*, 7654-7656.

(8)   Penner-Hahn, J. E.; McMurry, T. J.; Renner, M.; Latos-Grazynsky, L.; Eble, K. S.; Davis, I. M.; Balch, A. L.; Groves, J. T.; Dawson, J. H.; Hodgson, K. O. *J. Biol. Chem.* **1983**, *258*, 12761-12764.

(9)   (a) Terner, J.; Sitter, A. J.; Reczek;, C. M. *Biochim. Biophys. Acta* **1985**, *828*, 73-80. (b) Hashimoto, S.; Tatsuno, Y.; Kitagawa, T. *Proc. Jpn. Acad.* **1984**, *Ser B, 60*, 345-348. (c) Hashimoto, S.; Tatsuno, Y.; Kitagawa, T. *Proc. Natl. Acad. Sci.* **1986**, *83*, 2417-2421. (d) Sitter, A. J.; Reczek, C. M.; Terner, J. *J. Biol. Chem.* **1985**, *260*, 7515-7522. (e) Hashimoto, S.; Nakajima, R.; Yamazaki, I.; Tatsuno, Y.; Kitagawa, T. *FEBS Lett.* **1986**, *208*, 305-307. f) Hashimoto, S.; Teraoka, J.; Inubushi, T.; Yonetani, T.; Kitagawa, T. *J. Biol. Chem.* **1986**, *261*, 11110-11118.

(10)   Boso, B.; Lang, G.; McMurry, T. J.; Groves, T. *J. Chem. Phys.* **1983**, *79*, 1122-1126.

(11)   Simonneaux, G.; Scholz, W. F.; Reed, C. A.; Lang, G. *Biochim. Biophys. Acta*

1982, *716*, 1-7.

(12) Oertling, W. A.; Kean, R. T.; Wever, R.; Babcock, G. T. *Inorg. Chem.* **1990**, *29*, 2633-2645.

(13) (a) Imai, Y.; Nakamura, M. *Biochem. Biophys. Res. Commun.* **1989**, *158*, 717-722. (b) Atkins, W. M.; Sligar, S. G. *J. Am. Chem. Soc.* **1989**, *111*, 2715-2717. (c) Shimizu, T.; Hirano, K.; Takahashi, M.; Hatano, M.; Fujii-Kuriyama, Y. *Biochemistry* **1988**, *27*, 4138-4141.

(14) (a) Chin, D. -H.; Del Gandio, J.; LaMar, G. N.; Balch, A. L. *J. Am Chem. Soc.* **1977**, *99*, 5486-5488. (b) Chin, D. -H.; LaMar, G. N.; Balch, A. L. *J. Am. Chem. Soc.* **1980**, *102*, 4344-4350. (c) Balch, A. L.; Chan, Y. -W.; Cheng, R.-J.; LaMar, G. N.; Latos-Grazynski, L.; Renner, M. W. *J. Am. Chem. Soc.* **1984**, *106*, 7779-7785. (d) Balch, A. L.; LaMar, G. N.; Latos-Grazynski, L.; Renner, M. W.; Thanabal, V. *J. Am. Chem. Soc.* **1985**, *107*, 3003-3007.

(15) (a) Kitagawa, T.; Ozaki, Y. *Struct. and Bond* **1987**, *64*, 71-114. b) Spiro, T. G.; Li, X.-Y. In *Biological Application of Raman Spectroscopy*, Spiro, T. G. Ed. Wiley, New York, 1988; Chapter 1.

(16) (a) Bajdor, K.; Nakamoto, K. *J. Am. Chem. Soc.* **1984**, *106*, 3045-3046. (b) Proniewicz, L. M.; Bajdor, K.; Nakamoto, K. *J. Phys. Chem.* **1986**, *90*, 1760-1766.

(17) Schappacher, M.; Chottard, G.; Weiss, R. *J. Chem. Soc. Chem. Commun.* **1986**, 93-94.

(18) Hashimoto, S.; Tatsuno, Y.; Kitagawa, T. *Proc. 10th Intl. Conf. Raman Spectrosc.* Peticolas, W. L.; Hudson, B. Eds.; Univ. Printing Dept. of Oregon: Eugene, OR, 1986; pp.1.28-29.

(19) Wagner, W-D.; Paeng, I. R.; Nakamoto, K. *J. Am. Chem. Soc.* **1988**, *110*, 5565-5567.

(20) Paeng, I. R.; Shiwaku, H.; Nakamoto, K. *J. Am. Chem. Soc.* **1988**, *110*, 1995-1996.

(21) Kobayashi, H.; Higuchi, T.; Kaizu, Y.; Osada, H.; Aoki, M. *Bull. Chem. Soc. Jpn.* **1975**, *48*, 3137-3141.

(22) Cheng, R.-J.; Latos-Grazynski, L.; Balch, A. L. *Inorg. Chem.* **1982**, *21*, 2412-2418.

(23) Teraoka, J.; Hashimoto, S.; Sugimoto, H.; Mori, M.; Kitagawa, T. *J. Am. Chem. Soc.* **1987**, *109*, 180-184.

(24) (a) Kobayashi, H.; Yanagawa, Y. *Bull. Chem. Soc. Jpn.* **1972**, *45*, 450-456. (b)

Collman, J. P.; Hoard, J. L.; Kim, N.; Lang, G.; Reed, C. A. *J. Am. Chem. Soc.* **1975**, *97*, 2676-2681. (c) Kitagawa, T.; Teraoka, J. *Chem. Phys. Lett.* **1979**, *63*, 443-446.

(25) Li, X.-Y.; Czernuszewicz, R. S.; Kincaid, J. R.; Su, Y. O.; Spiro, T. G. *J. Phys. Chem.* **1990**, *94*, 31-47.

(26) Spiro, T. G.; Strekas, T. C. *J. Am. Chem. Soc.* **1974**, *96*, 338-345.

(27) (a) Kitagawa, T.; Iizuka;, T.; Saito, M.; Kyogoku, Y. *Chem. Lett.* **1975**, 849-852. (b) Kitagawa, T.; Kyogoku, Y.; Iizuka, T.; Ikeda-Saito, M. *J. Am. Chem. Soc.* **1976**, *98*, 5169-5173.

(28) Gold, A.; Joyaraj, K.; Doppelt, P.; Weiss, R.; Chottard, G.; Bill, E.; Ding, X.; Trautwein, A. X. *J. Am. Chem. Soc.* **1988**, *110*, 5756-5761.

(29) Latos-Grazynski, L.; Cheng, R-J.; La Mar, G. N.; Balch, A. L. *J. Am. Chem. Soc.* **1982**, *104*, 5992-6000.

(30) (a) Watanabe, T.; Ama, T.; Nakamoto, K. *J. Phys. Chem.* **1984**, *88*, 440-445. b) Nakamoto, K.; Paeng, I. R.; Kuroi, T.; Isobe, T.; Oshio, H. *J. Mol. Struct.* **1988**, *189*, 293-300.

(31) Collman, J. P.; Brauman, J. I.; Halbert, T. R.; Suslick, K. S. *Proc. Natl. Acad. Sci. U.S.A.* **1976**, *73*, 3333-3337.

(32) Kerr, E. A.; Mackin, H. C.; Yu, N. -T. *Biochemistry* **1983**, *22*, 4373-4379.

(33) Li, X. Y.; Spiro, T. G. *J. Am. Chem. Soc.* **1988**, *110*, 6024-6033.

(34) Su, Y. O.; Czernuszewicz, R. S.; Miller, L. A.; Spiro, T. G. *J. Am. Chem. Soc.* **1988**, *110*, 4150-4157.

Table II-1. Oxygen-oxygen and iron-oxygen stretching frequencies (cm^{-1}) of oxy-ferrous porphyrins.

Compound	$\nu(O_2)$	$\nu(Fe^{II}\text{-}O_2)$	Temp.	Ref.
Fe(TMP)O$_2$	1171	522	-100°C	This work
Fe(TPP)O$_2$				
end-on	1195	509	-248°C	19
side-on	1106		-258°C	30a
Fe(OEP)O$_2$				
end-on	1190		-258°C	30a
side-on	1104		-258°C	30a
Fe(T$_{piv}$PP)(1-MeIm)O$_2$	1159	571	RT	31,32
Fe(TPP)(Pip)O$_2$	1157	575	-70°C	30b

Abbreviations: TPP, tetraphenylporphyrin; OEP, octaethylporphyrin; T$_{piv}$PP, *meso*-tetra(α, α, α, α-o-pivalamidophenyl)porphyrin; Im, imidazole; Pip, piperidine.

129
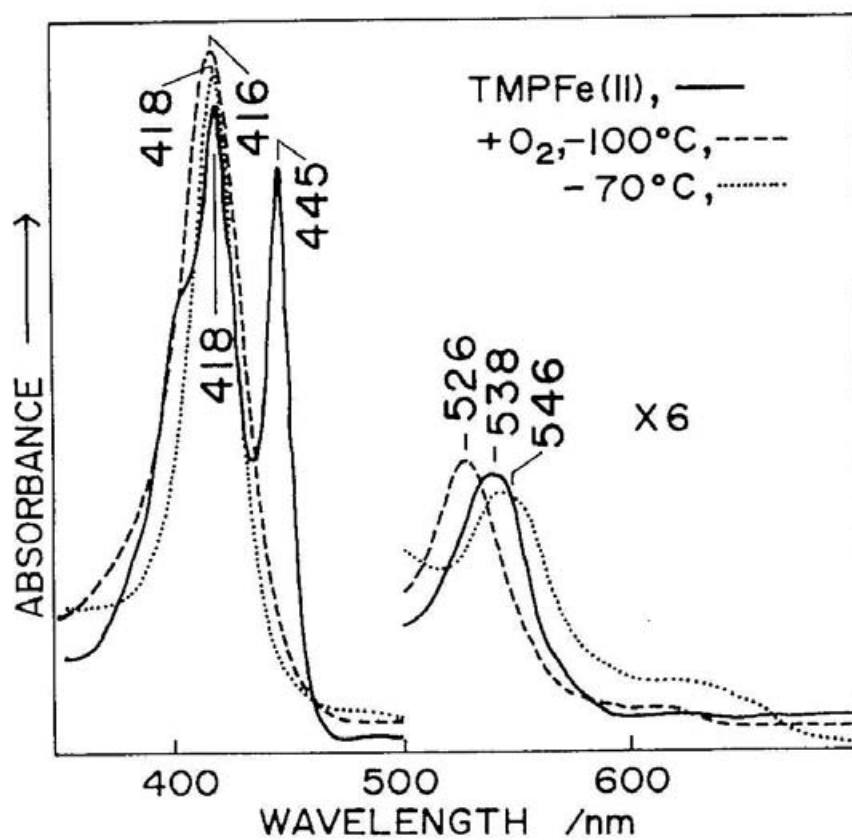
Figure II-1. Absorption spectra of (TMP)Fe[II] and its oxidized intermediates in toluene; solid line, (TMP)Fe[II]; broken line, intermediate 1; dotted line, intermediate 2. (see text).

130
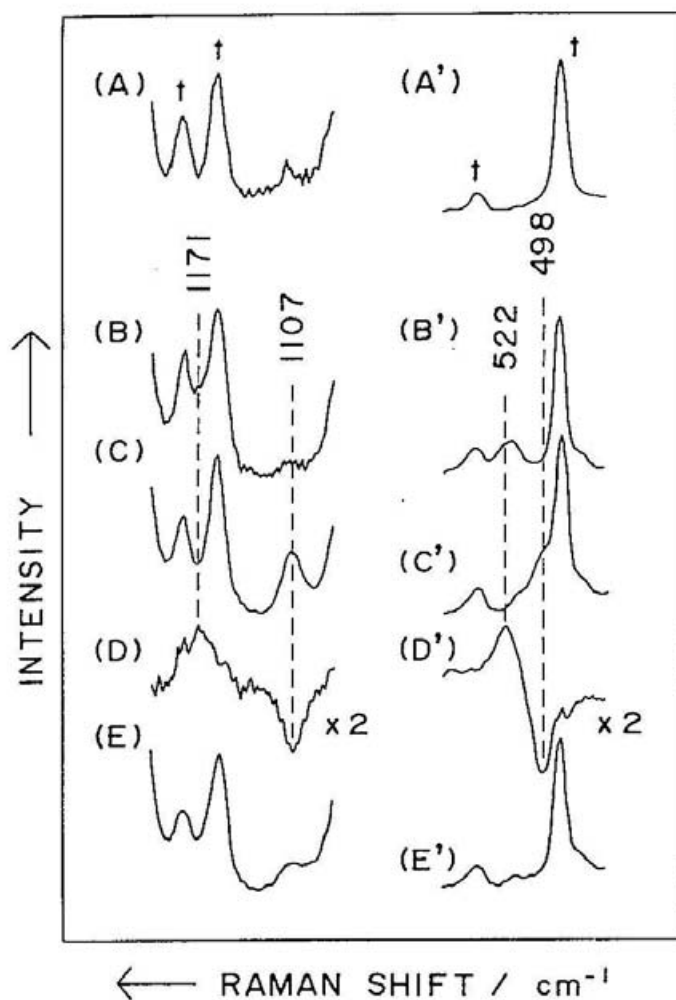
Figure II-2. RR spectra of (TMP)Fe^{II} and its oxidized intermediates in the ν(O$_2$) (left) and ν(Fe^{II}-O$_2$) stretching (right) regions; (A) and (A') (TMP)Fe^{II}; (B) and (B') Intermediate 1 obtained with ^{16}O$_2$; (C) and (C') Intermediate 1 obtained with ^{18}O$_2$; (D) Difference spectrum [= (B) - (C)]; (D') Difference spectrum [= (B') - (C')]; (E) Intermediate from ^{18}O$_2$ obtained after warming the sample used to record spectrum 2(C); (E') Intermediate from ^{16}O$_2$ obtained after warming the sample used to record spectrum 2(B'). The spectra in the ν(O$_2$) and ν(Fe^{II}-O$_2$) regions were obtained for toluene-h$_8$ and -d$_8$ solutions, respectively. Daggers denote Raman bands of solvent.

131
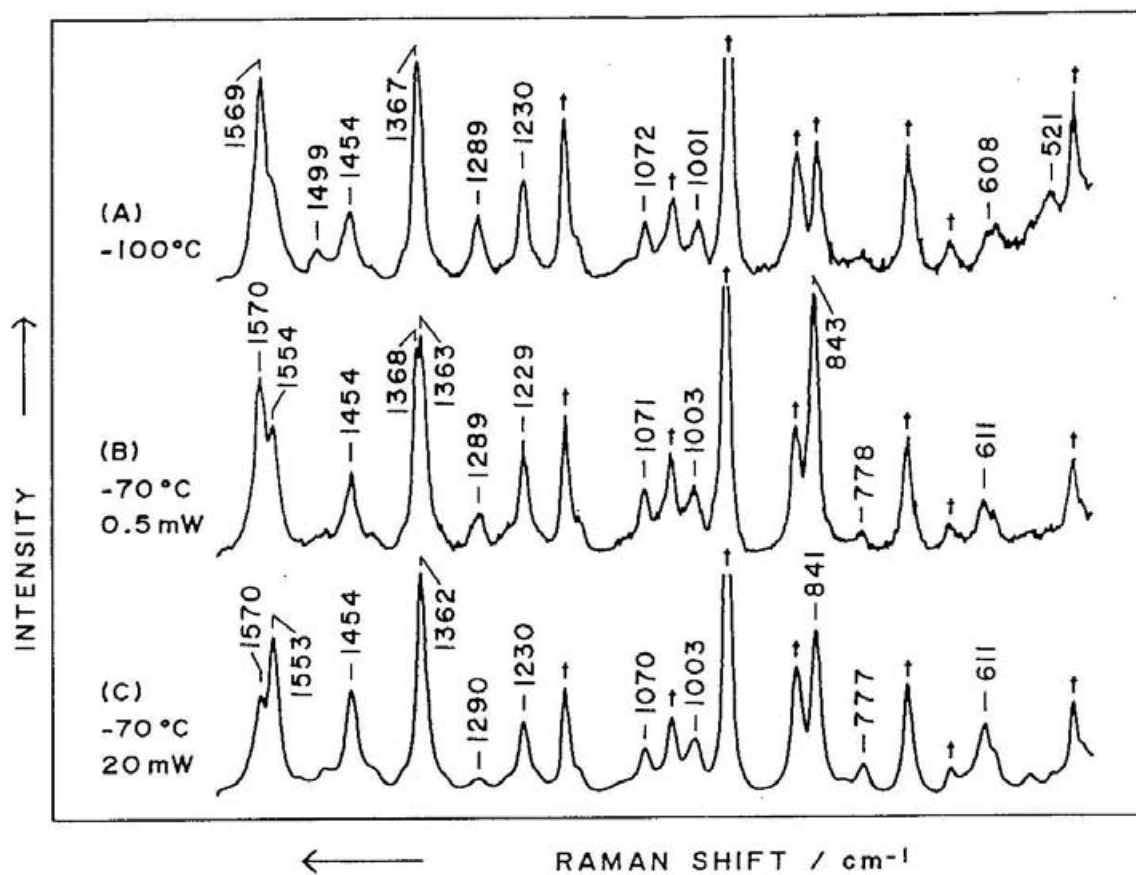
Figure II-3. RR spectra of the intermediate **1** and **2** + **3** + **4** in toluene-d_8; (A) Intermediate **1** observed at -100°C; (B) Intermediate **2** + **3** + **4** observed at -70°C with minimum laser power (0.5 mW at the sample point); (C) Intermediate **3** + **4** observed at -70°C with a higher laser power (20 mW at the sample point). Daggers denote Raman bands of solvent.
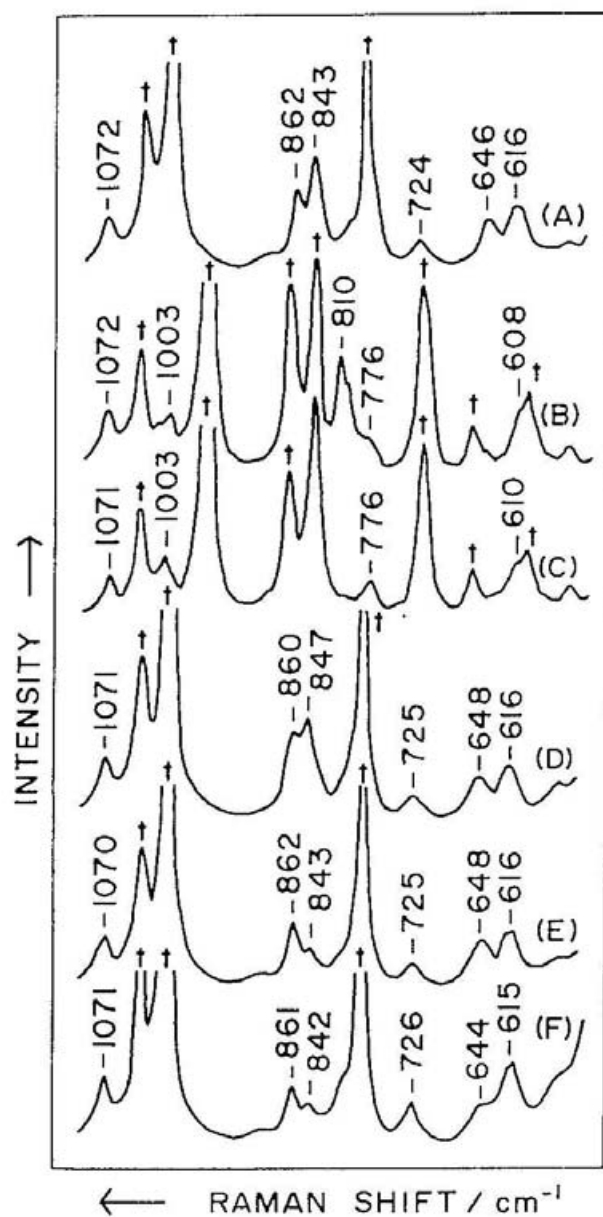
132

Figure II-4. Isotopic substitution effects of intermediates 3 on RR spectra in the 1100-550 cm^{-1} region; (A) ^{16}O derivative in toluene-h_8; (B) ^{18}O derivative in toluene-d_8; (C) ^{16}O derivative in toluene-d_8; (D) ^{54}Fe ^{16}O derivative in toluene-h_8; (E) ^{16}O derivative after warming up to -30°C and cooled to -70°C in toluene-h_8; (F) (TMP)Fe^{III}-OH in toluene-h_8. Daggers denote Raman bands of solvent.
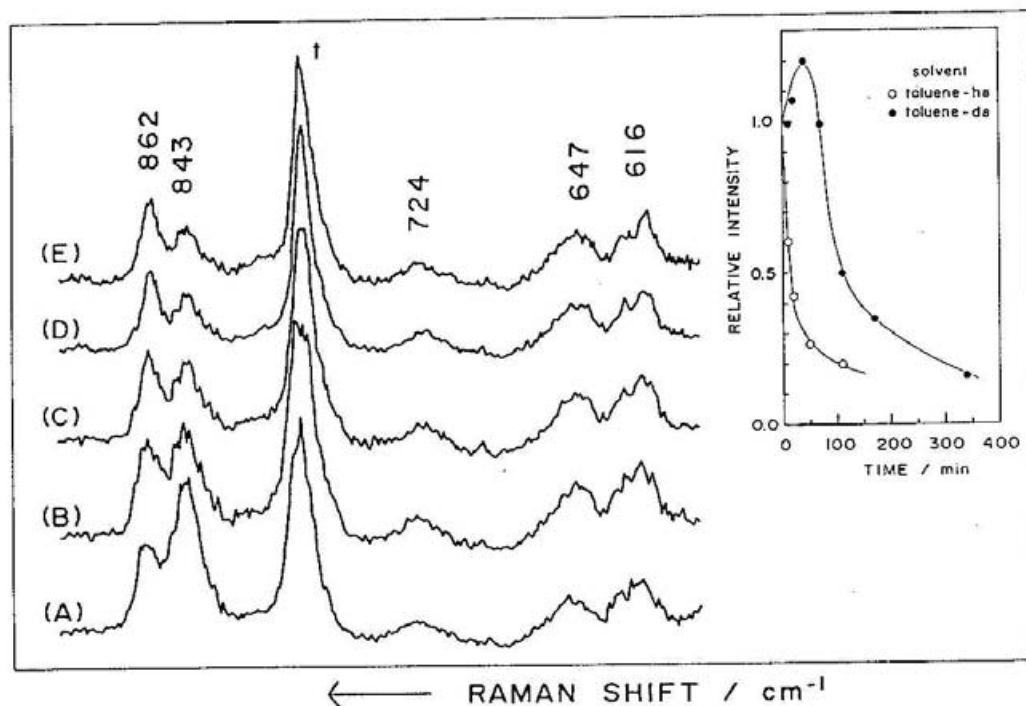
133

Figure II-5. Intensity change of the $\nu\,(\text{Fe}^{IV}=\text{O})$ RR band due to thermal decomposition of **3**. Spectrum (A) was observed in toluene-h_8 at -70°C just after preparation at -100°C whereas spectra (B), (C), (D) and (E) were observed at -100°C after keeping the sample at -30°C for 10, 20, 50 and 110 min, respectively. The inset shows the relative intensity of the $\nu\,(\text{Fe}^{IV}=\text{O})$ RR band to the solvent band (at 783 cm^{-1} for toluene-h_8 and at 869 cm^{-1} for toluene-d_8) plotted against the period in which the sample was kept at -30°C; (○): in toluene-h_8, (●): in toluene-d_8. A dagger deontes the solvent band used as reference.
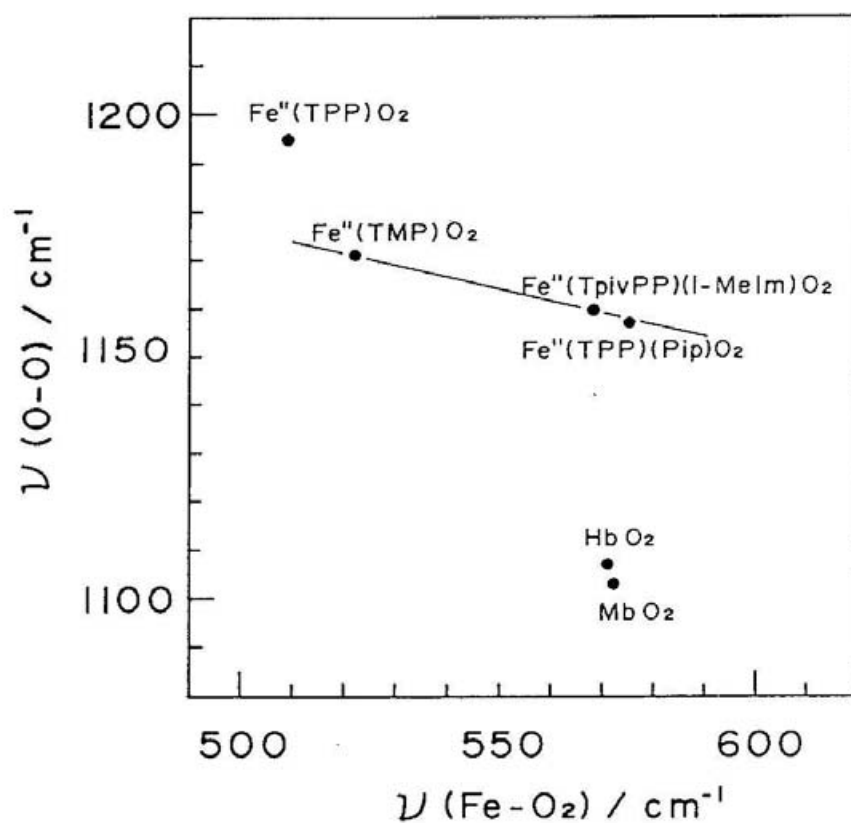
134

Figure II-6. The $\nu(O_2)$ vs $\nu(Fe^{II}-O_2)$ plot for oxygenated ironporphyrins and heme proteins; $Fe^{II}(TPP)O_2$, data from Refs. 30a (IR) and 19 (Raman); $Fe^{II}(TPP)(Pip)O_2$, data from Ref. 30b; $Fe^{II}(T_{piv}PP)(1-McIm)O_2$, data from Refs. 32 (IR) and 31 (Raman). The straight line represents $\nu(O_2) = -0.264 \cdot \nu(Fe^{II}-O_2) + 1309$ (see text).

135

Chapter III

Resonance Raman Characterization
of Ferric- and Ferrylporphyrin π Cation Radicals
and the $Fe^{IV}=O$ Stretching Frequency

Abstract

Resonance Raman (RR) spectra of porphyrin π cation radicals were investigated for the Fe^{III} and Fe^{IV} states by using tetramesitylporphyrinatoiron(III) complexes [(TMP)Fe]. Vibrational modes were assigned on the basis of the isotopic frequency shifts upon ^{15}N and meso-^{13}C substitution and the reported normal coordinate analysis. For both Fe^{III} and Fe^{IV} porphyrin π cation radicals, the ν_4 band was significantly shifted to the lower frequency side and thus the previous assignment by Kincaid et al. (*J. Am. Chem. Soc.* **1989**, *111*, 735-737) should be modified. The RR spectra exhibited no temperature dependence between -100 and 10°C and between -100 and -80°C for the Fe^{III}- and Fe^{IV} porphyrin π cation radicals, respectively, indicating the presence of one type of radicals, presumably the a_{2u} radical judging from the low frequency shifts of the ν_2 mode. The controversy about the $Fe^{IV}=O$ stretching mode ($\nu(Fe^{IV}=O)$) of the $Fe^{IV}=O$ porphyrin π cation radical was clarified by demonstrating that the two $\nu(Fe^{IV}=O)$ RR bands appear at 829 and 801-802 cm^{-1} in the presence of EtOH and *n*-PrOH, respectively, while a single band appears at 831 and 801 cm^{-1} in the presence of MeOH and *t*-BuOH, respectively. The difference between the $\nu(Fe^{IV}=O)$ frequencies in the presence and absence of MeOH was interpreted reasonably in terms of the effect of the fifth ligand.

III-1. Introduction

Oxidation states of iron-porphyrins higher than the ferric state play a key role in the catalytic reactions by heme enzymes[1,2] such as peroxidases, catalases and cytochrome P-450 and also in epoxidation of olefins by oxoferryl porphyrins.[3] Localization of the oxidative equivalent particularly in the Fe^V oxidation state has been a matter of debate. The corresponding intermediate for horseradish peroxidase (HRP, Compound I) is considered to have the $Fe^{IV}=O$ porphyrin π cation radical on the basis of Mössbauer[4], visible absorption[5], ENDOR[6], NMR[7], EPR[8], and EXAFS[9] spectroscopies, while that of cytochrome c peroxidase (CcP, compound ES)[10] was demonstrated to have the $Fe^{IV}=O$ neutral porphyrin and protein cation radical.[11] A question to be answered is how the $Fe^{IV}=O$ bond is affected by the localization of the oxidative equivalent to the porphyrin ring or the protein moiety. Furthermore, when the oxidative equivalent is localized in a porphyrin ring, the orbital occupancy of the unpaired electron is suggested to relate to the functional differences of enzymes; the intermediates of catalase and peroxidase were deduced to have the $^2A_{1u}$ and $^2A_{2u}$ ground states, respectively, on the basis of absorption spectra of model compounds.[5] However, recent studies with NMR[12] and ESR[13] assigned both reference model compounds to a_{1u} radicals.

Resonance Raman (RR) spectroscopy is a powerful technique for characterizing the iron-porphyrins in heme proteins as well as in organic solvents.[14] While some in-plane vibrations exhibit frequency shifts depending on delocalization of π electrons between the iron ion and the porphyrin macrocycle, the frequency of the $Fe^{IV}=O$ stretching vibration ($\nu(Fe^{IV}=O)$) serves as the most direct probe of the $Fe^{IV}=O$ bond. The $\nu(Fe^{IV}=O)$ RR band was identified for HRP compound II,[15-17] CcP compound ES[18] and myeloperoxidase.[19] The corresponding $\nu(Fe^{IV}=O)$ band for the $Fe^{IV}=O$ porphyrins in organic solvents was also elucidated by several groups.[20-23] However, the RR spectra of HRP compound I with one more higher oxidation state than compound II has been controversial due to its photolability.[24-28] Therefore, it is quite important to establish in a model system how RR spectra are altered by further oxidation of the $Fe^{IV}=O$ porphyrin and how the $Fe^{IV}=O$ bond is affected by it.

Previously we reported the $\nu(Fe^{IV}=O)$ RR band of the $Fe^{IV}=O$ porphyrin π cation radical,[29] but it was claimed by Kincaid et al.[30] who suggested that the previous $\nu(Fe^{IV}=O)$ RR band might arise from a photoreacted product. On the other hand, RR spectra of metalloporphyrin π cation radicals were reported for (TPP)M (TPP:

139

tetraphenylporphyrin) and (OEP)M (OEP: octaethylporphyrin) complexes,[31-33] in which M = Co^{II}, Cu^{II}, Zn^{II}, Ni^{II}, Co^{III}, and $V^{IV}=O$, and the RR spectral differences between the a_{1u} and a_{2u} radicals have been established. However, an iron-porphyrin was not included in such studies. Accordingly, in the present study, we investigated the RR spectra of Fe^{III}- and Fe^{IV}-porphyrin π cation radicals by using tetramesityl-porphyrinatoiron(III) complexes [(TMP)Fe]. Here we assign the vibrational modes of the cation radicals on the basis of ^{15}N and ^{13}C isotopic frequency shifts, explain how the porphyrin macrocycle is altered by removal of an electron, and solve the remaining controversy about the $\nu(Fe^{IV}=O)$ RR band stated above.

III-2. Experimental Section

Materials. ^{15}N-enriched pyrrole (95%) and ^{13}C-enriched potassium cyanide (99%) were purchased from Cambridge Isotope Laboratories and used without further purification. The latter was used after conversion to $Zn(^{13}CN)_2$ by using $ZnSO_4$.[34] $^{54}Fe_2O_3$ (97% enriched) was purchased from Rohstoff Einfuhr and converted to $^{54}FeSO_4$ with the method reported previously.[35] The ^{15}N-enriched $TMPH_2$ ($TMP-^{15}N_4H_2$) was synthesized from pyrrole-^{15}N and mesitaldehyde in the presence of BF_3Et_2O according to Lindsey et al.[36] Its mass spectrum gave a peak at m/e = 786.57 for the calculated value of 786.42 expected for $C_{56}H_{54}^{15}N_4$. The meso-^{13}C-incorporated $TMPH_2$ ($TMP-^{13}C_4H_2$) was obtained similarly from the ^{13}C-enriched mesitaldehyde which was prepared in 77% yield from the $AlCl_3$ catalyzed Gattermann reaction of mesitylene with $Zn(^{13}CN)_2$.[37] The IR spectrum of mesitaldehyde gave the $^{13}CH=O$ stretching band at 1650 cm^{-1} but no band of the $^{12}CH=O$ stretching mode. The mass spectrum of $TMP-^{13}C_4H_2$ exhibited a single peak at m/e = 786.00 for the calculated value of 786.45 expected for $C_{52}H_{54}N_4^{13}C_4$.

(TMP)Fe^{III}Cl was obtained from the reaction of $FeSO_4$ with $TMPH_2$ in N,N-dimethylformamide (DMF), followed by the treatment with 3M HCl according to Kobayashi et al.[38] The (TMP)Fe^{III}Cl was converted to (TMP)Fe^{III}ClO$_4$ by treatment with AgClO$_4$ and then oxidized to a porphyrin π cation radical [(TMP$^{+\cdot}$)Fe^{III}(ClO$_4$)$_2$] by Fe(ClO$_4$)$_3$. This exhibited dark-green color and its absorption spectrum was in agreement with that reported[39]. The ferryloxo porphyrin π cation radical [(TMP$^{+\cdot}$)Fe$^{IV}=O$] was prepared through oxidation of (TMP)Fe^{III}Cl by m-chloroperoxybenzoic acid (mCPBA) in the Raman cell kept in the ethanol bath at -80°C according to Groves et al.[40] and its formation was confirmed by the color change to

140

the characteristic green color. For the experiments with alcohol containing solvents, the mixing ratio of alcohol to CH_2Cl_2 was 1:19 in volume. Since this complex was not so stable that its RR spectrum was measured within 6 min after formation.

Raman Measurements. Raman scattering was excited at 406.7 nm with a Kr^+ ion laser (Spectra Physics, 2016) and detected with a photodiode array (PAR 1420) attached to a double monochromator (Spex 1404). The spectral resolution in terms of the width/pixel was 1.4 cm^{-1}. Raman shifts were calibrated with indene as standard with the accuracy of ± 1 cm^{-1}. All measurements were carried out with a spinning cell with a diameter of 2 cm. The cell was span at 1600 rpm in a cryostat which was cooled to -80°C by cold N_2 gas. The laser power was brought to the lowest possible (5 mW) to avoid photoreaction except for the experiments of power dependence.

III-3. Results

Ferric Neutral Compounds. Figure III-1 shows the RR spectra of (TMP)Fe^{III}Cl and its pyrrole-^{15}N and meso-^{13}C isotopomers. In order to draw structural information from the observed RR spectra, it is indispensable to characterize the vibrational properties of some marker bands to be used in this study. The vibrational properties of the porphyrin skeleton of (TMP)M would be close to those of (TPP)M, for which Spiro and coworkers[41] and Bocian and coworkers[42] worked out the normal coordinate analyses with M=Ni^{II} and M=Cu^{II}, respectively. Even though the absolute frequencies depend on a metal ion coordinated, the isotopic frequency shifts should generally be close between the corresponding vibrational modes if these modes were alike. Accordingly, we assign the observed RR bands of (TMP)Fe^{III}Cl on the basis of the isotopic frequency shifts upon ^{15}N [$\Delta\nu(^{15}N)$] and ^{13}C substitutions [$\Delta\nu(^{13}C)$]. Since the observed frequency shifts are closer to those of (TPP)Ni^{II} than to those of (TPP)Cu^{II}, we adopt the mode numbering by Spiro and coworkers.[41]

The observed frequency shifts for (TMP)Fe^{III}Cl and plausible assignments are summarized in Table III-I together with the corresponding reported data of (TPP)Ni^{II}.[41] Two polarized (p) bands at 1364 and 1003 cm^{-1} exhibit large $\Delta\nu(^{15}N)$ and therefore are assigned to ν_4 and ν_6, respectively. They involve mainly the $C_\alpha N$ and $C_\alpha C_\beta$ stretching vibrations.[41] The p bands at 1554 and 1454 cm^{-1} gives large $\Delta\nu(^{13}C)$ and zero $\Delta\nu(^{15}N)$, in agreement with the properties of the ν_2 and ν_3 modes of (TPP)Ni^{II}. These frequencies reflect mainly the strength of the $C_\beta C_\beta$ and $C_\alpha C_m$ bonds. The p band at 1073 cm^{-1} shows little shift upon both ^{15}N and ^{13}C substitutions

and is assigned to ν_9, which mainly involves the in-plane C_β-H bending vibration. It is puzzling that the 1080 cm^{-1} band of (TPP)Cu^{II} shows large isotopic frequency shifts $[\Delta\nu(^{15}N)=6$ and $\Delta\nu(^{13}C)=3$ cm$^{-1}]$[42] contrary to small shifts for (TPP)Ni^{II} and the present iron complexes. The highest frequency depolarized (dp) band at 1493 cm^{-1} is insensitive to both ^{15}N and ^{13}C substitutions and is assigned to ν_{11} which is predominantly associated with the $C_\beta C_\beta$ stretching mode.[41] The dp band at 1274 cm^{-1} gives large $\Delta\nu(^{15}N)$ and small $\Delta\nu(^{13}C)$, while the dp band at 1254 cm^{-1} shows large shifts for both ^{15}N and ^{13}C substitutions. These properties of the bands at 1274 and 1254 cm^{-1} are in agreement with those of ν_{12} and ν_{27}, respectively.[41] The ν_{12} and ν_{27} frequencies reflect primarily the strength of $C_\alpha N$ bond, although the latter contains significantly the C_m-phenyl stretching character. The dp band at 1183 cm^{-1} shows little shift for both ^{15}N and ^{13}C substitutions, and this is anticipated for ν_{17} and ν_{34}.[41] Since the absolute frequency is close to ν_{34} of (TPP)Ni^{II}, the band is tentatively assigned to ν_{34}, which contains mainly the C_β-H in-plane bending vibration. The dp band at 1018 cm^{-1} exhibits large $\Delta\nu(^{15}N)$ and moderate $\Delta\nu(^{13}C)$, and is assigned to ν_{15}, which arises mainly from the $C_\alpha C_\beta$ stretching vibration. The dp band at 863 cm^{-1} shows very large $\Delta\nu(^{13}C)$ and small $\Delta\nu(^{15}N)$. This is incompatible with the property of ν_{32}, but around 800-900 cm^{-1} region there is no dp band of (TPP)Ni^{II} which shows such a large $\Delta\nu(^{13}C)$. In contrast, the dp band at 846 cm^{-1} exhibits moderate sizes of $\Delta\nu(^{15}N)$ and $\Delta\nu(^{13}C)$ which are smaller than those of ν_{16} of (TPP)Ni. Therefore, with regard to ν_{32} and ν_{16}, the actual vibrational mode would be appreciably different between (TMP)Fe^{III}Cl and (TPP)Ni, but this vagueness would have no problem in this study, since these modes contain mainly the angle deformation character.

The RR spectra of a six-coordinate low-spin derivative with imidazole (Im) as axial ligands are shown in Figure III-2, where the spectra of pyrrole-^{15}N and meso-^{13}C derivatives are also contained. The assignments of bands based on the polarization properties and isotopic frequency shifts are summarized in Table III-II. The skeletal double bond stretching frequencies such as ν_2, ν_{11}, ν_3 and ν_4 are shifted to a higher frequency by 4-8 cm^{-1} upon the change from the five-coordinate high-spin to six-coordinate low-spin state, while other bands exhibit smaller shifts. The ν_{34} band seems to exist at 1187 cm^{-1} but it is too weak to confirm. It is interesting that the intense ν_{12} band of (TMP)Fe^{III}Cl is missing for (TMP)Fe^{III}(Im)$_2$. General behavior about the isotopic frequency shifts is similar between the two kinds of complexes. Therefore, the vibrational modes themselves are little altered by the change of the coordination

number and the spin state of the iron(III) ion.

Ferric π Cation Radical. Figure III-3 shows the RR spectra of $(TMP^{+\cdot})Fe^{III}(ClO_4)_2$ and its isotopomers. As seen from the relative intensity to the solvent peak at 1423 cm^{-1}, Raman intensities of $(TMP^{+\cdot})Fe^{III}(ClO_4)_2$ are noticeably weak despite of the fact that the absorbance of the Soret band of the π cation complex is not low.[39] This ferric porphyrin π cation was stable against laser illumination and, accordingly, the use of the higher laser power did not yield any RR spectral changes. The RR band at 1325 cm^{-1} (p) exhibits a frequency shift by -6 cm^{-1} upon ^{15}N substitution and is therefore assignable to ν_4. Note that the ν_4 frequency of the π cation radical is distinctly lower than that of the ferric neutral porphyrins shown in Figures III-1 and -2 (1364-1368 cm^{-1}), although the vibrational mode itself might be slightly altered from them. The dp band at 1250 cm^{-1}, which is probably berried under the 1234 cm^{-1} band for the ^{15}N derivative but can be identified at 1247 cm^{-1} with the ^{13}C derivative, has large $\Delta\nu(^{15}N)$ and small $\Delta\nu(^{13}C)$. These features suggest to assign the 1250 cm^{-1} band to ν_{12}, which also arises from the $C_\alpha N$ stretching vibrations. This is also downshifted from that of $(TMP)Fe^{III}Cl$. Thus, all the vibrations containing the $C_\alpha N$ stretching character are shifted to lower frequencies in the π cation radical.

The nearby band at 1231 cm^{-1} (p) is assignable to ν_1. The assignment of an intense and polarized band at 1509 cm^{-1}, which shows a large shift (-12 cm^{-1}) upon ^{13}C substitution, is a key of this spectrum and will be discussed later. Note that the 1509 cm^{-1} band exhibits an appreciable shift upon ^{15}N substitution contrary to expectation to the ν_2 mode. Frequencies of other bands below 1240 cm^{-1} are not greatly different from those of $(TMP)Fe^{III}Cl$. The frequency of the phenyl ring mode at 1611 cm^{-1} remains unaltered by ionization of the porphyrin ring, suggesting that the electronic states of phenyl rings are almost completely separated from those of porphyrin rings. Plausible assignments of the Raman bands of $(TMP^{+\cdot})Fe^{III}(ClO_4)_2$ are summarized in Table III-III. Although the mode numbers are commonly used in the neutral porphyrins and the π cation radical, actual vibrational modes would be appreciably different between them. The results indicate that removal of an electron from the porphyrin ring causes changes of a relatively limited number of double-bond stretching frequencies. The RR spectrum little changed between 10 and -100°C.

Ferryl π Cation Radicals. Figure III-4 shows RR spectra of $(TMP^{+\cdot})Fe^{IV}=O$ and its isotopomers in CH_2Cl_2 containing methanol (MeOH). The formation of the target compound was confirmed with visible absorption spectrum.[29] The Raman

143

intensity is considerably weak probably due to low Soret absorbance. In contrast with $(TMP^{+\cdot})Fe^{III}(ClO_4)_2$, $(TMP^{+\cdot})Fe^{IV}=O$ was readily photo-decomposed upon stop of spinning of the Raman cell and the RR spectrum of the photoproduct observed then was the same as that of $(TMP)Fe^{III}OH$.

Recently Kincaid et al.[30] assigned the RR band of $(TMP^{+\cdot})Fe^{IV}=O$ at 1358 cm^{-1} to the ν_4 band. However, as evident from Figures III-4D and -4A, this band is depolarized and exhibits no frequency shift upon ^{15}N substitution. Therefore, the 1358 cm^{-1} band cannot be ν_4. On the other hand, the RR band at 1335 cm^{-1} is shifted to 1319 cm^{-1} upon ^{15}N substitution and is therefore assigned to ν_4. This frequency is significantly lower than that (1371 cm^{-1}) of the oxoferryl neutral porphyrin $[(TMP)Fe^{IV}=O]$ reported previously.[23] If there were contaminants of any ferric TMP derivatives, a polarized band corresponding to their ν_4 band should be observed around 1364-1368 cm^{-1} as seen in Figures III-1 and -2. Since such a band is not seen in Figure III-4A, this sample seems to contain scarcely the photo-decomposed ferric compounds.

The polarized band at 1517 cm^{-1} is shifted to 1514 and 1502 cm^{-1} upon ^{15}N and meso-^{13}C substitutions, respectively, and is assignable to the ν_2 mode. However, similar to the 1509 cm^{-1} band of $(TMP^{+\cdot})Fe^{III}(ClO_4)_2$, it would not be the same mode as that expected from ν_2 of $(TPP)Ni^{II}$ due to the appreciable ^{15}N shift. The weak dp band at 1457 cm^{-1} might arise from ν_{11} although it gives large $\Delta\nu(^{13}C)$. The RR spectrum of $(TMP^{+\cdot})Fe^{IV}=O$ did not change between -100 and -80°C, although at higher temperature the decomposed compounds appeared. Tentative assignments of other RR bands of $(TMP^{+\cdot})Fe^{IV}=O$ are summarized in Table III-IV together with the observed frequencies of the corresponding bands of oxoferryl neutral porphyrin $[(TMP)Fe^{IV}=O]$.[23]

In our previous report,[29] the RR band at 831 cm^{-1}, which is seen at similar frequencies for the ^{15}N and ^{13}C derivatives in Figure III-4, was assigned to the $Fe^{IV}=O$ stretching vibration $(\nu(Fe^{IV}=O))$ of $(TMP^{+\cdot})Fe^{IV}=O$ on the basis of the ^{18}O and ^{54}Fe isotopic frequency shifts. However, Kincaid et al.[30] claimed that this band arose from a photo-decomposed compound and the $\nu(Fe^{IV}=O)$ band of $(TMP^{+\cdot})Fe^{IV}=O$ was located at 801 cm^{-1}. As noted previously, when the spinning of the cell was abolished, the 831 cm^{-1} band disappeared and therefore, it cannot be ascribed to a stable photo-product. Furthermore, the relative intensity of the 831 cm^{-1} band to other porphyrin bands was not altered by the laser power change from 5 to 0.5

mW that was the lowest possible power for the Raman measurements, and a Raman band was not recognized around 800 cm^{-1} with the weakest laser power. In this regard the reported results shown in Figure III-1 of Ref. 30 were partly nonreproducible. According to the initial report on $(TMP^{+\bullet})Fe^{IV}=O$ by Groves et al.,[40] this compound is more stabilized in the presence of MeOH than in its absence. Therefore, in a previous study[29] we carried out the experiments for a solution containing MeOH. However, MeOH might have coordinated to the trans position of oxo-oxygen and altered the $\nu(Fe^{IV}=O)$ frequency. In order to solve this controversy, we prepared the π cation radical without MeOH. The results are shown in Figure III-5.

A prominent RR band at 1355 cm^{-1} shows no shift upon ^{15}N substitution but is shifted to a lower frequency by 6 cm^{-1} upon ^{13}C substitution. The ν_4 band, which should be polarized and is expected to shift upon ^{15}N substitution, cannot be identified in Figure III-5. This band might be buried in a wing of the 1355 cm^{-1} band, but a difference calculation failed to reveal the presence of the ^{15}N isotope-sensitive band. A new band appears at 1526 cm^{-1}, which exhibits -4 and -8 cm^{-1} shifts upon ^{15}N and ^{13}C substitutions, respectively, similar to the 1509 cm^{-1} band of $(TMP^{+\bullet})Fe^{III}(ClO_4)_2$ and is considered to arise from the modified ν_2. Frequencies of other bands and their behavior upon isotopic substitutions bear close resemblance between Figures III-4 and -5, although the relative intensity of the band at 1003 cm^{-1} to others is slightly higher. It is noted that an intense band is observed at 801 cm^{-1} in Figure III-5.

The inset of Figure III-6 compares the visible absorption spectra of $(TMP^{+\bullet})Fe^{IV}=O$ observed in the presence and absence of MeOH. The difference in the α band is clear, although the difference was little in the Soret band. Figure III-6 shows the behavior of the 801 cm^{-1} band for the use of $(TMP)^{54}FeCl$ and ^{18}O-labeled mCPBA. The 801 cm^{-1} band shifts to a higher frequency by 3 cm^{-1} with the ^{54}Fe porphyrin and to a lower frequency by 37 cm^{-1} with the ^{18}O derivative. These agree closely with the expected shifts of $\Delta\nu(^{54}Fe)=3.3$ cm^{-1} and $\Delta\nu(^{18}O)=-35.2$ cm^{-1} calculated for a diatomic Fe=O harmonic oscillator. Therefore, this band is assigned to the $\nu(Fe^{IV}=O)$ band of $(TMP^{+\bullet})Fe^{IV}=O$, in agreement with Kincaid et al.[30] When the laser power was raised, the 831 cm^{-1} band did not appear but the 801 cm^{-1} band simply disappeared. To gain an insight into the compound obtained in the presence of MeOH, we added various kinds of alcohols to the solvent and the results are summarized in Figure III-7.

As shown by spectra B and C in Figure III-7, the two bands around 831 and 801

cm^{-1} are coexistent for the solvent containing ethanol (EtOH) (precisely, 829 and 802 cm^{-1}) and 1-propanol (n-PrOH) (829 and 801 cm^{-1}), while frequencies of other bands are little altered. For the solution with 2-methyl-2-propanol (t-BuOH) (D), the 831 cm^{-1} band was missing but a band was present at 801 cm^{-1} similar to the case of the absence of alcohol (E). In a separate study on (OEP)Fe^{III}(2-MeIm),[43] coordination of MeOH, EtOH, and n-PrOH to the sixth coordination position of the Fe^{III} ion was confirmed by observations of the Fe^{III}-alcohol stretching RR band and a CT absorption band around 570-590 nm, but t-BuOH did not give such evidence for coordination. Accordingly, it is deduced that steric hindrance between a bulky alkyl group and pyrrole nitrogens interferes with coordination of t-BuOH. The frequency difference in $\nu(Fe^{IV}=O)$ between the presence and absence of alcohol might be attributed to the difference between the alcohol-coordinated and non-coordinated compounds. However, this is not compatible with a general idea that the five coordinate oxo-ferryl complexes give rise to a $\nu(Fe^{IV}=O)$ frequency higher than that in the six-coordinate complexes.[20-23]

An alternative idea comes from the fact that the RR spectra in Figures III-7B, -7C and -7D are very alike except for the 801/831 cm^{-1} features. Comparison of RR spectra between the five- and six-coordinate ferric complexes shown in Figures III-1 and -2 suggests that the structural difference appears in the intensity of the ν_{16} band (846 cm^{-1} in Figure III-1 and 848 cm^{-1} in Figure III-2) which is noticeably weaker for the six-coordinate complex, while frequencies of RR bands below 1100 cm^{-1} are almost the same between the two kinds of complexes. The absence of the ν_{16} band in Figure III-7 despite of the presence of the ν_{32} band which is characterized by a large $\Delta\nu(^{13}C)$ in Figures III-4 and -5, suggests that the compound in question adopts the six-coordinate structure irrespective of the presence or absence of alcohol. Previously, Groves et al.[40] inferred that the reaction product of mCPBA, that is, m-chlorobenzoic acid (mCBA), was coordinated to the trans position of oxo-oxygen. In the presence of alcohol, mCBA would compete with alcohol for coordination at the axial position but the equilibrium becomes biased to alcohol. In this interpretation, the frequency difference in $\nu(Fe^{IV}=O)$ is ascribed to the difference in σ donation of the trans ligand; the larger the σ donation is, the lower the $\nu(Fe^{IV}=O)$ frequency is. If the σ donation from mCBA is larger than that of alcohol, the lower $\nu(Fe^{IV}=O)$ in the absence of alcohol is reasonably interpreted. In fact, for oxoferryl neutral complexes, the $\nu(Fe^{IV}=O)$ frequency is lower when the trans ligand is N-MeIm (807 cm^{-1}) than when

it is THF (829 cm^{-1}).[21] One may argue that the ligand with higher σ donor property wins in the competition for coordination. It would be true if the concentration of mCBA were the same as that of alcohol. Actually, however, the concentration of alcohol is much higher than that of mCBA.

III-4. Discussion

Nature of the Fe=O Bond in the Ferryl π Cation Radical. An oxoferryl porphyrin π cation radical has a catalytic activity as a monoxygenase in contrast to the oxoferryl neutral porphyrins. It is curious to know an origin of the differences in nature of the Fe=O bond between the two kinds of complexes. The $\nu(Fe^{IV}=O)$ RR bands have been studied for various Fe-porphyrins,[20-23] and they can be categorized into three groups; five-coordinate complexes ($\nu(Fe^{IV}=O) = 852$ cm^{-1} for O_2 matrix[20] and 843 cm^{-1} in toluene solution[23]), six-coordinate with a weak trans ligand ($\nu(Fe^{IV}=O) = 829-820$ cm^{-1})[21] and those with strong trans ligand ($\nu(Fe^{IV}=O) = 807$ cm^{-1})[21]. In the present study, the $\nu(Fe^{IV}=O)$ frequency of the π cation radicals was located at 831 cm^{-1} for weak trans ligand (alcohol) and at 801 cm^{-1} for stronger trans ligand (mCBA). Consequently, the difference in $\nu(Fe^{IV}=O)$ frequencies between the porphyrin π cation radical and neutral porphyrin is smaller than that caused by the effect from the trans ligand.

Recently, Su et al.[44] observed the upshift of the $V^{IV}=O$ stretching frequency ($\nu(V^{IV}=O)$) of (OEP)$V^{IV}=O$ upon formation of a π cation radical (a_{1u}) and ascribed it to the polarization effect of a π electrons. They observed 1.00% downshift of the $\nu(V^{IV}=O)$ band of (OEP)$V^{IV}=O$ when solvent was changed from benzene to CH_2Cl_2 and 1.52% upshift of it upon the formation of a π cation radical without a change of the coordination number. Upon coordination of alcohol or a strong ligand like imidazolate to the trans position of oxygen, they observed 2.35% or 5.99% decrease of the $\nu(V^{IV}=O)$ frequency. If the same rate is applied to (TMP)$Fe^{IV}=O$ with $\nu(Fe^{IV}=O)$ at 843 cm^{-1} in toluene,[23] the $\nu(Fe^{IV}=O)$ frequency of the five coordinate neutral state in CH_2Cl_2 would be 835 cm^{-1}, and the hypothetical five coordinate (TMP$^{+\cdot}$)$Fe^{IV}=O$ would have $\nu(Fe^{IV}=O) = 848$ cm^{-1}. If mCBA was regarded as a strong ligand like imidazolate, the (TMP$^{+\cdot}$)$Fe^{IV}=O$(alcohol) and (TMP$^{+\cdot}$)$Fe^{IV}=O$(mCBA) would have $\nu(Fe^{IV}=O)=828$ and $\nu(Fe^{IV}=O)=797$ cm^{-1}, respectively. These are unexpectedly in good agreement with the observed values. Therefore, the difference between two frequencies is reasonably ascribed to the trans

147

effect.

Macor et al.[45] pointed out that the $\nu(V^{IV}=O)$ frequency is different between the a_{1u} and a_{2u} radicals; it is lower than that of neutral mode by 16 cm^{-1} for the a_{2u} radical $[(TPP^{+\bullet})V^{IV}=O]$ and higher than it by 15 cm^{-1} for the a_{1u} radical $[(OEP^{+\bullet})V^{IV}=O]$. However, one cannot rule out a possibility that a difference in porphyrin peripheral substituents (ethyl vs. phenyl) causes some differences in coordination of the trans ligand, which yields some difference in the $\nu(V^{IV}=O)$ frequency without direct interaction with the half occupied a_{1u} or a_{2u} orbital.

State of Porphyrin Macrocycle in the π Cation Radical. The characteristic feature of $(TMP^{+\bullet})Fe^{IV}=O(MeOH)$ is the considerable downshift of the ν_4 frequency and this is also true with $(TMP^{+\bullet})Fe^{III}(ClO_4)_2$. Since the peak position for $(^{13}C\text{-}TMP^{+\bullet})Fe^{IV}=O(MeOH)$ is not clear, it is difficult to deduce how close to that of (TPP)Ni the ν_4 vibrational mode of $(TMP^{+\bullet})Fe^{IV}=O(MeOH)$ is. However, judging from the large value of $\Delta\nu(^{15}N)$ compared with those of ferric compounds, the ν_4 mode of $(TMP^{+\bullet})Fe^{IV}=O(MeOH)$ should involve significant $C_\alpha N$ stretching character. Accordingly, the formation of the π cation radical with (TMP)Fe^{III} and (TMP)Fe$^{IV}=O$ is accompanied by weakening of the $C_\alpha N$ bonds and/or the vibrational mode itself became more pure $C_\alpha N$ stretching vibration. This contrasts with the case of (TPP)V$^{IV}=O$ which exhibited only 2 cm^{-1} downshift of ν_4 upon formation of the π cation radical.[45]

It is also noted that the phenyl mode becomes noticeably stronger upon formation of the π cation radical for (TPP)V$^{IV}=O$ but it remains weak for the $(TMP^{+\bullet})Fe$ system. The intensification of the phenyl band is also seen for $(TPP^{+\bullet})Cu^{II}$.[33] This may imply that in the electronic excited state or both the ground and excited states the peripheral phenyl rings of TPP become more coplanar to the porphyrin plane and thus π electrons of the phenyl group are more delocalized to the half-filled radical orbital for $(TPP^{+\bullet})M$. Since the orbital density at C_m is high for the a_{2u} radical, although it is zero for the a_{1u} radical, a slight change of the C_m-C_{phenyl} dihedral angle easily changes an amount of π delocalization. If it occurs only in the excited state, the Soret excitation causes a change of π electron distribution and thus strength of C=C bonds of the phenyl ring. Then more resonance enhancement of the phenyl mode is reasonably interpreted. In the case of $(TMP^{+\bullet})M$ π cation radicals, however, the internal rotation around the C_m-C_{phenyl} bond is interfered by the steric hindrance between two o-CH$_3$ groups of the phenyl ring and the pyrrole groups of the porphyrin, and there-

148

fore, the π conjugation between the phenyl and porphyrin rings remains unchanged upon electronic excitation even for the π cation radical. This would be a reason why the RR intensity of the phenyl mode is unaltered with $(TMP^{+\bullet})Fe$ radicals.

If such torsion around the C_m-C_{phenyl} bond also took place in the ground state of $(TPP^{+\bullet})M$ radicals, the radical property might be slightly diluted due to the delocalized electrons of the phenyl group. In the EPR study of $(TPP^{+\bullet})Zn^{II}$, leakage of the electron spin density to the phenyl rings has been detected.[47a-c] A theoretical calculation on phenyl hyperconjugation[48] which describes π-σ spin delocalization into twisted phenyl rings predicts larger leakage of the spin density for larger torsion around the C_m-C_{phenyl} bond. In a crystal, the phenyl group of (TMP)M is nearly perpendicular to the porphyrin plane[46] but that of (TPP)M is slightly rotated around the C_m-C_{phenyl} axis.[39] If similar torsion is present for $(TPP^{+\bullet})M$ in solutions, this would affect frequencies of double bond stretching modes of porphyrins and cause some difference between RR spectra of $(TMP^{+\bullet})Fe^{IV}=O$ and $(TPP^{+\bullet})V^{IV}=O$ porphyrin π cation radicals. Indeed, the ^1H NMR shift of m-protons of the phenyl ring is appreciably different between $(TMP^{+\bullet})Fe^{III}(ClO_4)_2$[40] and $(TPP^{+\bullet})Fe^{III}(ClO_4)_2$.[39] In the case of heme proteins, there should be no inflow of π electrons at C_m upon formation of the π cation radical. In this regard, the results from the RR studies on $(TPP)V=O$[45] should be carefully applied to heme proteins.

Vibrational Modes of π Cation Radicals. According to the reports on the porphyrin π cation radicals of divalent metal,[31-33] the ν_2 band is the most intense RR band upon the Soret excitation. Therefore, it is likely that the 1507 cm^{-1} band of $(TMP^{+\bullet})Fe^{III}(ClO_4)_2$ arises from the ν_2 mode. The ν_2 mode of neutral metalloporphyrins contains mainly the $C_\alpha C_m$ stretching character and is expected to show no shift upon ^{15}N substitution but a large shift upon ^{13}C substitution.[41] Indeed, such a feature was confirmed in this study for the five-coordinate high-spin and six-coordinate low-spin ferric (TMP)Fe complexes as shown in Tables III-I and -II. However, the 1507 cm^{-1} band of $(TMP^{+\bullet})Fe^{III}(ClO_4)_2$ exhibited an appreciable shift upon ^{15}N substitution as well as upon meso-^{13}C substitution. Therefore, the ν_2 mode of the porphyrin π cation radical is inferred to contain the $C_\alpha N$ stretching character, which is different from the ν_2 mode of (TPP)Ni and (TMP)Fe^{III}Cl. Since an electron is removed from the π orbital which is bonding or antibonding regarding a given bond, it is rather natural that the force constants and thus vibrational energy distributions for the π cation radicals are appreciably altered from those of neutral state. The low

149

frequency shift of ν_2 might be partly due to weakening of the $C_\alpha N$ bond. When the difference in the vibrational mode is admitted, the corresponding bands of the $Fe^{IV}=O$ porphyrin π cation radical observed at 1517 cm^{-1} for $(TMP^{+\cdot})Fe^{IV}=O(MeOH)$ (Figure III-4) and at 1526 cm^{-1} for $(TMP^{+\cdot})Fe^{IV}=O(mCBA)$ (Figure III-5) are also assignable to ν_2. Then, they are significantly lower than the ν_2 frequency (1570 cm^{-1}) of the $Fe^{IV}=O$ neutral porphyrin.

The ν_{11} band, which arises from the nearly pure $C_\beta C_\beta$ stretching vibration for Ni(TPP) and is expected to give no shift upon meso-^{13}C and ^{15}N substitutions,[41] is considered to appear at 1458 cm^{-1} for $(TMP^{+\cdot})Fe^{IV}=O(MeOH)$ and at 1457 cm^{-1} for $(TMP^{+\cdot})Fe^{IV}=O(mCBA)$, although they exhibited the meso-^{13}C isotopic shift of -8 cm^{-1}. These frequencies are significantly lower than that of $(TMP)Fe^{III}(Im)_2$ (1496 cm^{-1}), but it is not unreasonable from the fact that ν_2 band is significantly downshifted. We rather infer that this mode of the π cation radical contains the $C_\alpha C_m$ stretching character and therefore shows the meso-^{13}C isotopic frequency shift. Such changes of vibrational modes in the π cation radical are also apparent from the observed differences in the ^{15}N and meso-^{13}C isotopic frequency shifts between the ferric neutral porphyrins and π cation radicals studied here.

Czernuszewicz et al.[33] strengthened little change of vibrational modes between the neutral porphyrin and π cation radicals on the basis of similarity in deuteration shifts. They investigated $(TPP^{+\cdot})Cu^{II}$ and observed -10 and -32 cm^{-1} shifts for ν_4 and ν_2, respectively, upon formation of the π cation radical in contrast with -36 and -52 cm^{-1} for $(TMP^{+\cdot})Fe^{IV}=O$ (see Table III-IV). One of the plausible explanations for the smaller shifts for $(TPP^{+\cdot})Cu^{II}$ than those for $(TMP^{+\cdot})Fe^{IV}=O$ is that the radical character is reduced for $(TPP^{+\cdot})Cu^{II}$ due to the torsion around the C_m-C_{phenyl} bond and accordingly, its vibrational modes are closer to those of neutral porphyrins than the latter case. However, there have been no experimental data about ^{13}C and ^{15}N isotopic frequency shifts for $(TPP^{+\cdot})Cu^{II}$, and a correlation between the frequencies of the core-size marker bands and the core sizes has not been investigated for $(TPP^{+\cdot})M$ yet. Detailed discussion about the vibrational modes of $(TPP^{+\cdot})Cu^{II}$ should be postponed until such data are provided. Currently this is a sole study which gives the ^{13}C and ^{15}N isotopic shift data for (TPP)M-type π cation radicals.

a_{1u} *and* a_{2u} *Radicals.* Czernuszewicz et al.[33] revealed the RR spectral characteristics of the a_{1u} vs a_{2u} π-cation radicals of metalloporphyrins. According to them,

(OEP$^{+\bullet}$)M gives the a_{1u}-like radical and brings about upshift of ν_2 and downshift of ν_4 while (TPP$^{+\bullet}$)M gives the a_{2u}-like radical and brings about downshift of ν_2 and small but variable downshift of ν_4. The oxoferryl radical obtained in the present study is characterized by large downshifts of both ν_4 and ν_2. Therefore, this radical is categorized to the typical a_{2u} radical. This is consistent with the NMR and Mössbauer studies[40,49] which pointed out that (TMP$^{+\bullet}$)Fe^{III}(ClO$_4$)$_2$ has the a_{2u} radical character. Since the RR spectrum did not show any temperature dependence for both Fe^{III}- and Fe^{IV}=O porphyrin π cation radicals, coexistence of two kinds of radicals[50] is unlikely. In other words, the energy difference between the a_{1u} and a_{2u} radicals is fairly large.

Mössbauer, NMR and X-ray crystallographic analyses of the six-coordinate (TPP$^{+\bullet}$)Fe^{III}(ClO$_4$)$_2$ and five-coordinate (TPP$^{+\bullet}$)Fe^{III}(SbCl$_6$) revealed the presence of the ferro- and antiferro-magnetic coupling between the high-spin iron and the unpaired electron in the a_{2u} orbital.[39,49] Since the a_{2u} orbital has a large density at nitrogen,[51] the planarity of the FeN$_4$ core is expected to affect the spin arrangement; if it was domed, overlapping between the d_π orbitals of iron(III) and the a_{2u} orbital at nitrogen would increase and it would stabilize the antiferromagnetic structure. The structure of (TMP$^{+\bullet}$)M is reported to be planar,[46] and accordingly the ferromagnetic coupling would be dominant. Since the frequencies of the single-bond stretching- and deformation mode frequencies below 1240 cm^{-1} are scarcely altered between (TMP$^{+\bullet}$)Fe^{III}(ClO$_4$)$_2$ and (TMP$^{+\bullet}$)Fe^{IV}=O(MeOH), the planar structure would be maintained in the ferryl state, too.

Czernuszewicz et al.[33] observed a novel feature characteristic of π cation radicals. They observed an anomalously polarized (ap) band around 1000 cm^{-1} upon Soret excitation for both (TPP$^{+\bullet}$)Cu^{II} and (OEP$^{+\bullet}$)Ni^{II} and explained it in the following way; the $^2A_{1u}$ and $^2A_{2u}$ states are mixed through a vibration with the A_{2g} symmetry and the ap band around 1000 cm^{-1} corresponds to this mode. If so, the π cation radicals which yield the ap band around 1000 cm^{-1} can be regarded as the a_{1u}/a_{2u} admixture which should be distinguished from the a_{1u}/a_{2u} thermal mixture.[50] Unfortunately, we failed to detect it for both (TMP$^{+\bullet}$)Fe^{III}(ClO$_4$)$_2$ and (TMP$^{+\bullet}$)Fe^{IV}=O. (TPP$^{+\bullet}$)Cu^{II} and (TPP$^{+\bullet}$)Fe^{III}Cl(SbCl$_6$) are known to adopt a ruffled structure in a crystal[52] and probably so in solution. In contrast, (TMP$^{+\bullet}$)M are considered to adopt a planar structure.[39,46,49] This feature and the hindrance of the torsion around the C_m-C_{phenyl} bond stated above may suggest that the (TMP$^{+\bullet}$)M

system gives more pure a_{2u} radical than the $(TPP^{+\cdot})M$ system.

Since the $C_\beta C_\beta$ bond is antibonding and bonding for the a_{1u} and a_{2u} HOMOs, respectively,[51] removal of an electron from the a_{1u} or a_{2u} orbital is expected to cause the up- or down-shift of the $C_\beta C_\beta$ stretching vibrations. On the other hand, the $C_\alpha N$ bond is non-bonding and anti-bonding for the a_{1u} and a_{2u} HOMOs,[51] respectively, the downshift of the $C_\alpha N$ stretching frequency is never expected upon formation of a cation radical from the simple consideration. This implies that significant configuration interaction occurs in the cation radical state and the resultant electronic state cannot be easily inferred from the ground state wavefunctions of neutral porphyrins.

In conclusion, it became evident that the both ν_4 and ν_2 bands are shifted significantly to a lower frequency in the π cation radical of Fe^{III} and Fe^{IV}-porphyrins. Little shift of the ν_4 frequency upon the formation of Compound I of HRP raises a question about the established assignment of the π cation radical at ambient temperatures. The RR spectrum of the oxo-ferryl porphyrin π cation radical is along the extension of the a_{2u}-type divalent metalloporphyrin π cation radicals but it might be different from other a_{2u} type π cation radicals given by $(TPP^{+\cdot})M$ with regard to the torsion around the C_m-C_{phenyl} bond. The $\nu(Fe^{IV}=O)$ frequency is not greatly perturbed by formation of the π cation radical, but is more sensitive to its trans ligand. The controversy between Kincaid et al.[30] and our previous report[29] was reasonably explained in terms of difference of the trans ligand.

References

(1)   (a) Yamazaki, I.; Tamura, M.; Nakajima, R. *Mol. Cell. Biochem.* **1981**, *40*, 143-153. b) Schonbaum, G. R.; Chance, B. In *The Enzyme*; Boyer, P. Ed. ; Academic Press: Orlando, FL, 1976; Vol. 13, pp 363-408.

(2)   Hewson, W. D.; Hager, L. P. In *The Porphyrins* Dolphin, D. H. Ed.; Academic Press: New York, 1978; Vol 7, pp 295-332.

(3)   Groves, J. T. In *Cytochrome P-450: Structure, Mechanism, and Biochemistry*, Ortiz de Montellano, P., Ed.; Plenum Press: New York, 1986; Chapter 1.

(4)   (a) Maeda, Y.; Morita, Y. *Biochem. Biophys. Res. Commun.* **1967**, *29*, 680-685. (b) Moss, T. H.; Ehrenberg, A.; Bearden A. J. *Biochemistry* **1969**, *8*, 4159-4162. (c) Schultz, C. E.; Rutter, R.; Sage, J. T.; Debrunner, P. G. Hager, L. P. *Biochemistry* **1984**, *23*, 4743-4754.

(5)   (a) Dolphin, D.; Forman, A.; Borg, D. C.; Fajer, J.; Felton, R. H. *Proc. Natl. Acad. Sci. U.S.A.* **1971**, *68*, 614-618. (b) DiNello, R. K.; Dolphin, D. H. *J. Biol. Chem.* **1981**, *256*, 6903-6912.

(6)   (a) Roberts, J. E.; Hoffman, B. M.; Rutter, R.; Hager, L. P. *J. Biol. Chem.* **1981**, *256*, 2118-2121. (b) Roberts, J. E.; Hoffman, B. M.; Rutter, R.; Hager, L. P. *J. Am. Chem. Soc.* **1981**, *103*, 7654-7656.

(7)   (a) La Mar, G. N.; de Ropp, J. S. *J. Am. Chem. Soc.* **1980**, *102*, 395-397. (b) La Mar, G. N.; de Ropp, J. S.; Smith, K. M.; Langry, K. C. *J. Biol. Chem.* **1981**, *256*, 237-243.

(8)   Schultz, C. E.; Devaney, P. W.; Winkler, H.; Debrunner, P. G.; Doan, N.; Chiang, R.; Rutter, R.; Hager, L. P. *FEBS Lett.* **1979**, *103*, 102-105.

(9)   (a) Penner-Hahn, J. E.; Eble, K. S.; McMurry;, T. J.; Renner, M.; Balch, A. L.; Groves, J. T.; Dawson, J. H.; Hodgson, K. O. *J. Am. Chem. Soc.* **1986**, *108*, 7819-7825. (b) Chance, B.; Powers, L.; Ching, Y.; Poulos, T.; Schonbaum, G. R.; Yamazaki, I.; Paul, K. G. *Arch. Biochem. Biophys.* **1984**, *235*, 596-611.

(10)   Yonetani, T. In *The Enzymes*; Boyer, P. D. Ed.; Academic Press: Orlando, FL, 1976; Vol. 13, pp 345-361.

(11)   (a) Yonetani, T.; Schleyer, H.; Ehrenberg, A. *J. Biol. Chem.* **1966**, *241*, 3240-3243. (b) Hoffman, B. M.; Roberts, J. E.; Kang, C. H.; Margoliash, E. *J. Biol. Chem.* **1981**, *256*, 6556-6564. (c) Siraraja, M.; Goodin, D. B.; Smith, M.; Haffman, B. M. *Nature (London)* **1989**, *245*, 738-740.

(12)   (a) Morishima, I.; Takamuki, Y.; Shiro, Y. *J. Am. Chem. Soc.* **1984**, *106*, 7666-

7672. (b) Godziela, G. M.; Goff, H. M. *J. Am. Chem. Soc.* **1986**, *108*, 2237-2243.

(13)   Sandusky, P. O.; Salehi, A.; Chang, C. K.; Babcock, G. T. *J. Am. Chem. Soc.* **1989**, *111*, 6437-6439.

(14)   (a) Spiro, T. G. Ed. *Biological Application of Raman Spectroscopy*; Wiley: New York, 1987; Vol. 3.   (b) Kitagawa, T. *Adv. Spectrosc.* **1986**, *13*, 443-481.   (c) Kitagawa, T.; Ozaki, Y. *Structure and Bonding*, **1987**, *64*, 71-114.

(15)   (a) Hashimoto, S.; Tatsuno, Y.; Kitagawa, T. *Proc. Jpn. Acad. Ser. B* **1984**, *60*, 345-348.   (b) Hashimoto, S.; Tatsuno, Y.; Kitagawa, T. *Proc. Natl. Acad. Sci. U.S.A.* **1986**, *83*, 2417-2421.   (c) Hashimoto, S.; Nakajima, R.; Yamazaki, I.; Tatsuno, Y.; Kitagawa, T. *FEBS Lett.* **1986**, *208*, 305-307.

(16)   (a) Terner, J.; Sitter, A. J.; Reczek, C. M. *Biochim. Biophys. Acta* **1985**, *828*, 73-80.   (b) Sitter, A. J.; Reczek, C. M.; Terner, J. *J. Biol. Chem.* **1985**, *260*, 7515-7522.

(17)   Makino, R.; Uno, T.; Nishimura, Y.; Iizuka, T.; Tsuboi, M. ; Ishimura, Y. *J. Biol. Chem.* **1986**, *261*, 8376-8382.

(18)   Hashimoto, S.; Teraoka, J.; Inubushi, T.; Yonetani, T.; Kitagawa, T. *J. Biol. Chem.* **1986**, *261*, 11110-11118.

(19)   Oertling, W. A.; Hoogland, H.; Babcock, G. T.; Wever, R. *Biochemistry* **1988**, *27*, 5395-5400.

(20)   (a) Bajdor, K.; Nakamoto, K. *J. Am. Chem. Soc.* **1984**, *106*, 3045-3046.   (b) Proniewicz, L. M.; Bajdor, K.; Nakamoto, K. *J. Phys. Chem.* **1986**, *90*, 1760-1766.

(21)   Schappacher, M.; Chottard, G.; Weiss, R. *J. Chem. Soc. Chem. Commun.* **1986**, 93-94.

(22)   Kean, R. T.; Oertling, W. A.; Babcock, G. T. *J. Am. Chem. Soc.* **1987**, *109*, 2185-2187.

(23)   Mizutani, Y.; Hashimoto, S.; Tatsuno, Y.; Kitagawa, T. *J. Am. Chem. Soc.* **1990**, *112*, 6809-6814.

(24)   (a) Teraoka, J.; Ogura, T.; Kitagawa, T. *J. Am. Chem. Soc.* **1982**, *104*, 7354-7356.   (b) Ogura, T.; Kitagawa, T. *J. Am. Chem. Soc.* **1987**, *109*, 2177-2179.

(25)   (a) Oertling, W. A.; Babcock, G. T. *J. Am. Chem. Soc.* **1985**, *107*, 6406-6407. (b) Oertling, W. A.; Babcock, G. T. *Biochemsitry* **1988**, *27*, 3331-3338.

(26)   Paeng, K. J.; Kincaid, J. R. *J. Am. Chem. Soc.* **1988**, *110*, 7913-7915.

(27)   Van Wart, H. E.; Zimmer, J. *J. Am. Chem. Soc.* **1985**, *107*, 3379-3381.

(28)   Palaniappan, V; Terner, J. *J. Biol. Chem.* **1989**, *264*, 16046-16053.

(29)   Hashimoto, S.; Tatsuno, Y.; Kitagawa, T. *J. Am. Chem. Soc.* **1987**, *109*, 8096-

8097.

(30) Kincaid, J. R.; Schneider, A. J.; Paeng, K. J. *J. Am. Chem. Soc.* **1989**, *111*, 735-737.

(31) Yamaguchi, H.; Nakano, M.; Itoh, K. *Chem. Lett.* **1982**, 1397-1400.

(32) (a) Salehi, A.; Oertling, W. A.; Babcock, G. T.; Chang, C. K. *J. Am. Chem. Soc.* **1986**, *108*, 5630-5631. (b) Oertling, W. A.; Salehi, A.; Chang, C. K.; Babcock, G. T. *J. Phys. Chem.* **1987**, *91*, 3114-3116. (c) Oertling, W. A.; Salehi, A.; Chung, Y. C.; Leroi, G. E.; Chang, C. K.; Babcock, G. T. *J. Phys. Chem.* **1987**, *91*, 5887-5898. (d) Oertling, W. A.; Salehi, A.; Chang, C. K.; Babcock, G. T. *J. Phys. Chem.* **1989**, *93*, 1311-1319.

(33) Czernuszewicz, R. S.; Macor, K. A.; Li, X. Y.; Kincaid, J. R.; Spiro, T. G. *J. Am. Chem. Soc.* **1989**, *111*, 3860-3869.

(34) Puff, H.; Sievers, R. In *Handbuch der Praparative Anorganischen Chemie II*; Brauer, V. G., Ed.; Ferdin and Enke Verlag: Stuttgart, 1978; p 1036.

(35) Tatsuno, Y.; Saeki, Y.; Nozaki, M.; Otsuka, S.; Maeda, Y. *FEBS Lett.* **1980**, *112*, 83-85.

(36) Wagner, R. W.; Lawrence, D. S.; Lindsey, J. S. *Tetrahedron Lett.* **1987**, *28*, 3069-3070.

(37) Fuson, R. C.; Horning, E. C.; Rowland, S. P.; Ward, M. L. *Org. Synth. III* **1987**, 549-551.

(38) Kobayashi, H.; Higuchi, T.; Kaizu;, Y.; Osada, H.; Aoki, M. *Bull. Chem. Soc. Jpn.* **1975**, *48*, 3137-3141.

(39) Gans, P.; Buisson, G.; Duee, E.; Marchon, J-C.; Erler, B. S.; Scholz, W. F.; Reed, C. A. *J. Am. Chem. Soc.* **1986**, *108*, 1223-1234.

(40) Groves, J. T.; Quinn, R.; McMurry, T. J.; Nakamura, M.; Lang, G.; Boso, B. *J. Am. Chem. Soc.* **1985**, *107*, 354-360.

(41) Li, X. Y.; Czernuszewicz, R. S.; Kincaid, J. R.; Su, Y. O.; Spiro T. G. *J. Phys. Chem.* **1990**, *94*, 31-47.

(42) Atamian, M.; Donohoe, R. J.; Lindsey;, J. S.; Bocian, D. F. *J. Phys. Chem.* **1989**, *93*, 2236-2243.

(43) (a) Fidler, V.; Ogura, T.; Sato, S.; Aoyagi;, K.; Kitagawa, T. *Bull. Chem. Soc. Jpn.* **1991**, *64*, 2315-2322. (b) Ogura, T.; Fidler, V.; Ozaki, Y.; Kitagwa, T. *Chem. Phys. Lett.* **1990**, *169*, 457-459.

(44) Su, Y. O.; Czernuszewicz, R. S.; Miller, L. A.; Spiro, T. G. *J. Am. Chem. Soc.* **1988**, *110*, 4150-4157.

155

(45) Macor, K. A.; Czernuszewicz, R. S.; Spiro, T. G. *Inorg. Chem.* **1990**, *29*, 1996-2000.

(46) Song, H.; Reed, C. A.; Scheidt, W. R. *J. Am. Chem. Soc.* **1989**, *111*, 6865-6866.

(47) (a) Fajer, J.; Borg, D. C.; Forman, A.; Dolphin, D.; Felton, R. H. *J. Am. Chem. Soc.* **1970**, *92*, 3451-3459. (b) Fajer, J.; Davis, M. S. In *The Porphyrins*; Dolphin, D. Ed.; Academic Press, New York, 1978, Vol. IV, p 197. (c) Harris, K. D. M.; Thomas, J. M. *J. Chem. Soc. Faraday Trans.* **1990**, *86*, 1095-1101.

(48) Pople, J. A.; Beveridge, D. L. *J. Chem. Phys.* **1968**, *49*, 4725-4726.

(49) Buisson, G.; Derozier, A.; Duee, E.; Gans, P.; Marchon, J. C.; Regnard, J. R.; *J. Am. Chem Soc.* **1982**, *104*, 6793-6796.

(50) Fujii, H.; Morishima, I. *to be published*.

(51) Kashiwagi, H.; Obara, S. *Int. J. Quant. Chem.* **1981**, *20*, 843-859.

(52) Scheidt, W. R. *Struct. Bonding* **1987**, *64*, 1-70.

Table III-I. Observed frequencies, isotopic frequency shifts, and the mode assignments for Raman bands of (TMP)Fe^{III}Cl and the corresponding data for (TPP)Ni^{II}.

		(TMP)Fe^{III}Cl				(TPP)Ni^{II}	
$\nu_i{}^a$	P^b	$\Delta\nu(^{15}N)^c$	$\Delta\nu(^{13}C)^d$	assignments^e	$\nu_i{}^f$	$\Delta\nu(^{15}N)$	$\Delta\nu(^{13}C)$
1612	p	0	-1	phenyl(ν_{8a})			
1554	p	0	-7	ν_2	1572	0	-8
1493	dp	0	-1	ν_{11}	1504	0	0
1454	p	0	-8	ν_3	1470	0	-6
1364	p	-5	-4	ν_4	1374	-6	0
1274	dp	-10	+1	ν_{12}	1302	-11	0
1254	dp	-9	-9	ν_{27}	1269	-8	-5
1229	p	-1	-4	ν_1	1235	-1	-6
1183	dp	0	0	$\nu_{34}(\nu_{17})$	1190	0	0
1073	p	-2	-1	ν_9	1079	-1	-1
1018	dp	-9	-4	ν_{15}	1005	-10	-8
1003	p	-15	-3	ν_6	1004	-20	-2
863	dp	-1	-13	ν_{32}	869	-2	-4
846	dp	-4	-7	ν_{16}	846	-7	-10

a) observed frequencies. b) polarization. c) isotopic frequency shift for ^{15}N substitution. d) isotopic frequency shift for ^{13}C substitution. e) mode number is based on Ref. 41. f) all data for (TPP)Ni^{II} were observed values reported in Ref. 41.

Table III-II. Observed frequencies, isotopic frequency shifts, and the mode assignments for Raman bands of $(TMP)Fe^{III}(Im)_2$.

ν_i	P	$\Delta\nu(^{15}N)$	$\Delta\nu(^{13}C)$	assignments
1612	p	0	+1	phenyl(ν_{8a})
1562	p	0	-9	ν_2
1496	dp	-1	+1	ν_{11}
1462	p	0	-8	ν_3
1368	p	-6	-3	ν_4
1260	dp	-9	-9	ν_{27}
1231	p	-2	-5	ν_1
1072	p	-2	+2	ν_9
1022	dp	-10	-3	ν_{15}
1004	p	-14	-1	ν_6
864	dp	-1	-12	ν_{32}
848	dp	-4	-9	ν_{16}

Table III-III. Observed frequencies, isotopic frequency shifts, and the mode assignments for Raman bands of $(TMP^{+ \bullet})Fe^{III}(ClO_4)_2$.

ν_i	P	$\Delta\nu(^{15}N)$	$\Delta\nu(^{13}C)$	assignments
1611	p	0	-2	phenyl(ν_{8a})
1509	p	-4	-12	ν_2
1325	p	-6	+2	ν_4
1299	p	0	-1	
1250	p	-	-3	ν_{12}
1231	p	+3	-5	ν_1
1181	dp	-1	-2	ν_{34}
1068	p	-2	0	ν_9
1022	dp	-3	-2	ν_{15}
894	p	0	-4	
862	dp	0	-14	ν_{32}

Table III-IV. Observed frequencies, isotopic frequency shifts, and the mode assignments for Raman bands of $(TMP^{+\cdot})Fe^{IV}=O(MeOH)$ and the corresponding data for $(TMP)Fe^{IV}=O$.

$(TMP^{+\cdot})Fe^{IV}=O(MeOH)$					$(TMP)Fe^{IV}=O$
ν_i	P	$\Delta\nu(^{15}N)$	$\Delta\nu(^{13}C)$	assignments	ν_i
1614	p	-1	-1	phenyl(ν_{8a})	
1517	p	-3	-15	ν_2	1570
1457	dp	-1	-8	ν_{11}	
1358	dp	+2	-16		
1335	p	-16		ν_4	1371
1236	p	+1	-6	ν_1	1229
1181	dp	0	0	ν_{34} or (ν_{17})	
1067	p	-2	0	ν_9	1071
1024	dp	-9	-4	ν_{15}	
1003	p	-12	-3	ν_6	
894	p	0	0		
862	dp	0	-10	ν_{32}	862
831	p	0	+1	$\nu(Fe^{IV}=O)$	843

Figure III-1. Resonance Raman spectra of (TMP)Fe^{III}Cl and its isotopomers in CH$_2$Cl$_2$ at room temperature. A) unlabeled species, B) pyrrole-^{15}N derivative, C) meso-^{13}C derivative, D) polarized spectra for unlabeled species. Raman bands marked by a dagger are due to solvent.
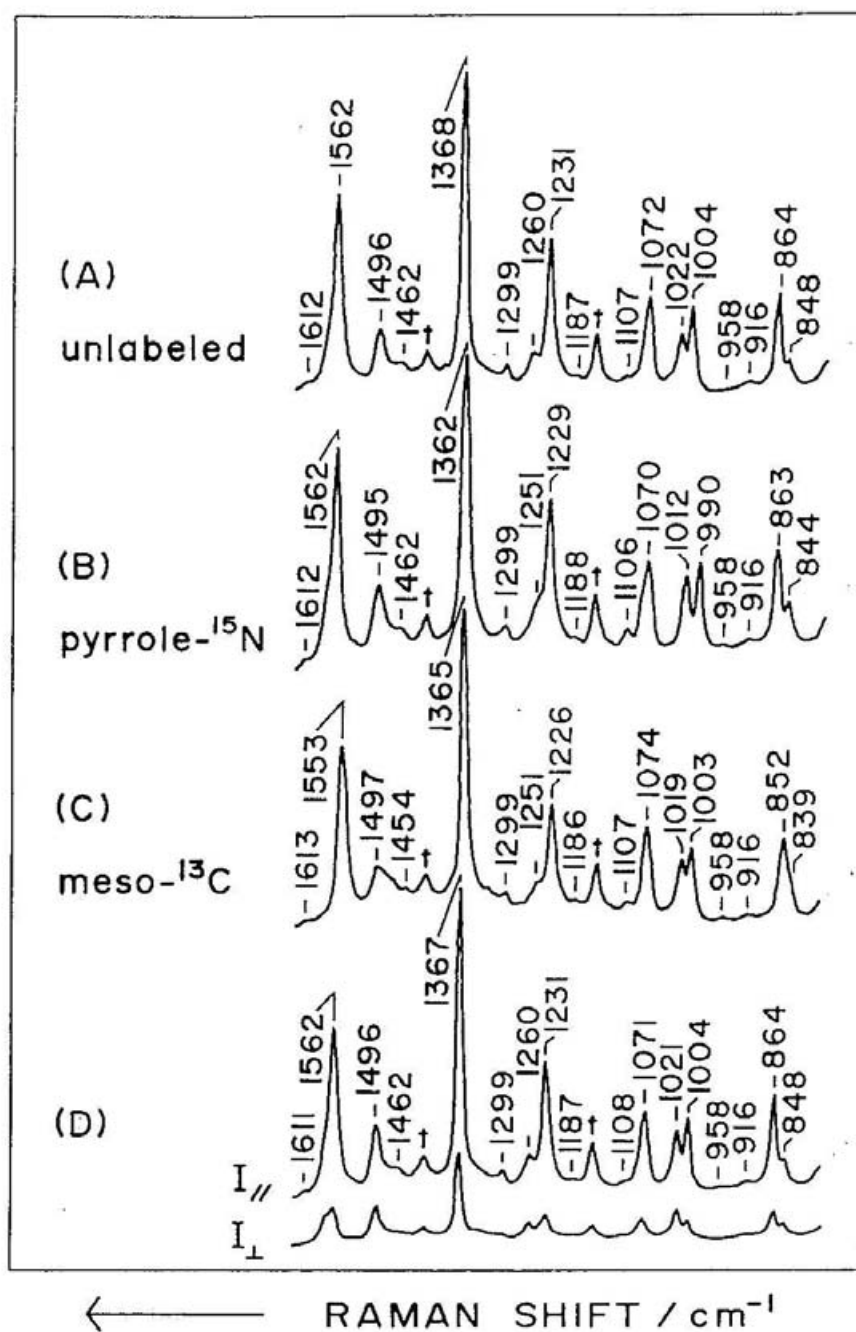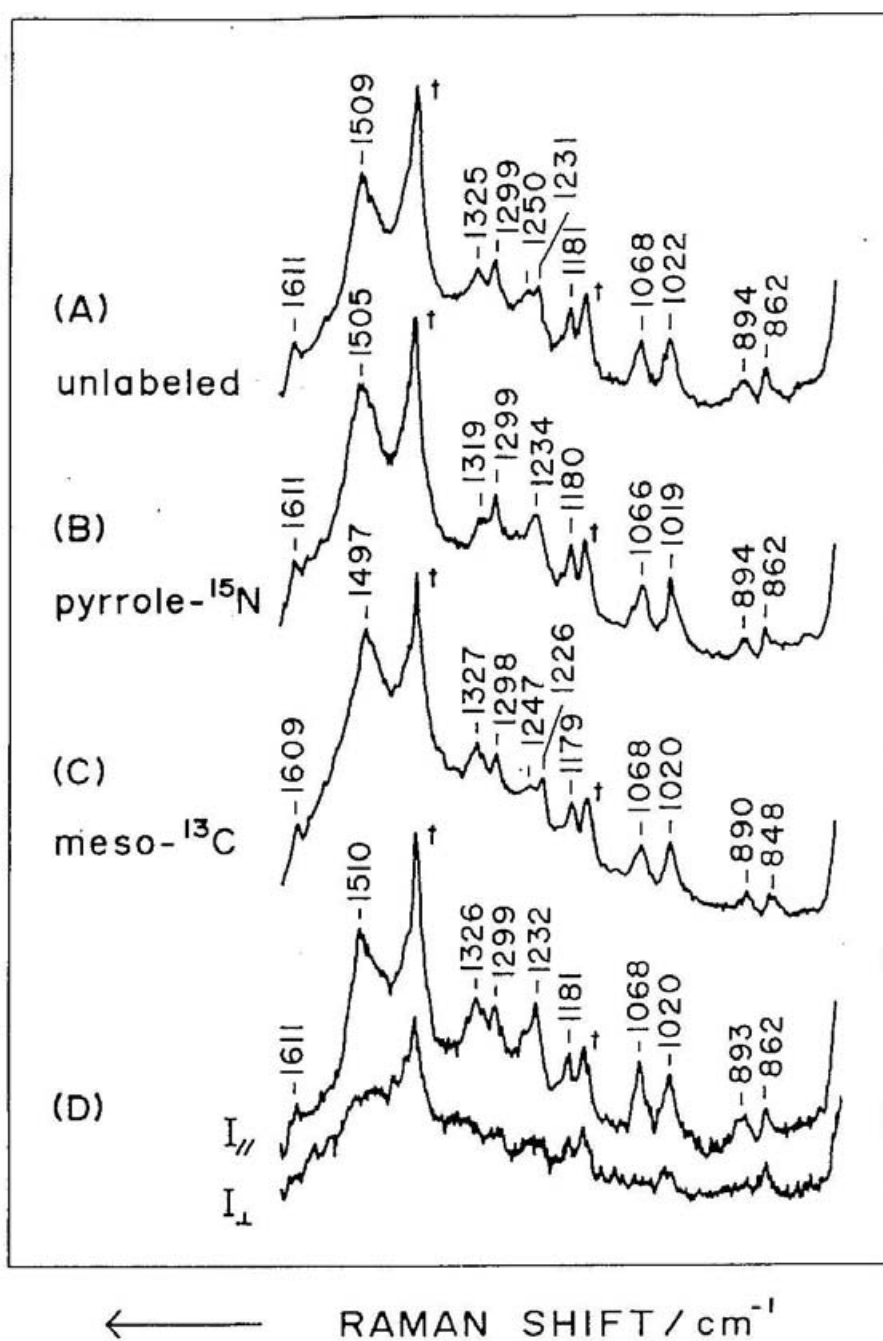
161

Figure III-2. Resonance Raman spectra of (TMP)Fe^{III}(Im)$_2$ and its isotopomers in CH$_2$Cl$_2$ at room temperature. A) unlabeled species, B) pyrrole-^{15}N derivative, C) meso-^{13}C derivative, D) polarized spectra for unlabeled species. Raman bands marked by a dagger are due to solvent.

162

Figure III-3. Resonance Raman spectra of $(TMP^{+•})Fe^{III}(ClO_4)_2$ and its isotopomers in dried CH_2Cl_2 at room temperature. A) unlabeled species, B) pyrrole-^{15}N derivative, C) meso-^{13}C derivative, D) polarized spectra for unlabeled species. Raman bands marked by a dagger are due to solvent. The spectra were observed with the spinning cell.

163
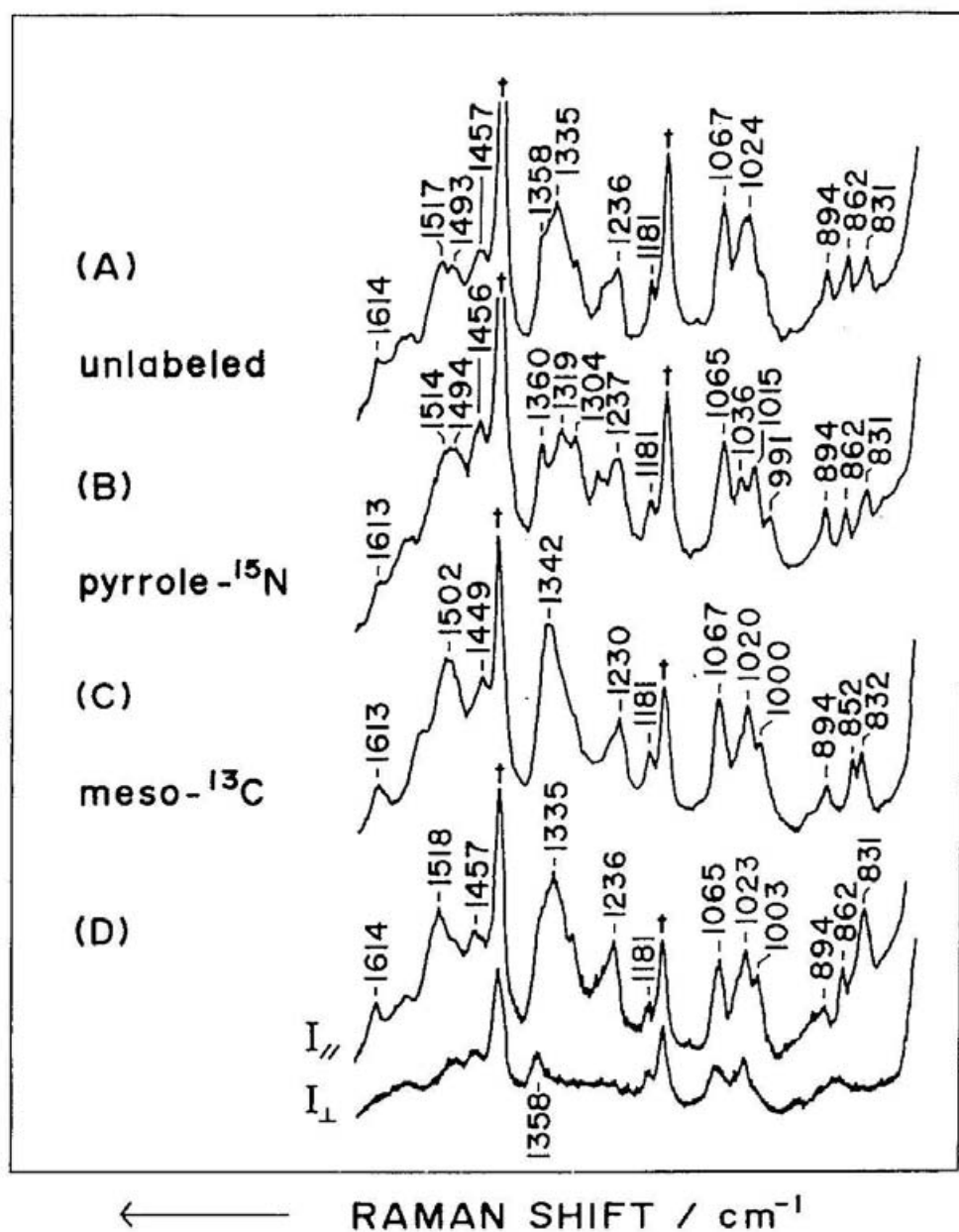
Figure III-4. Resonance Raman spectra of $(TMP^{+\bullet})Fe^{IV}=O(MeOH)$ and its isotopomers in CH_2Cl_2 containing MeOH at -80°C. A) unlabeled species, B) pyrrole-^{15}N derivative, C) meso-^{13}C derivative, D) polarized spectra for unlabeled species. The spectra were observed with the spinning cell. Raman bands marked by a dagger are due to solvent. The ratio of mCPBA to porphyrin was ca. 20.
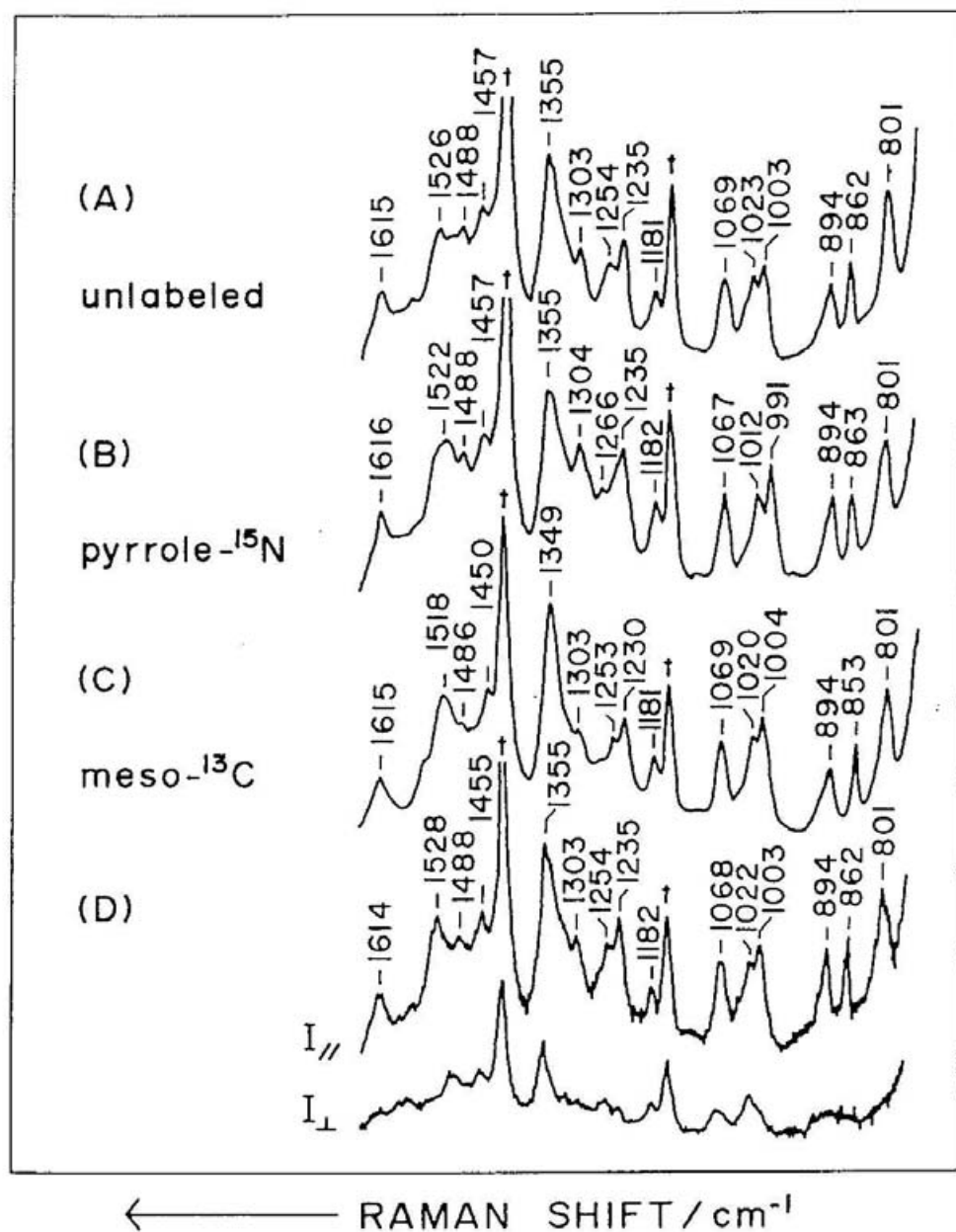
164

Figure III-5. Resonance Raman spectra of $(TMP^{+\bullet})Fe^{IV}=O(mCBA)$ and its isotopmers in dried CH_2Cl_2 at -80°C. A) unlabeled species, B) pyrrole-^{15}N derivative, C) meso-^{13}C derivative, D) polarized spectra for unlabeled species. Raman bands marked by a dagger are due to solvent. The spectra were observed with the spinning cell. The ratio of mCPBA to porphyrin was 2.
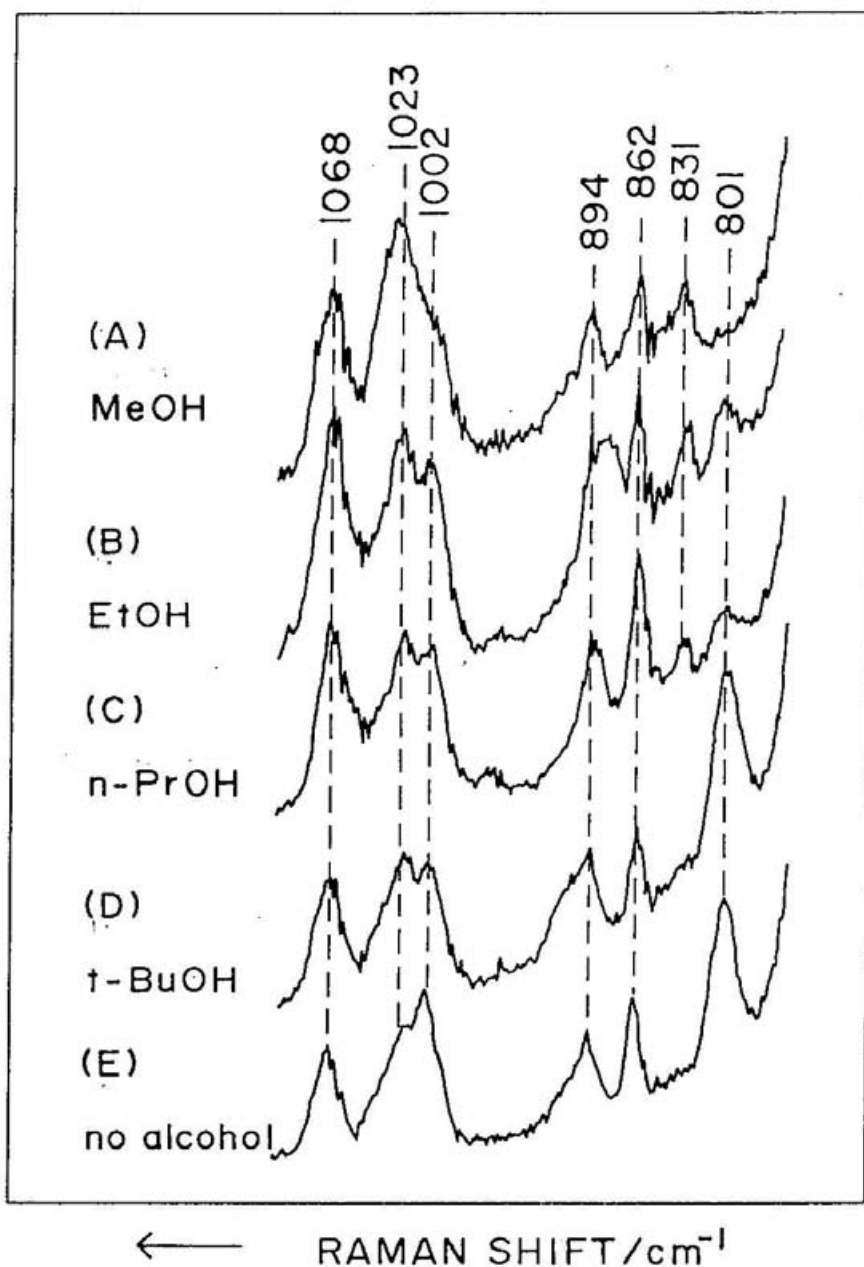
165

Figure III-6. Resonance Raman spectra of $(TMP^{+•})Fe^{IV}=O(mCBA)$ in dried CH_2Cl_2 at -80 °C. A) derived from ^{56}Fe porphyrin and ordinary mCPBA, B) derived from ^{54}Fe porphyrin and ordinary mCPBA, C) derived from ^{56}Fe porphyrin and ^{18}O mCPBA. Others are the same in the caption of Figure III-5. The inset figure shows the absorption spectra in the α band region of $(TMP^{+•})Fe^{IV}=O(MeOH)$ (solid line) and $(TMP^{+•})Fe^{IV}=O(mCBA)$ (broken line).

166
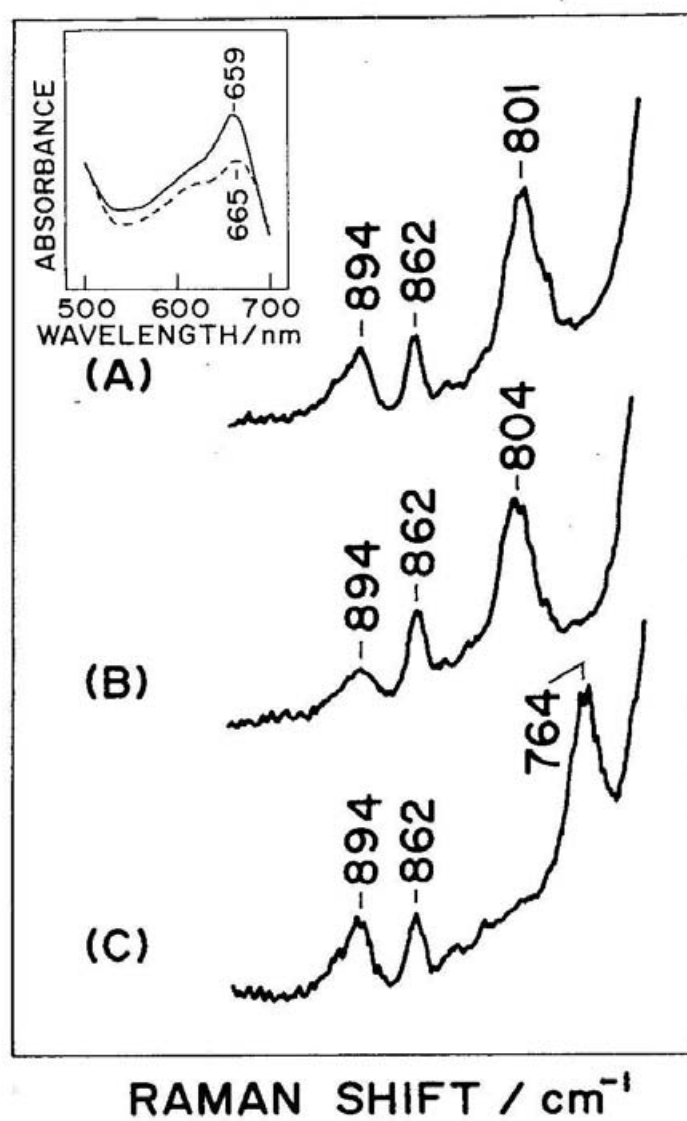
Figure III-7. Resonance Raman spectra of $(TMP^+ \cdot)Fe^{IV}=O(alcohol)$ and $(TMP^{+ \cdot})Fe^{IV}=O(mCBA)$ at -80 °C in dried CH_2Cl_2 with methanol (A), ethanol (B), n-propylalcohol (C), or t-butylalcohol (D) and in the absence of any alcohol (E). The spectra were observed with the spinning cell.